Titre: Title:	Numerical studies of melting process in a cylindrical enclosure
Auteur: Author:	Yongke Wu
Date:	1990
Type:	Mémoire ou thèse / Dissertation or Thesis
Référence: Citation:	Wu, Y. (1990). Numerical studies of melting process in a cylindrical enclosure [Thèse de doctorat, Polytechnique Montréal]. PolyPublie. https://publications.polymtl.ca/57965/

UNIVERSITE DE MONTREAL

NUMERICAL STUDIES OF MELTING PROCESS IN A CYLINDRICAL ENCLOSURE

par

Yongke Wu
DEPARTEMENT DE GENIE MECANIQUE
ECOLE POLYTECHNIQUE

THESE PRESENTEE EN VUE DE L'OBTENTION
DU GRADE DE PHILOSOPHIAE DOCTOR (Ph. D.)
(GENIE MECANIQUE)

Septembre 1990

ISBN 0-315-64324-2

UNIVERSITE DE MONTREAL

ECOLE POLYTECHNIQUE

Cette thèse intitulée:

NUMERICAL STUDIES OF MELTING PROCESS IN A CYLINDRICAL ENCLOSURE

présentée par: Yongke Wu

en vue de l'obtention du grade de: Philosophia Doctor (Ph.D.)

a été dûment acceptée par le jury d'examen constitué de:

M.	Luc Robillard	Ph.D., président
M.	Marcel Lacroix	Ph.D.
M.	Réné Kahawita	Ph.D.
M.	T. Hung Nguyen	Ph.D.
M.	Michel Prud'homme	Ph.D.

SOMMAIRE

On considère le processus de fusion d'un matériau à changement de phase porté à la température de fusion à l'intérieur d'une enceinte cylindrique verticale. Le Chapitre 1 passe en revue la biblographie des études analytiques, numériques et expérimentales sur les phénomènes de changement de phase pertinentes à ce problème et permet de situer celui–ci dans un contexte d'ingénierie global.

On suppose que la phase liquide constitue un fluide de propriétés thermodynamiques constantes qui satisfait aux conditions de l'approximation de Boussineq. Le problème est traité pour différentes conditions limites en adoptant une formulation vorticité–fonction de courant, étant donné la symétrie axiale du problème. Les équations gouvernant l'écoulement thermoconvectif dans la cavité formée par la phase liquide sont données au Chapitre 2 en coordonnées curvilignes générales.

La méthode de solution fait appel à une technique de transformation des coordonnées décrite au Chapitre 3 qui permet d'immobiliser l'interface liquide–solide dans le plan transformé où le système d'équations pour la vorticité, la fonction de courant et la température sont alors résolues par différences finies. On génère ainsi un maillage adapté à la géométrie de la cavité à chaque pas de calcul dans le temps. La transformation s'effectue également via la solution par différences fines d'une paire d'équations de type elliptique. Cette technique permet un bon contrôle du maillage généré dans le plan physique tout en gardant un maillage uniforme dans le plan transformé.

Notre étude comporte ensuite quatre volets couvrant chacun un ou plusieurs aspects nouveaux du problème de la fusion dans un cylindre vertical, qui n'a été que très peu étudié d'une façon ou d'une autre jusqu'ici. On considere plus précisément

les effets d'un chauffage par le bas, d'un flux de chaleur imposé à la paroi verticale et de l'inversion de densité dans le cas de la glace en traitant à chaque fois le problème pour des nombres de Rayleigh modérés.

Le Chapitre 4 est consacré à l'étude du cas où l'on impose une température constante à la paroi verticale en supposant les parois horizontales adiabatiques. Les résultats obtenus pour $Ra = 10^4 - 10^6$, $Pr = 7$, $Ste = 0.15$ et $A = 2$ révèlent que le nombre de Nusselt moyen présente des oscillations lorsque Ra devient important. On se penche également sur le cas de la fusion autour d'une enceinte verticale ayant fait l'objet d'une étude précédente. L'effet de certaines approximations courantes est examiné et des prédictions numériques sont obtenues pour des nombres de Rayleigh allant jusqu à $Ra = 7 \times 10^5$ pour une température constante imposée à la paroi verticale et $Ra = 7 \times 10^8$ pour un flux de chaleur constant. Les résultats présentés pour $Ste = 0.15$ et pour $Pr = 7$ sont pratiquement indépendants de ces paramètres lorsque $Ste < 0.15$ et $Pr > 7$. Pour un flux de chaleur constant, Nu moyen en régime permanent est proportionnel à $Ra^{1/4}$ et la fusion s'effectue plus lentement que pour une température constante.

On étudie le chauffage par le bas à température constante au Chapitre 5 pour $Ste = 0.1$, $Pr = 7$ et $Ra = 10^6$ en supposant une paroi verticale adiabatique. Le nombre de Rayleigh critique pour l'apparition des cellules de Bénard est de 2197 en se basant sur l'épaisseur de la couche liquide. On passe progressivement d'un régime multicellulaire à un régime unicellulaire, durant lequel se forme une couche limite thermique au bas du cylindre qui tend à s'opposer au transfert de chaleur à travers la cavité. Le nombre de Nusselt local subit une évolution marquée et fortement tributaire de la configuration cellulaire avant de se stabiliser à un niveau d'autant plus élevé qu'on se rapproche de l'axe de symétrie.

Le Chapitre 6 résume le cas de la fusion dans une enceinte entièrement isotherme pour $Ra = 10^5, 10^6$. Le transfert de chaleur dans la partie supérieure de la cavité, qui constitue alors une zone de stratification stable, est essentillement conductif et Nu décroît de façon monotone. La fonte au bas de la cavité présente un seuil critique tout comme dans le cas précédent, mais plus bas (environ 830) car la convection dans la zone latérale favorise l'apparition des cellules de Bénard beaucoup plus tôt.

Le Chapitre 7 traite de la fusion de la glace pour une paroi verticale à $T_w = 4$, 6, 8 et $10°C$, pour $Ra = 7 \times 10^5$ et $A = 2$. Le transfert de chaleur est maximum pour une paroi à $4°C$. On observe un écoulement unicellulaire dans la cavité dont le sens est inversé par rapport au cas d'un fluide normal: l'ecoulement descend le long de la paroi au lieu de monter. Pour $T_w = 6$ et $8°C$, on observe deux cellules de sens de rotation opposé, séparées par l'isotherme de $4°C$. L'intensité des deux cellules est comparable lorsque cet isotherme est situé au milieu de cavité et Nu est alors minimun, ce qui se produit pour $T_w = 8°C$. Lorsque $T_w = 10°C$, on se rapproche du cas d'un fluide normal, sans inversion de densité.

Le Chapitre 8 présente les grandes conclusions de cette étude et formule quelques recommandations en vue de travaux subséquents.

ABSTRACT

Melting of a solid matrix at fusion temperature in a vertical cylindrical enclosure is being studied. The problem is treated for several boundary conditions, assuming a fluid phase of constant thermal properties. The vorticity–stream function formulation is adopted and the Boussineq approximation is made. Governing equations for heat and fluid flow are given in general curvilinear coordinates in Chapter 2, after a comprehensive literature review in Chapter 1.

Solution is carried out based on a numerical coordinate transformation technique described in Chapter 3. The set of governing equations is then solved by standard finite–difference techniques in the transformed plane, where the solid–liquid interface is at rest. Transformation is achieved through an elliptic boundary value problem, thereby generating a new set of body–fitted coordinates at each time step.

Chapter 4 describes results obtained in the case of adiabatic top and bottom walls, for an isothermal vertical wall, for $Ra = 10^4 - 10^6$, $Pr = 7$, $Ste = 0.15$, and $A = 2$. Melting around a cylinder is also considered. The effect of some simplifying assumptions is examined and numeral prediction are obtained for $Ra < 7 \times 10^5$ for a constant temperature and $Ra < 7 \times 10^8$ for a constant heat flux. Results obtained for $Ste = 0.15$ and $Pr = 7$ are virtually independent of these parameters when $Ste < 0.15$ and $Pr > 7$. For a constant heat flux, Nu is proportional to $Ra^{1/4}$ and melting occurs more slowly than for a constant temperature.

Heating from the bottom is studied in Chapter 5, for $Ste = 0.1$, $Pr = 7$ and $Ra = 10^6$. The critical Rayleigh number for Bénard convection is 2197 based on the melt thickness. The flow configuration evolves from a multicellular regime

to a single cell regime during which a thermal boundary layer is formed at the bottom wall.

Chapter 6 investigates melting within a completely isothermal enclosure for $Ra = 10^5$ and 10^6. The top part of the cavity is then a stable layer with no convection, while the bottom part shows a critical Ra around 830 as the lateral cells trigger the onset of convection much earlier than in the previous case. Chapter 7 treats the melting of ice for T_w = 4, 6, 8 and $10°C$, for $Ra = 7 \times 10^5$ and $A = 2$. Nu is maximum when $T_w = 4°C$. There is only one cell in the cavity, with downward flow along the cylinder wall, the flow direction is opposite from that of normal fluid with no density inversion. For T_w=6 and $8°C$, two counter–rotating cells are found, separated by the $T_w = 4°C$ isotherm. The intensity of both cells is similar, and Nu minimum when $T_w = 8°C$ and the $4°C$ isotherm lies midway between the wall and the interface. Chapter 8 concludes and offers recommendations for future work.

ACKNOWLEDGEMENTS

First of all, I would like to express my greatest appreciation to Professor T. Hung Nguyen, my research supervisor for his encouragement and friendly guidance during the course of this thesis. I am very pleased to have the opportunity to work under his supervision and counselling in all phases of my graduate study at Ecole Polytechnique, University of Montréal.

Grateful acknowledgements are also expressed to Professor Michel Prud'homme, my co-supervisor, for his patience and rigor in examining all the mathematical formulae in this thesis, and for many helpful discussions during this study.

I would like to extend my special appreciations to my fellow graduate students and colleagues in the Department of Mechanical Engineering, for many invaluable discussions both in professional and in computer knowledge.

Finally, my sincere gratitude goes to my wife Yuping Shu for her love and encouragement throughout my graduate study, and also for her debugging and improving my computer graphic software.

This work was supported by the National Science and Engineering Research Council of Canada, through grants No OGP626 and OGP4982.

TABLE OF CONTENTS

LIST OF FIGURES

LIST OF TABLES

LIST OF SYMBOLS

a_n	nth coefficient of nonlinear thermal expansion term
A	aspect ratio H/r_0
$\mathbf{A}$	
$\vdots$	
$\mathbf{G}$ and $\mathbf{U}$	component vectors
$\mathbf{A}'$	
$\vdots$	
$\mathbf{G}'$ and $\mathbf{U}'$	transformed component vectors
A^u	
$\vdots$	
E^u	coefficients of the upwind schemes
A_i^f	
$\vdots$	
F_i^f	coefficients of the finite difference representation of equation f
c_p	specific heat at constant pressure
Fo	Fourier number $\alpha t/r_0$
g	acceleration of gravity; scale factor $g = J^2$
$g_{i,j}$	covariant scale factor
$g^{i,j}$	contravariant scale factor
h	latent heat of fusion
H	height of cylinder
J	determinant of the Jacobian
k_l	thermal conductivity in the melt
k_s	thermal conductivity in the solid

k^*	k_s/k_l
$\mathbf{n}$	unit vector
Nu	Nusselt number $Q/(Hk\Delta T)$
Nu_{local}	local Nusselt number
p	pressure
P	dimensionless pressure $p/(\alpha r_0 \rho)$
$P(\xi,\eta)$	control function for concentrating coordinates in direction of ξ
Pr	Prandtl number ν/α
q_c	heat flux
$\mathbf{q}$	primitive variable vectors
Q	heat transfer rate at cylinder wall
$Q(\xi,\eta)$	control function for concentrating coordinates in direction of η
Ra	Rayleigh number $g\beta r_0^3(T_w - T_r)/(\alpha\nu)$
Ra_1	Rayleigh number $g\beta_1 r_0^3(T_w - T_r)/(\alpha\nu)$
Ra_2	Rayleigh number $g\beta_2 r_0^3(T_w - T_r)^2/(\alpha\nu)$
Ra_i	internal Rayleigh number $g\beta\delta^3(T_w - T_r)/(\alpha\nu)$
Ra_e	external Rayleigh number $Ra_e = Ra$
r	radial coordinate
r_0	radius of cylinder
R	radius in dimensionless form r/r_0
Ste	Stefan number $c_p(T_w - T_f)/h$
t	time
T	temperature
T_f	fusion temperature
T_l	temperature of the melt liquid
T_s	temperature of the solid

u	radial velocity
U	dimensionless velocity ur_0/α
v	axial velocity
$\dot{v}$	local interface velocity $d\mathbf{n}/dt$
$\tilde{U}, \tilde{V}, \widetilde{W}$	contravariant velocities
V	dimensionless velocity vr_0/α
V_f	molten volume fraction
w	velocity component in z direction
x, y	transformed coordinates in physical plane
z	axial coordinate
Z	axial coordinate in dimensionless form z/r_0

Greek symbols

α_l	thermal diffusivity of the melt $k_l/\rho_l c_p$
α_s	thermal diffusivity of the solid $k_s/\rho_s c_p$
α^*	α_s/α_l
β	thermal expansion coefficient
β_1	first order thermal expansion coefficient $\beta_2(T_r - T_m)$
β_2	second order expansion coefficient $\beta/[1 - \beta(T_r - T_m)]$
$\delta(t)$	thickness of the melt layer
Δ	subcool $(T_f - T_i)/(T_w - T_f)$
ϵ	perturbation parameter
$\Gamma^l_{i,j}$	Christoffel symbol
λ	ratio of thermal diffusivities α_l/α_s
θ	dimensionless temperature $(T - T_f)/(T_w - T_f)$
θ_l	temperature in the liquid region $(T_l - T_f)/(T_w - T_f)$

θ_s	temperature in the solid region $(T_s - T_f)/(T_w - T_f)$
μ	dynamic viscosity
ν	kinematic viscosity
ξ, η, ζ	coordinate directions in transformed space
ρ	density of water expressed by $\rho_r[1 - 2\beta_1(T - T_r) - \beta_2(T - T_R)]^2$
ρ_l	density of the melt
ρ_r	reference density $\rho_m[1 - \beta(T_r - T_m)^2]$
ρ_s	density of the solid
τ	dimensionless time $Ste \cdot Fo$
σ	dimensionless interface speed $dr_f/d\tau$
$\phi(\xi, \eta)$	parameters of the grid control function
$\varphi(\xi, \eta)$	parameters of the grid control function
ψ	stream function
ω	vorticity $\dfrac{\partial v}{\partial r} - \dfrac{\partial u}{\partial z}$
∇^2	Laplace operator in cylindrical coordinate
$\widetilde{\nabla}^2$	transformed Laplace operator

Subscripts

f	fusion
i	index, l for liquid, s for solid
m	mean value
r	reference point
w	cylinder wall
x, y, z, t	derivatives with respect to x, y, z, t
ξ, η, ζ, τ	derivatives with respect to ξ, η, ζ, τ

Chapter 1

INTRODUCTION

The study of phase-change problems is of great interest in a wide range of natural and industrial processes. As a matter of fact, phase-change phenomena are significant and must be dealt with in a broad range of fields, such as aeroscience, energy storage, surgery, cryobiology as well as in the chemical, food, and metallurgical industries. In recent years latent heat-recovery systems have attracted considerable attention in many applications requiring large a mount of heat to be stored and recovered during the phase-change process.

This process is of theoretical significance as well. In the past decades, most of the studies dealing with phase-change problems have considered heat conduction as the sole heat transfer mechanism. Because of their simplicity, one-dimensional, analytical methods, either exact or approximate, have been widely developed. However, these analyses are valid only when the temperature of the melt is uniform and equal to the fusion temperature. These situations are not very realistic since even small temperature differences in the melt can induce buoyancy forces, and give rise to appreciable convective flows. Experimental studies have shown clearly that the heat transport mechanism is mainly due to conduction only in the very early stage of the phase-change process; as the melting progresses, natural convection becomes dominant.

When natural convection is taken into account, exact closed-form solutions

can not be obtained as in the simple one-dimensional models, as irregular geometry becomes an inherent feature of the phase-change problem. A solution method must be found then to handle the complex and moving boundaries. In this respect, the body fitted coordinates have been widely adopted. At the present time, the problem of moving boundaries can be efficiently analyzed by this method. Although for extremely complex geometries and large time scales, numerical methods are currently limited by the storage capability and speed of the computer, it seems that such a restriction can be overcome in a near future.

Literature Review

The study of the phase-change process can be traced back to a century ago. In 1831, Lame and Clapeyon [1] published the first analytical work on the phase-change problem. Since then substantial efforts have been devoted by many investigators. Among them, Stefan developed a general approach to the phase-change problem [2], which has been named Stefan problem in his honor.

Phase-change or Stefan problems have been extended to such a wide range that an exhaustive review is beyond the scope of this thesis. Therefore, our intention is focused on two main categories: the conduction dominated phase-change problem, and the convection dominated phase-change problem in some typical geometries, namely plane and cylindrical.

Section 1 of this review is concerned with analytical approaches usually adopted in the study of one-dimensional conduction models, while section 2 is devoted to the analyses of phase-change problems in the presence of natural convection in different geometries.

Finally, the scope of the present investigation is outlined in light of the prior studies.

1.1 The Conduction Dominated Phase-Change Problem

The conduction-dominated Stefan problem may be regarded as a classical subject to which tremendous efforts have been devoted. Meanwhile, a large number of techniques has been developed as no single method appears general enough to handle all cases. The purpose of this review is to present methods that are mostly used in the investigations of phase-change problems.

1.1.1 Similarity Transformation

Similarity transformation, also known as Boltzman transformation [3] is a method which reduces the heat diffusion equation to an ordinary differential equation by introducing a variable of the form

$$\mu = x/(\alpha t)^{1/2} \tag{1.1}$$

In the case of one-dimensional problems with isothermal boundary conditions, an exact closed form solution can be obtained for the melting of a semi-infinite domain as shown in Fig. 1.1.

The governing equations can be stated as

$$\frac{\partial T_l}{\partial t} + (1 - \rho_s/\rho_l)\frac{\partial \delta}{\partial t}\frac{\partial T_l}{\partial x} = \alpha_l \frac{\partial^2 T_l}{\partial x^2} \tag{1.2}$$

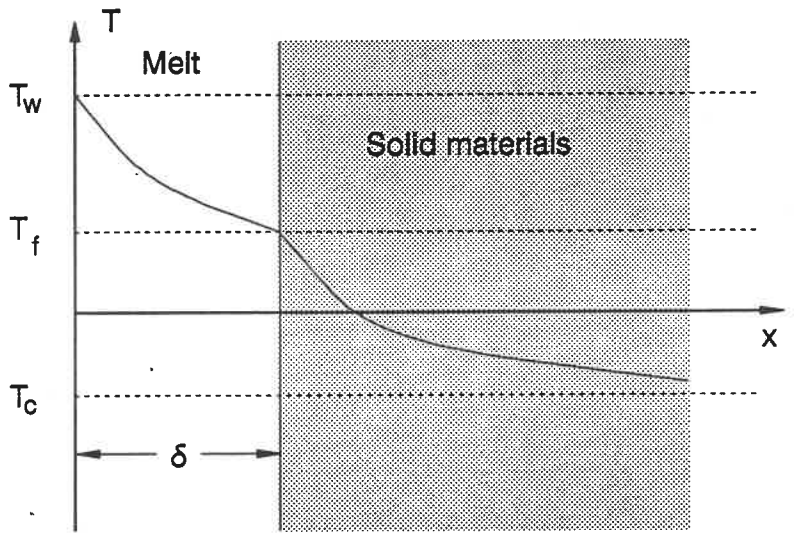

Figure 1.1: One-dimensional Stefan problem

$$\frac{\partial T_s}{\partial t} = \alpha_s \frac{\partial^2 T_s}{\partial x^2} \tag{1.3}$$

$$\rho_s h \frac{\partial \delta}{\partial t} = -\left[k_l \frac{\partial T_l}{\partial x} - k_s \frac{\partial T_s}{\partial x}\right]_{x=\delta} \tag{1.4}$$

Equation (1.4) is also known as the Stefan condition.

Introducing a scale factor, $\delta \frac{\partial \delta}{\partial t}/\alpha_l = 2\mu^2$, where μ is a constant to be determined and the similarity transform $\eta_l = x/\delta + \rho_s/\rho_l - 1$ and $\eta_s = x/\delta$, the governing equations (1.2)-(1.4) reduce to a coupled system of ordinary differential equations

$$\frac{d^2\theta_l}{d\eta_l^2} + 2\mu^2 \eta_l \frac{d\theta_l}{d\eta_l} = 0 \tag{1.5}$$

$$\frac{d^2\theta_s}{d\eta_s^2} + 2\mu^2\eta_s\lambda\frac{d\theta_s}{d\eta_s} = 0 \tag{1.6}$$

$$2\rho^*\mu^2 = -Ste\left[\frac{d\theta_l}{d\eta_l} - k^*\Delta\frac{d\theta_s}{d\eta_s}\right] \tag{1.7}$$

where

$$\theta_l = \frac{T_l - T_f}{T_w - T_f} \qquad \theta_s = \frac{T_s - T_i}{T_f - T_i} \quad \rho^* = \rho_s/\rho_l \quad k^* = k_s/k_l$$

$$Ste = \frac{C_l(T_w - T_f)}{h} \quad \Delta = \frac{T_f - T_i}{T_w - T_f} \quad \lambda = \alpha_l/\alpha_s \quad \varepsilon = \rho^* - 1$$

Eq. (1.5),(1.6) and (1.7) may be solved independently to obtain [4]

$$\theta_l = \frac{erf(\mu\rho^*) - erf(\mu\eta_l)}{erf(\mu\rho^*) - erf(\mu\varepsilon)} \tag{1.8}$$

$$\theta_s = \frac{erfc(\mu\lambda^{1/2}\eta_s)}{erfc(\mu\lambda^{1/2})} \tag{1.9}$$

$$\mu = \frac{Ste}{\sqrt{\pi}}\left\{\frac{e^{-\mu^2\rho^2}}{erf(\mu\rho^*) - erf(\mu\varepsilon)} - \frac{k^*\Delta\lambda^{1/2}e^{-\mu^2\lambda}}{erfc(\mu\lambda^{1/2})}\right\} \tag{1.10}$$

For given values of Ste, Δ, λ, ρ^* and k^*, μ can be determined, and the temperature distribution then becomes known. The interface position is given by

$$\delta(t) = 2\mu(\alpha_l t)^{1/2} \tag{1.11}$$

The above result indicates that the melt thickness $\delta(t)$ grows like $t^{1/2}$, which is a characteristic of one-dimensional conduction-dominated phase-change problems driven by isothermal boundary conditions.

An analytical solution for the one-dimensional freezing/melting of a saturated liquid in a semi-infinite geometry subjected to a constant heat flux was found by El-Gernk and Cronenberg[5]. The temperature distribution can be expressed as

$$T_s(x,t) = T_f + \frac{2q_c}{k_s}\sqrt{\alpha_s t}\left[ierfc\frac{\delta}{2\sqrt{\alpha_s t}} - ierfc\frac{x}{2\sqrt{\alpha_s t}}\right] \tag{1.12}$$

while the thickness of the melt can be obtained from the formula

$$\frac{d\delta}{dt} = \frac{q_c}{\rho_s L} erfc\left(\frac{\delta}{2\sqrt{\alpha_s t}}\right) \tag{1.13}$$

A general description of exact solutions for conduction dominated phase-change problem is presented in Table I.

Very few additional Stefan problems are known to have exact closed form solutions. The only known exact solutions obtained by similarity transformation are those for an unbounded domain, such as a semi-infinite slab [6] and some symmetric geometries, *e.g.* cylindrical and spherical systems [2], [3], [8] with constant thermal physical properties.

1.1.2 Power Series Expansions

For some boundary conditions, the similarity transformation is not useful. Power series expansions provide an alternative approach. Evans et al. [9] was probably

Item	Constant temperature		Constant heat flux	
	Freezing/melting	Similar transient heat	Freezing/melting	Similar transient heat
Governing equation	$\frac{\partial T_s}{\partial t} = \alpha_s \frac{\partial^2 T_s}{\partial x^2}$	the same	the same	the same
Boundary condition	$t_s(0,t) = t_o$ $t_s(\delta,t) = T_f$ $\frac{\partial T_s(\delta,t)}{\partial x} = \frac{\rho_s L}{k_s}\frac{d\delta}{dt}$	$t_s(0,t) = t_o$ $t_s(\infty,t) = T_\infty$ $\frac{\partial T_s(\infty,t)}{\partial x} = 0$	$k_s\frac{\partial T_s(0,t)}{\partial x} = q_c$ $T_s(\delta,t) = T_f$ $\frac{\partial T_s(\delta,t)}{\partial x} = \frac{\rho_s L}{k_s}\frac{d\delta}{dt}$	the same $T_s(\infty,t) = T_\infty$ $\frac{\partial T_s(\infty,t)}{\partial x} = 0$
Initial condition	$\delta(t=0) = 0$	$T_s(x,0) = T_\infty$	$\delta(t=0) = 0$	$T_s(x,0) = T_\infty$
General form of solution	$T_s(x,t) = C + Derf\frac{x}{2\sqrt{\alpha_s t}}$	the same	$T_s(x,t) = A + B(t)ierfc\frac{x}{2\sqrt{\alpha_s t}}$	the same
Complete solution	$T_s(x,t) = T + (T_f - T_o)\frac{erf\frac{x}{2\sqrt{\alpha_s t}}}{erf\frac{\delta}{2\sqrt{\alpha_s t}}}$ where $\delta(t) = 2\sqrt{\alpha_s t}$	$T_s(x,t) = T_o$ $+(T_\infty - T_o)erf\frac{x}{2\sqrt{\alpha_s t}}$	$T_s(x,t) = T_f + \frac{2q_c}{k_s}\sqrt{\alpha_s t}$ $\left(ierfc\frac{\delta}{2\sqrt{\alpha_s t}} - ierfc\frac{x}{2\sqrt{\alpha_s t}}\right)$	$T_s(x,t) = T_\infty - \frac{2q_c}{k_s}\sqrt{\alpha_s t}$ $\left(ierfc\frac{x}{2\sqrt{\alpha_s t}}\right)$

Table 1.1: Exact solutions for the conduction-dominated phase-change problem

the first to use power series expansions to deal with phase-change problems. They assumed a power series in time for the position of the phase-change front, $\delta(t)$, and double power series in time and space for the temperature distribution in the melt layer, that is

$$\theta = \sum_{i,j=0}^{\infty} a_{i,j} x^i t^j \tag{1.14}$$

$$\delta = \sum_{i=0}^{\infty} c_i t^i \tag{1.15}$$

These series can be substituted into Eq.(1.2)-(1.4) and the unknown coefficients can be determined. Evans *et al* [9] presented a series solution for melting with a variable flux. Tao [10], [11], [12], [13] obtained solutions for one-dimensional Stefan problems with an arbitrary initial condition and a convection boundary condition, by using three different types of polynomials of complementary error functions.

For a semi-infinite domain with constant heat flux or convection, the solutions for the position of the solid-liquid interface can be written as [4]

$$\delta(t)/(\alpha_l t/l) = Ste + O(Ste^2 t/(l^2 \alpha_l)) \tag{1.16}$$

From the previous results, one can see that the fundamental difference between one-dimension Stefan problems with isothermal boundary conditions and those with heat flux or convection boundary conditions lies in the growth rate of the melt thickness. For the isothermal boundary condition, the melt thickness increases as $t^{1/2}$, while for heat flux or convection boundary condition, it increases linearly with time.

Power series expansions can be of great use in the determination of short time solutions to the Stefan problem and can give very accurate solutions near the singularity. But for a large time scale, more terms are required, which entail very tedious mathematical manipulations, and the power series method then looses its attractiveness.

1.1.3 Integrodifferential Equations

The integrodifferential method reduces the Stefan problem to a system of integrodifferential equations. Mathematically, this method can also be regarded as a superposition method, in which the phase-change process may be divided into two distinct problems:

(a) The pure heat conduction without phase change;

(b) The moving source of heat at the interface, which replaces the latent heat generated by the phase change.

The superposition method is stated mathematically as

$$T(x,y,t) = P(x,y,t) + Q(x,y,t) \tag{1.17}$$

where $P(x,y,t)$ is the solution to the conduction problem without phase-change and $Q(x,y,t)$ is the solution to the "moving source problem".

By choosing an appropriate Green's function, which must satisfy the conduction equation with the Neumann boundary condition, $P(x,y,t)$ and $Q(x,y,t)$ are governed by coupled integrodifferential equations.

The Stefan problem can also be solved by Fourier and Laplace transformations. Over infinite intervals, Fourier transformation may reduce the Stefan problem to an initial-value problem. For finite intervals, the Laplace transformation leads to a boundary-value problem.

These transformations all lead to integrodifferential equations. The resulting integrals have to be evaluated by a numerical method.

1.1.4 Perturbation Method

Before presenting the perturbation method, two concepts, "quasi-steady" and "quasi-stationary" approximations, are worth discussing, as they are widely used in the analysis of phase-change problems.

In the quasi-steady approximation, the unsteady term in the conduction equation is neglected [1]. The unsteady behavior appears only in the Stefan condition. The gradient at the interface is determined by solving the steady state diffusion equation with the stationary interface. The solutions by Bankoff [3] and Rosner [14] were obtained using this approximation. In general, quasi-steady solutions are not capable of satisfying initial conditions.

In the quasi-stationary approximation, the unsteady term is retained in the conduction equation, which is solved by assuming the interface is stationary [15]. The quasi-stationary solution is capable of satisfying an initial temperature distribution. However, the solution is not valid for all times if the temperature ahead of the advancing interface is not uniform and is changing due to the interface motion.

In order to discuss these approaches, consider a general heat flow within the

solid phase governed by the unsteady, one-dimensional heat conduction equation. For constant thermal properties, the governing equations are [16]

$$\frac{\partial T}{\partial t} = \frac{\alpha}{R^n}\frac{\partial}{\partial R}\left(R^n \frac{\partial T}{\partial R}\right) \tag{1.18}$$

with $n = 0, 1, 2$ for plane, cylindrical and spherical geometries, respectively. An energy balance equation at the solid-liquid interface yields

$$\frac{dR}{dt} = \frac{k}{\rho L}\frac{\partial T}{\partial R}\bigg|_{R = R_f} \tag{1.19}$$

To simplify the description, let the boundary condition be isothermal, and introduce the dimensionless physical parameter $\epsilon = Ste$, and the dimensionless variables r, τ, r_f, θ for the appropriately scaled space, time, interface position, and temperature, respectively. Then, the governing equations can be expressed in the following dimensionless form

$$\epsilon\sigma\frac{\partial \theta}{\partial r} = \frac{1}{r^n}\frac{\partial}{\partial r}\left(r^n \frac{\partial \theta}{\partial r}\right) \tag{1.20}$$

$$\theta(r, r = r_f) = 1 \tag{1.21}$$

$$\theta(r_f, r = 1) = 0 \tag{1.22}$$

$$\sigma = \frac{\partial \theta}{\partial r}\bigg|_{r = r_f} \tag{1.23}$$

where σ is the speed of the melting front, *i.e.*

$$\sigma = \frac{dr_f}{d\tau} \tag{1.24}$$

Using regular perturbation methods, the asymptotic expansion of θ about $\epsilon \rightarrow 0$, yields the following perturbation series

$$\theta(r, r_f; \epsilon) = \sum_{i=0}^{\infty} \epsilon^{i/2} \theta_i(r, r_f) \tag{1.25}$$

$$\sigma(r; \epsilon) = \sum_{i=0}^{\infty} \epsilon^{i/2} \sigma_i(r_f) \tag{1.26}$$

Substituting Eqs. (1.25)-(1.26) into Eqs. (1.20)-(1.23) and equating coefficients of equal powers of ϵ yields

$$\frac{1}{r^n} \frac{\partial}{\partial r} \left(r^n \frac{\partial \theta_i}{\partial r} \right) = \begin{cases} 0 & for \quad i = 0 \\ \sum_{j=1}^{i} \sigma_{j-1} \frac{\partial \theta_{i-j}}{\partial r_f} & for \quad i \geq 1 \end{cases} \tag{1.27}$$

$$\theta_i(r_f, r = r_f) = \begin{cases} 1 \quad for \quad i = 0 \\ 0 \quad for \quad i \geq 1 \end{cases} \tag{1.28}$$

$$\theta_i(r_f, r = 1) = 0 \tag{1.29}$$

$$\sigma_i = \left. \frac{\partial \theta_i}{\partial \tau} \right|_{r = r_f} \tag{1.30}$$

The linear system of equations(1.27)-(1.30) has been solved by Jiji and Weinbaum [17] for the zero-order, the first-order and the second-order terms.

The asymptotic expansions (1.25)-(1.26) are the outer expansions. The procedure above is equivalent to a quasi-steady approximation, which, however, is only valid for the long-time scale. The outer expansion is singular as $\tau \rightarrow 0$.

Inner expansions based upon the short-time scale are

$$\hat{\theta}(r, r_f; \epsilon) = \sum_{i=0}^{\infty} \epsilon^{i/2} \hat{\theta}_i(r, r_f) \tag{1.31}$$

$$\hat{\sigma}(r; \epsilon) = \sum_{i=0}^{\infty} \epsilon^{i/2} \hat{\sigma}_i(r_f) \tag{1.32}$$

A similar procedure can be performed to find the inner solutions, which is equivalent to the quasi-stationary approximation and valid only in the short-time scale.

It is possible to construct a series solution in the perturbation parameter ϵ which is uniformly valid for all times by using the matched asymptotic expansion method [17]. Most perturbation solutions published in the literature [15], [16] [18], [19] are up to the second order. For higher order terms, the perturbation method becomes increasingly difficult, if not intractable.

1.1.5 Coordinate Transformation

One of the main difficulties in dealing with phase-change problems is that both the liquid and solid regions vary with time and their interface is not know *a priori*. Coordinate transformations allow the moving-boundary problem to be transformed into a fixed-boundary problem. There are a number of ways of performing this transformation. For the one-dimensional conduction-dominated phase-change problem, the transformation consists simply of a coordinate stretching

A general form of stretching of the spatial coordinate may be written as

$$\eta = \frac{x - R}{\delta(t) - R} + A \tag{1.33}$$

where $\delta(t)$ is the interface position, R a reference boundary, and A the distance over which the coordinate origin is to be translated. Either R or A can be a constant or function of time.

By using η instead of x in the governing equations, the moving-boundary problem becomes a "fixed" boundary problem. While the coordinate transformation does not solve the phase-change problem by itself, it does make the moving boundary problem more tractable. After the transformation, the boundaries become "fixed" and many procedures, exact or approximate, may be used to obtain the solutions.

In fact, the transformation (1.33) is not exclusive. Many alternatives exist. With $A = 0$, the transformation is the well-known the Landau transformation [20]. In recent years, the coordinate transformation method became very popular not only in conduction dominate phase-change problems but also in convection dominated phase-change problems [21], [22], [23], [24]. This transformation method can be extended from one-dimension to two-dimension, and will be discussed in Chapter 3.

1.1.6 Other Methods

There are a number of additional methods for phase-change problems. The enthalpy method is often used in solving both conduction dominated and convection dominated problems [25], [26] and [27]. The complex variable method can also "transfer" a moving boundary problem into a "fixed" problem by conformal map-

ping [28], [29]. For certain classes of problems, the isotherm migration method [30], as well as the boundary element or boundary integral methods [31], [32], *etc.*, can be of interest.

1.2 Convection-Dominated Phase-Change Problems

Oddly enough, the importance of natural convection in the phase-change process has been recognized only in recent years. The first theoretical results concerned with natural convection were presented by Tien and Yen [33]. They studied a melting problem with heating from below. The numerical solutions showed that convection significantly enhanced the melting rate. They also found that the critical Rayleigh number for the onset of natural convection in the melt layer is 1720. Boger and Westwater [34] investigated the same the problem experimentally. The agreement between the experimental and numerical results [33] was fairly good. By studying large Rayleigh number flows, they also found that natural convection can significantly enhance melting or retard freezing.

Another early work on natural convection effects was done by Hale and Viskanta [35]. Both experimental and analytical results were presented for melting with heating from below and for freezing with cooling from above. By assuming one-dimensional heat transfer and considering natural convection effects by placing a convection term into the Stefan condition, they found that natural convection is of great importance. The melting rate was found to increase almost linearly with time.

All the above investigations have shown that the results obtained for conduction dominated phase-change problems are not valid in the presence of natural

convection.

Literature on natural convection effects in phase-change problem is generally focused on three geometries: the rectangular cavity, horizontal and vertical cylinders.

1.2.1 Phase-Change in Rectangular Geometries

An experimental investigation of melting within a rectangular enclosure was performed by Hale and Viskanta [36]. They presented the photographs of the melting front and heat transfer rate, showing that conduction plays an important role only at early times, and natural convection dominates thereafter. As a consequence, the melting progresses near the top of the heated wall faster than near the bottom. They found that the temperature at a small distance from the heated wall rises rapidly from an initial temperature close to the melting point and then reaches a maximum, followed by a slow decrease and then approaches a steady value in contrast with the pure conduction model, which predicts a monotonic increase of temperature with time. The results show that the heat transfer coefficient increases along the heated plate. The highest is at the top of the test cell where the natural convection is the strongest. The variation of the heat transfer coefficient with time shows that a minimum exists due to the natural convection in the melt region.

Okada [37] studied experimentally and numerically a melting in a vertical cavity with adiabatic upper and lower surfaces. He used the coordinate transformation technique to immobilize the solid-liquid interface and made a quasi-steady assumption in the simulation. The numerical solution shows a good agreement with the experimental data. He found that after the early stage natural convec-

tion dominates in the melt region. As the melting progresses, the average Nusselt number on the vertical wall varies linearly with the dimensionless time. He therefore concluded that the thermal energy stored as latent heat varies about linearly with dimensionless time. A simple relationship between thermal energy storage and Rayleigh number was proposed. He studied the effect of Prandtl number in the melting process and found that the melting rate is unaffected by Pr as long as $Pr \geq 7$.

Gadgil and Gobin [38] analysed melting in a rectangular enclosure by a numerical method. They decoupled the calculation of the melting front motion and the calculation of the natural convective flow in the melt region by dividing the process in a number quasi-static steps. To start the computation, they assumed a quasi-static step melt representing 5% in volume of the phase-change material. The predicted melting front were compared with the experimental data [35]. The predicted speed of propagation of the melting front is 37% larger than that observed experimentally. The agreement is quite good when based on the fraction of the melt rather than on the time elapsed. Two kinds of boundary conditions from full slip to no-slip on the top of the rectangle were simulated. No significant difference of the melting propagation was found, though the horizontal velocity profile near the top does change as expected. The variation of heat transfer rate with the time elapsed shows that at the beginning the Nusselt number rapidly decreases. As convection becomes fully developed, the Nusselt number increases slightly. The molten fraction varies linearly with time.

Webb and Viskanta [40] studied the melting process of gallium. They employed algebraic stretching functions to map the irregular domain into a non-orthogonal curvilinear grid. The numerical solutions were compared with their experimental data. The theoretical solutions overpredicted the experimental re-

sults. They explained the discrepancy by noting that for highly conductive materials, heat conduction in the solid cannot be neglected; and by pointing out that the experiment had not clearly controlled the steady-state temperature. The molten fraction was again almost linear with time after the conduction dominated regime.

Solidification within a rectangular enclosure with convection and radiation boundary conditions at the surface of the mold and at the top of the enclosure was analyzed by Ramachandran *et al* [41]. Equations governing the temperature and velocity fields in the melt and the temperature fields in the solid and in the mold were established. The Landau transformation was employed. The effect of radiation and convection at the surface was examined by determining the interface movement for different radiation constants and Biot numbers. They found that the heat transferred at the interface and the interface shape differ markedly from the solution obtained by neglecting natural convection. They also studied the effects on solidification of Rayleigh number, Prandtl number, Stefan number and superheat [42]. Their results show that the low Rayleigh numbers ($Ra = 5 \times 10^2$) can significantly influence the solidification. The Prandtl number influences the interface movement only up to $Pr = 10$. After this point, an asymptotic solution is reached.

Benard *et al* [43] investigated melting in a rectangular enclosure, driven by the coupling of heat conduction in the solid phase and natural convection in the melt. Both numerical and experimental studies were performed. The test cell was heated from one side and cooled from the other. The results showed that heat conduction in the solid phase significantly modified the kinetics of the melting process compared with the case of phase change with an isothermal solid phase, since the heat extraction from the cold wall greatly influences the evolution of the

interface shape and position. As the melt thickness becomes larger, temperature gradients in the melt decrease while temperature gradients in the solid phase increase with time, as the thickness of the solid decreases. Finally, a balance of temperature gradients in the solid and in the melt is established. Therefore, the interface reaches a stationary position and the heat transfer rate becomes constant.

1.2.2 Summary

Studies in melting of rectangular geometries taking into account the natural convection have shown that:

1. Convection significantly increases the melting velocity and heat transfer rate.

2. The heat transfer rate evolves with time as follow: at the beginning of the melting, the heat transfer rate decreases sharply in conduction-dominated regime. As the melt region becomes thicker, natural convection begins to increase the heat transfer rate. When the melt region becomes large enough to allow boundary layers to develop, the heat transfer rate decreases gradually.

3. The molten fraction varies linearly with time except at the very beginning of the melting, that is when conduction dominates.

4. For materials with a high thermal conductivity, the heat conduction in the solid phase may not be neglected. In other words, the saturated temperature assumption may not be valid for the high thermal conductivity materials in the phase-change problem.

5. There exists a limit on the Prandtl number beyond which it does not have any influence on the melting process.

1.2.3 Phase-Change around/in Horizontal Cylinders

Bathelt *et al* [44] investigated melting around an electrically heated horizontal cylinder embedded in paraffin. The photographs showed that at early times, heat transfer in the melt region is dominated by conduction, the molten region is symmetrical about the axis of the cylinder. At the same time a plume start to develop at the top of the cylinder where the local heat transfer rate reaches a maximum. Below the cylinder, the local heat transfer rate is minimum. The average Nusselt number decreases with time when heat transfer is done by conduction; at large times the Nusselt number reaches a constant value even though the liquid-solid interface continues to move as melting progresses. This behavior is characteristic of natural convection heat transfer.

By using a coordinate transformation to immobilize the moving boundary, Prusa and Yao studied melting around a horizontal cylinder with an isothermal boundary [45] and a constant heat flux boundary condition [46]. Using both numerical and perturbation methods, they determined that the melting process could be divided into three stages:

1. Conduction stage: at early time of the melting, heat transfer is dominated by conduction. The melt region appears annular, and all characteristics of the melting process are dominated by Stefan number.

2. Transition stage: as time advances, natural convection becomes more important, and the effects of conduction and convection are comparable.

3. Convection stage: natural convection is the dominant mode of heat transfer. Although natural convection dominates conduction, the average heat transfer does not increase as natural convection develops.

A numerical solution for melting around a horizontal heated cylinder was also obtained by Rieger *et al* [47]. They employed a stream function-vorticity formulation to model the fluid flow in the melt. The resulting governing equations were transformed onto a rectangular domain by using the method of body-fitted coordinates. Thus, the computations of the moving boundary problem could be performed on a fixed domain. They found that the natural coordinates tend to cluster in certain areas. To overcome this difficulty, they employed implicit rezoning procedure to generate more uniform coordinates at each time step. The numerical solutions show that the melting front has a pear-like profile. Besides the three stages mentioned by Prusa and Yao [45], they pointed out the existence of a flow regime in which heat transfer is governed mainly by boundary layers.

The melting process inside a horizontal cylinder was studied by Rieger *et al* [48]. Both experimental and numerical melting profiles were presented. The melt contours reveal that heat transfer is greatly enhanced due to natural convection in the upper part of the annulus where the propagation of the melt is accelerated. The inverse effect occurs in the lower part of the melt region. The cold fluid flowing down along the solid-liquid interface inhibits heat transport. These counteracting transport mechanisms lead to an almost total stop of the melting process at the bottom. The variations of Nusselt number are qualitatively the same as for the melt process around a cylinder except for high Rayleigh numbers. For a Rayleigh number $Ra = 10^6$, the Nusselt number first decreases, to reach a minimum as before, and then increases. After reaching a maximum,

it decreases again. They found that for Rayleigh numbers $Ra \geq 10^6$, secondary vortices occur at the bottom, where three dimensional unsteady rolls induced by thermal instability developed. In this region, Bénard convection was observed. Ho and Viskanta [49] also studied melting inside a horizontal cylinder using experimental and numerical methods. They also observed the secondary vortices in the bottom of the melt region for high Rayleigh numbers.

Ho and Chen [50] studied outward melting of ice around a isothermal horizontal cylinder, taking into account the effect of the density inversion of water. The governing equations were modeled by the stream function-vorticity formulation. The numerical solutions were obtained by finite difference method with grid transformation. Due to the density anomaly of water, the melting process is more complex than that of a normal phase change material. When the heated boundary temperature $T_w = 4°C$, the water near the cylinder is of higher density than that near the ice interface, thus the water near the surface of the cylinder moves downward while the water near the ice interface moves upward, in contrast to the behavior of a normal fluid. As consequence, the melting profiles has an upright pear-like shape *i.e.* in opposition to the case of a normal fluid. For the surface temperature $T_w = 8°C$, the densities of water at the cylinder surface and at the ice interface are approximately the same. The maximum density line of water is located somewhere in the melt, resulting in two counter-rotating flows in the melt region. As a result, the melting process is retarded. For the surface temperature $T_w = 10°C$, the melting profile has a pear-like shape as in the case of a normal fluid and exhibits the counter-circulation in the melt region. The average heat transfer coefficient reaches a maximum value when the surface temperature $T_w = 4°C$, and a minimum value around $T_w = 9°C$, instead of $T_w = 8°C$ as postulated by Herrmann *et al* [51].

1.2.4 Summary

Studies of the phase-change process around/in a horizontal cylinder show that natural convection can play an important role in the following aspects:

1. There exists a counteracting heat transfer mechanism which leads to an almost total stop of the melting process at the bottom for the normal fluid. As a consequence, the melting profiles appear pear-like shaped.

2. Density inversion could significantly influence the melting profiles. Depending on the boundary temperature, the melting profiles may appear in pear-like shape or upside down pear-like shape.

3. There exists a minimum heat transfer rate for density inversion phase-change materials.

4. For very high Rayleigh numbers, three-dimensional convection may occur at the bottom of horizontal cylinders.

1.2.5 Phase-Change around/in Vertical Cylinders

Sparrow *et al* [52] studied numerically the melting around a vertical cylinder embedded in the phase-change material. To deal with the irregularity of the melting domain, they employed the Landau transformation. Based on the assumption that the interface radius varies slowly with height, they dropped all the terms involving the first order and the second order derivatives of the radius with respect to the height. As a matter of fact, this assumption is invalid for high Rayleigh number as the slope of the melting profiles at the top of the melt region is not negligible. The discrepancy has been discussed in [53].

Sparrow *et al* considered moderate Rayleigh numbers from 7×10^4 to 7×10^6. The characteristics of heat transfer are similar to those in rectangular geometries. Again, it was found that the Prandtl number does not influence the melting rate when $Pr \geq 7$.

The experimental studies on the melting process in a vertical cylindrical enclosure have been carried out by Bareiss and Beer [54], [55]. Several kinds of phase-change materials were used in the experiments. They proposed a correlation for heat transfer rate as $Nu_z = f(Ra_z, Fo, Ste, z/H)$.

Kemink and Sparrow [56] studied melting about a vertical cylinder with or without subcooling and for open or closed cavities. The results showed that the heat transfer coefficients are not affected by whether the upper surface of the cylinder is closed by a cover which imposes a no-slip velocity boundary condition or is bounded by an insulated air space which imposes a full slip velocity boundary condition. This result was found applicable to both melting of a subcooled or a non-subcooled phase-change materials. In the case of subcooling, they found that subcooling tends to delay the onset of the convection-dominated regime and the heat transfer coefficients in the presence of subcooling are $10\% - 15\%$ lower than those for the non-subcooled case. For sufficiently large times, after the onset of convection, the heat transfer coefficients were found to become time-independent. The correlation between the Nusselt number and Rayleigh number was established. They also found that the functional dependence of the steady-state Nusselt numbers in the absence of subcooling agrees well with the literature for natural convection in vertical parallel-walled enclosures without melting.

The experimental studies mentioned above were obtained at very large Rayleigh numbers, typically in the range of $10^8 - 10^{10}$. In many applications, however,

moderate Rayleigh numbers are quite important. Unfortunately, less attention has been paid to these studies.

As the literature review reveals, the problems of phase-change in rectangular and horizontal cylinder geometries have received considerable attention. For melting in vertical cylinder however, only a few studies have been performed, in which the many features that make the problem interesting have been neglected, for example, melting by heating from the bottom of the cylinder, the effect of density inversion in the melting process, and melting of subcooled materials. Also the intermediate range of Rayleigh numbers still needs further investigation.

1.3 Scope of Thesis

This thesis is devoted to the numerical simulation of the melting process in a vertical cylindrical enclosure. One of the motivations for this research lies in the belief that a fundamental comprehensive study of phase-change process will eventually lead to better engineering design and industrial production.

In order to facilitate the reading of the rest of this thesis, we present here a brief description of the contents of the following chapters.

In Chapter 2, the general mathematical modelling of the phase-change problem is formulated. Chapter 3 describes the coordinate transformation used for the subsequent numerical solutions. Chapter 4 treats the problem of melting of a laterally heated cylinder, with adiabatic conditions at the top and bottom. Both outward and inward melting are studied. Melting by heating from the bottom of a vertical cylinder is the subject of Chapter 5. In Chapter 6 we study the melting within a cylinder subject to a constant temperature at all boundaries. Chapter 7

is devoted to the problem of melting in the presence of a density inversion. The conclusion and recommendation for the further research are presented in Chapter 8.

Chapter 2

MATHEMATICAL MODELLING OF PHASE CHANGE PROBLEMS

This chapter is devoted to the mathematical modelling of the phase-change problem, including fluid flow and heat transfer in the liquid region and conduction in the solid to be melted. Several formulations will be presented for phase-change problems in Cartesian coordinates, in curvilinear coordinates and in cylindrical coordinates.

Basically, the mathematical description consists of a set of partial differential equations, *i.e.* the equation of conservation of mass, momentum and energy, and the interface energy equation. The most common formulation of these equations is written in the Cartesian coordinates.

In phase-change problems, we have to deal with moving boundaries as well as with irregular domains for both liquid and solid domains. The Cartesian formulation is therefore unsuitable and more general formulations are required. These formulations can be derived from their Cartesian counterpart. To solve the equations by the finite difference method, a curvilinear grid system has to be established, which is the subject of the next chapter.

In curvilinear coordinates, the most common system is the cylindrical coordinates. As we are concerned with the phase-change problem in a vertical cylindrical

enclosure, a general formulation describing the phase-change process in the cylindrical coordinates will be presented and thereafter, the governing equations for our study will be cast.

2.1 General Formulation for Phase-Change Problems

The melting/freezing processes are usually considered in two separate regions: (a) The melt liquid region, where the fluid flow and heat transfer are coupled. (b) The solid region to be melted, where the mechanism of heat transfer is just heat conduction. The interaction between the two regions is described by an interface equation.

For compactness of the following development, we define primitive variables as a vector

$$\mathbf{q} = [u, v, w, p, T_i]^T \tag{2.1}$$

Where u, v and w are velocities components in x, y and z directions respectively; p is the pressure, and T_i is the temperature. The subscript i denotes the temperature in the liquid or solid, depending on whether $i = l$ or s. With these notations, a general mathematical model in both the liquid and solid regions can be expressed in the Cartesian coordinates as

$$\frac{\partial \mathbf{U(q)}}{\partial t} + \frac{\partial \mathbf{A(q)}}{\partial x} + \frac{\partial \mathbf{B(q)}}{\partial y} + \frac{\partial \mathbf{C(q)}}{\partial z} = \frac{\partial \mathbf{D(q)}}{\partial x} + \frac{\partial \mathbf{E(q)}}{\partial y} + \frac{\partial \mathbf{F(q)}}{\partial z} + \mathbf{G} \tag{2.2}$$

where $\mathbf{U(q)}$, $\mathbf{A(q)}$, $\mathbf{B(q)}$, $\mathbf{C(q)}$, $\mathbf{D(q)}$, $\mathbf{E(q)}$, $\mathbf{F(q)}$ and $\mathbf{G}$ are five-component

vectors:

$$\mathbf{U} = \begin{bmatrix} \rho \\ \rho u \\ \rho v \\ \rho w \\ \rho c_p T_i \end{bmatrix} \quad \mathbf{A} = \begin{bmatrix} \rho u \\ p + \rho u^2 \\ \rho uv \\ \rho uw \\ \rho c_p u T_i \end{bmatrix} \quad \mathbf{B} = \begin{bmatrix} \rho v \\ \rho uv \\ p + \rho v^2 \\ \rho vw \\ \rho c_p v T_i \end{bmatrix} \quad \mathbf{C} = \begin{bmatrix} \rho w \\ \rho uw \\ \rho vw \\ p + \rho w^2 \\ \rho c_p w T_i \end{bmatrix}$$

$$\mathbf{D} = \begin{bmatrix} 0 \\ 2\mu \dfrac{\partial u}{\partial x} \\ \mu(\dfrac{\partial v}{\partial x} + \dfrac{\partial u}{\partial y}) \\ \mu(\dfrac{\partial w}{\partial x} + \dfrac{\partial u}{\partial y}) \\ k_i \dfrac{\partial T_i}{\partial x} \end{bmatrix} \quad \mathbf{E} = \begin{bmatrix} 0 \\ \mu(\dfrac{\partial u}{\partial y} + \dfrac{\partial v}{\partial x}) \\ 2\mu \dfrac{\partial v}{\partial y} \\ \mu(\dfrac{\partial w}{\partial y} + \dfrac{\partial v}{\partial z}) \\ k_i \dfrac{\partial T_i}{\partial y} \end{bmatrix} \quad \mathbf{F} = \begin{bmatrix} 0 \\ \mu(\dfrac{\partial u}{\partial z} + \dfrac{\partial w}{\partial x}) \\ \mu(\dfrac{\partial v}{\partial z} + \dfrac{\partial w}{\partial y}) \\ 2\mu \dfrac{\partial w}{\partial z} \\ k_i \dfrac{\partial T_i}{\partial z} \end{bmatrix} \quad \mathbf{G} = \begin{bmatrix} 0 \\ \rho g_x \\ \rho g_y \\ \rho g_z \\ 0 \end{bmatrix}$$

where the first component is the continuity equation; the second, third and fourth components are the momentum equations in x, y and z direction respectively; the last one is the energy equation in the liquid or solid region, depending on the subscript $i = l$ or s.

The interface equation can be developed by considering the local interface energy balance

$$\rho h \dot{v} = -(k_l \frac{\partial T_l}{\partial n} - k_s \frac{\partial T_s}{\partial n}) \cdot \mathbf{n} \tag{2.3}$$

where $\dot{v}$ is the local velocity of the moving interface pointing in the solid phase, $\mathbf{n}$ is a normal vector to the interface, and h is the latent heat.

Equations (2.2), (2.3) and the appropriate boundary conditions constitute the complete mathematical description of the problem under consideration.

2.2 General Formulation in Curvilinear Coordinates

In the analysis of phase-change problem, the main difficulty is due to the moving boundary and irregular domain. Since once the melting/freezing begins, the geometry of the domain becomes unknown. In the past, conduction was considered as the sole mechanism in the melting/freezing process, the melting/freezing front could be uniform along the boundary. In presence of natural convection, however, the interface motion is nonuniform, depending on the strength of the convection; the stronger the natural convection, the faster the interface moves. Therefore, the solid-liquid interface could become curved and the corresponding domains become irregular. As a consequence, the mathematical formulation will be best written in a curvilinear system.

2.2.1 Theory of the Transformation

The general transformation from the physical plane $[x, y, z]$ to the transformed plane $[\xi, \eta, \zeta]$ is given by the vector-valued function

$$\begin{bmatrix} \xi \\ \eta \\ \zeta \end{bmatrix} = \begin{bmatrix} \xi(x,y,z) \\ \eta(x,y,z) \\ \zeta(x,y,z) \end{bmatrix} \tag{2.4}$$

The inverse function or transformation of (2.4) is

$$\begin{bmatrix} x \\ y \\ z \end{bmatrix} = \begin{bmatrix} x(\xi,\eta,\zeta) \\ y(\xi,\eta,\zeta) \\ z(\xi,\eta,\zeta) \end{bmatrix} \tag{2.5}$$

To find the transformation relations, the following equations will be used

$$\begin{bmatrix} dx \\ dy \\ dz \end{bmatrix} = \begin{bmatrix} x_\xi & x_\eta & x_\zeta \\ y_\xi & y_\eta & y_\zeta \\ z_\xi & z_\eta & z_\zeta \end{bmatrix} \begin{bmatrix} d\xi \\ d\eta \\ d\zeta \end{bmatrix} \tag{2.6}$$

and

$$\begin{bmatrix} d\xi \\ d\eta \\ d\zeta \end{bmatrix} = \begin{bmatrix} \xi_x & \xi_y & \xi_z \\ \eta_x & \eta_y & \eta_z \\ \zeta_x & \zeta_y & \zeta_z \end{bmatrix} \begin{bmatrix} dx \\ dy \\ dz \end{bmatrix} \tag{2.7}$$

From the above equations one can obtain

$$\begin{bmatrix} \xi_x & \xi_y & \xi_z \\ \eta_x & \eta_y & \eta_z \\ \zeta_x & \zeta_y & \zeta_z \end{bmatrix} = \frac{1}{J} \begin{bmatrix} \begin{vmatrix} y_\eta & y_\zeta \\ z_\eta & z_\zeta \end{vmatrix} & - \begin{vmatrix} x_\eta & x_\zeta \\ z_\eta & z_\zeta \end{vmatrix} & \begin{vmatrix} x_\eta & x_\zeta \\ y_\eta & y_\zeta \end{vmatrix} \\ - \begin{vmatrix} y_\xi & y_\zeta \\ z_\xi & z_\zeta \end{vmatrix} & \begin{vmatrix} x_\xi & x_\zeta \\ z_\xi & z_\zeta \end{vmatrix} & - \begin{vmatrix} x_\xi & x_\zeta \\ y_\xi & y_\zeta \end{vmatrix} \\ \begin{vmatrix} y_\xi & y_\eta \\ z_\xi & z_\eta \end{vmatrix} & - \begin{vmatrix} x_\xi & x_\eta \\ z_\xi & z_\eta \end{vmatrix} & \begin{vmatrix} x_\xi & x_\eta \\ y_\xi & y_\eta \end{vmatrix} \end{bmatrix} \tag{2.8}$$

where J is the Jacobian determinant

$$
\begin{aligned}
J &= \begin{vmatrix} x_\xi & x_\eta & x_\zeta \\ y_\xi & y_\eta & y_\zeta \\ z_\xi & z_\eta & z_\zeta \end{vmatrix} \\
&= x_\xi y_\eta z_\zeta + x_\eta y_\zeta z_\xi + x_\zeta y_\xi z_\eta - x_\xi y_\zeta z_\eta - x_\eta y_\xi z_\zeta - x_\zeta y_\eta z_\xi
\end{aligned} \tag{2.9}
$$

With the above relations, all the partial derivatives in the Cartesian coordinates can be transformed into any curvilinear system $[\xi, \eta, \zeta]$. For example

$$
\begin{aligned}
f_x &= \frac{\partial(f,y,z)}{\partial(\xi,\eta,\zeta)} \Big/ \frac{\partial(x,y,z)}{\partial(\xi,\eta,\zeta)} \\
&= \frac{1}{J} \begin{vmatrix} f_\xi & f_\eta & f_\zeta \\ y_\xi & y_\eta & y_\zeta \\ z_\xi & z_\eta & z_\zeta \end{vmatrix} \\
&= f_\xi \frac{\begin{vmatrix} y_\eta & y_\zeta \\ z_\eta & z_\zeta \end{vmatrix}}{J} + f_\eta \frac{-\begin{vmatrix} y_\xi & y_\zeta \\ z_\xi & z_\zeta \end{vmatrix}}{J} + f_\zeta \frac{\begin{vmatrix} y_\xi & y_\eta \\ z_\xi & z_\eta \end{vmatrix}}{J} \\
&= \xi_x f_\xi + \eta_x f_\eta + \zeta_x f_\zeta
\end{aligned} \tag{2.10}
$$

Other derivatives can be transformed in a similar way to obtain

$$
\begin{bmatrix} f_x \\ f_y \\ f_z \end{bmatrix} = \begin{bmatrix} \xi_x & \eta_x & \zeta_x \\ \xi_y & \eta_y & \zeta_y \\ \xi_z & \eta_z & \zeta_z \end{bmatrix} \begin{bmatrix} f_\xi \\ f_\eta \\ f_\zeta \end{bmatrix} \tag{2.11}
$$

The time derivative can be transformed as

$$
\left(\frac{\partial f}{\partial t}\right)_{x,y,z} = \frac{\partial(x,y,z,f)}{\partial(\xi,\eta,\zeta,t)} \Big/ \frac{\partial(x,y,z,t)}{\partial(\xi,\eta,\zeta,t)} \tag{2.12}
$$

$$
\begin{aligned}
&= \frac{1}{J}\begin{vmatrix} x_\xi & x_\eta & x_\zeta & x_t \\ y_\xi & y_\eta & y_\zeta & y_t \\ z_\xi & z_\eta & z_\zeta & z_t \\ f_\xi & f_\eta & f_\zeta & f_t \end{vmatrix} \\
&= f_t\frac{1}{J}\begin{vmatrix} x_\xi & x_\eta & x_\zeta \\ y_\xi & y_\eta & y_\zeta \\ z_\xi & z_\eta & z_\zeta \end{vmatrix} \\
&\quad -f_\xi\frac{1}{J}\begin{vmatrix} x_\eta & x_\zeta & x_t \\ y_\eta & y_\zeta & y_t \\ z_\eta & z_\zeta & z_t \end{vmatrix} + f_\eta\frac{1}{J}\begin{vmatrix} x_\xi & x_\zeta & x_t \\ y_\xi & y_\zeta & y_t \\ z_\xi & z_\zeta & z_t \end{vmatrix} - f_\zeta\frac{1}{J}\begin{vmatrix} x_\xi & x_\eta & x_t \\ y_\xi & y_\eta & y_t \\ z_\xi & z_\eta & z_t \end{vmatrix} \\
&= \left(\frac{\partial f}{\partial t}\right)_{\xi,\eta,\zeta} \\
&\quad -f_\xi\left(x_t\frac{\begin{vmatrix} y_\eta & y_\zeta \\ z_\eta & z_\zeta \end{vmatrix}}{J} - y_t\frac{\begin{vmatrix} x_\eta & x_\zeta \\ z_\eta & z_\zeta \end{vmatrix}}{J} + z_t\frac{\begin{vmatrix} x_\eta & x_\zeta \\ y_\eta & y_\zeta \end{vmatrix}}{J}\right) \\
&\quad +f_\eta\left(x_t\frac{\begin{vmatrix} y_\xi & y_\zeta \\ z_\xi & z_\zeta \end{vmatrix}}{J} - y_t\frac{\begin{vmatrix} x_\xi & x_\zeta \\ z_\xi & z_\zeta \end{vmatrix}}{J} + z_t\frac{\begin{vmatrix} x_\xi & x_\zeta \\ y_\xi & y_\zeta \end{vmatrix}}{J}\right) \\
&\quad -f_\zeta\left(x_t\frac{\begin{vmatrix} y_\xi & y_\eta \\ z_\xi & z_\eta \end{vmatrix}}{J} - y_t\frac{\begin{vmatrix} x_\xi & x_\eta \\ z_\xi & z_\eta \end{vmatrix}}{J} + z_t\frac{\begin{vmatrix} x_\xi & x_\eta \\ y_\xi & y_\eta \end{vmatrix}}{J}\right) \\
&= \left(\frac{\partial f}{\partial t}\right)_{\xi,\eta,\zeta} + \xi_t f_\xi + \eta_t f_\eta + \zeta_t f_\zeta
\end{aligned}
$$

where

$$\begin{bmatrix} \xi_t \\ \eta_t \\ \zeta_t \end{bmatrix} = - \begin{bmatrix} \xi_x & \xi_y & \xi_z \\ \eta_x & \eta_y & \eta_z \\ \zeta_x & \zeta_y & \zeta_z \end{bmatrix} \begin{bmatrix} x_t \\ y_t \\ z_t \end{bmatrix} \tag{2.13}$$

with x_t, y_t and z_t being the grid point velocities.

In view of the above transformations, one can find that the time dependent variables in the Cartesian coordinates can not be just transformed in the time coordinate (if we use 4-D space). The grid point velocities are associated with the transformation. For a static grid system, $x_t = y_t = z_t = 0$. Therefore, $\xi_t = \eta_t = \zeta_t = 0$, the transformation then reduces to

$$\left(\frac{\partial f}{\partial t}\right)\Big|_{x,y,z} = \left(\frac{\partial f}{\partial t}\right)\Big|_{\xi,\eta,\zeta} \tag{2.14}$$

To summarize all the relations above, we can write a transformation matrix as

$$\begin{bmatrix} f_t \\ f_x \\ f_y \\ f_z \end{bmatrix} = \begin{bmatrix} 1 & \xi_t & \eta_t & \zeta_t \\ 0 & \xi_x & \eta_x & \zeta_x \\ 0 & \xi_y & \eta_y & \zeta_y \\ 0 & \xi_z & \eta_z & \zeta_z \end{bmatrix} \begin{bmatrix} f_\tau \\ f_\xi \\ f_\eta \\ f_\zeta \end{bmatrix} \tag{2.15}$$

2.2.2 General Formulation in Curvilinear Coordinates

With the transformations developed in the previous section, the general formula for the phase-change problem in curvilinear coordinates can be recast as

$$\frac{\partial \mathbf{U}'}{\partial t} + \frac{\partial \mathbf{A}'}{\partial \xi} + \frac{\partial \mathbf{B}'}{\partial \eta} + \frac{\partial \mathbf{C}'}{\partial \zeta} = \frac{\partial \mathbf{D}'}{\partial \xi} + \frac{\partial \mathbf{E}'}{\partial \eta} + \frac{\partial \mathbf{F}'}{\partial \zeta} + \mathbf{S}(\xi, \eta, \zeta) \tag{2.16}$$

where

$$\mathbf{U}' = \begin{bmatrix} \rho \\ \rho u \\ \rho v \\ \rho w \\ \rho c_p T_i \end{bmatrix} \quad \mathbf{A}' = \begin{bmatrix} \rho\tilde{U} \\ \rho u\tilde{U} + \xi_x p \\ \rho v\tilde{U} + \xi_y p \\ \rho w\tilde{U} + \xi_z p \\ \rho c_p \tilde{U} T_i \end{bmatrix} \quad \mathbf{B}' = \begin{bmatrix} \rho\tilde{V} \\ \rho u\tilde{V} + \eta_x p \\ \rho v\tilde{V} + \eta_y p \\ \rho w\tilde{V} + \eta_z p \\ \rho c_p \tilde{V} T_i \end{bmatrix} \quad \mathbf{C}' = \begin{bmatrix} \rho\widetilde{W} \\ \rho u\widetilde{W} + \zeta_x p \\ \rho v\widetilde{W} + \zeta_y p \\ \rho w\widetilde{W} + \zeta_z p \\ \rho c_p \widetilde{W} T_i \end{bmatrix}$$

$$\mathbf{D}' = \begin{bmatrix} 0 \\ \mu(g^{11}\frac{\partial u}{\partial \xi} + g^{12}\frac{\partial u}{\partial \eta} + g^{13}\frac{\partial u}{\partial \zeta}) \\ \mu(g^{11}\frac{\partial v}{\partial \xi} + g^{12}\frac{\partial v}{\partial \eta} + g^{13}\frac{\partial v}{\partial \zeta}) \\ \mu(g^{11}\frac{\partial w}{\partial \xi} + g^{12}\frac{\partial w}{\partial \eta} + g^{13}\frac{\partial w}{\partial \zeta}) \\ \mu(g^{11}\frac{\partial T_i}{\partial \xi} + g^{12}\frac{\partial T_i}{\partial \eta} + g^{13}\frac{\partial T_i}{\partial \zeta}) \end{bmatrix}$$

$$\mathbf{E}' = \begin{bmatrix} 0 \\ \mu(g^{21}\frac{\partial u}{\partial \xi} + g^{22}\frac{\partial u}{\partial \eta} + g^{23}\frac{\partial u}{\partial \zeta}) \\ \mu(g^{21}\frac{\partial v}{\partial \xi} + g^{22}\frac{\partial v}{\partial \eta} + g^{23}\frac{\partial v}{\partial \zeta}) \\ \mu(g^{21}\frac{\partial w}{\partial \xi} + g^{22}\frac{\partial w}{\partial \eta} + g^{23}\frac{\partial w}{\partial \zeta}) \\ \mu(g^{21}\frac{\partial T_i}{\partial \xi} + g^{22}\frac{\partial T_i}{\partial \eta} + g^{23}\frac{\partial T_i}{\partial \zeta}) \end{bmatrix}$$

$$\mathbf{F}' = \begin{bmatrix} 0 \\ \mu(g^{31}\frac{\partial u}{\partial \xi} + g^{32}\frac{\partial u}{\partial \eta} + g^{33}\frac{\partial u}{\partial \zeta}) \\ \mu(g^{31}\frac{\partial v}{\partial \xi} + g^{32}\frac{\partial v}{\partial \eta} + g^{33}\frac{\partial v}{\partial \zeta}) \\ \mu(g^{31}\frac{\partial w}{\partial \xi} + g^{32}\frac{\partial w}{\partial \eta} + g^{33}\frac{\partial w}{\partial \zeta}) \\ \mu(g^{31}\frac{\partial T_i}{\partial \xi} + g^{32}\frac{\partial T_i}{\partial \eta} + g^{33}\frac{\partial T_i}{\partial \zeta}) \end{bmatrix}$$

where $\tilde{U}, \tilde{V}$ and $\tilde{V}$ are contravariant velocities defined by

$$\tilde{U} = \rho(\xi_t + u\xi_x + v\xi_y + w\xi_z) \tag{2.16}$$

$$\tilde{V} = \rho(\eta_t + u\eta_x + v\eta_y + w\eta_z) \tag{2.17}$$

$$\widetilde{W} = \rho(\zeta_t + u\zeta_x + v\zeta_y + w\zeta_z) \tag{2.18}$$

The contravariant scale factors are

$$g^{11} = \xi_x^2 + \xi_y^2 + \xi_z^2 \tag{2.19}$$

$$g^{22} = \eta_x^2 + \eta_y^2 + \eta_z^2 \tag{2.20}$$

$$g^{33} = \zeta_x^2 + \zeta_y^2 + \zeta_z^2 \tag{2.21}$$

$$g^{12} = g^{21} = \xi_x\eta_x + \xi_y\eta_y + \xi_z\eta_z \tag{2.22}$$

$$g^{13} = g^{31} = \xi_x\zeta_x + \xi_y\zeta_y + \xi_z\zeta_z \tag{2.23}$$

$$g^{23} = g^{32} = \eta_x\zeta_x + \eta_y\zeta_y + \eta_z\zeta_z \tag{2.24}$$

The interface equation in the curvilinear coordinates becomes

$$\begin{bmatrix} \frac{\partial x}{\partial t} \\ \frac{\partial y}{\partial t} \\ \frac{\partial z}{\partial t} \end{bmatrix} = k_s \begin{bmatrix} \xi_x^s & \eta_x^s & \zeta_x^s \\ \xi_y^s & \eta_y^s & \zeta_y^s \\ \xi_z^s & \eta_z^s & \zeta_z^s \end{bmatrix} \begin{bmatrix} \frac{\partial T_s}{\partial \xi} \\ \frac{\partial T_s}{\partial \eta} \\ \frac{\partial T_s}{\partial \zeta} \end{bmatrix} - k_l \begin{bmatrix} \xi_x^l & \eta_x^l & \zeta_x^l \\ \xi_y^l & \eta_y^l & \zeta_y^l \\ \xi_z^l & \eta_z^l & \zeta_z^l \end{bmatrix} \begin{bmatrix} \frac{\partial T_l}{\partial \xi} \\ \frac{\partial T_l}{\partial \eta} \\ \frac{\partial T_l}{\partial \zeta} \end{bmatrix} \tag{2.25}$$

where the superscripts s and l denote the scale factors in the solid and liquid domains respectively.

2.3 General Formulation in Cylindrical Coordinates

The most commonly used curvilinear coordinate system is the cylindrical system with

$$\xi = r, \qquad \eta = \theta, \qquad \zeta = z$$

and

$$x = r\cos\theta, \qquad y = r\sin\theta, \qquad z = z$$

We redefine the vector $\mathbf{q} = [u_r, u_\theta, u_z, p, T_i]^\tau$, the governing equation (2.15) then becomes

$$\frac{\partial \mathbf{U}}{\partial t} + \frac{\partial \mathbf{A}}{\partial r} + \frac{\partial \mathbf{B}}{\partial \theta} + \frac{\partial \mathbf{C}}{\partial z} = \frac{\partial \mathbf{D}}{\partial r} + \frac{1}{r}\frac{\partial \mathbf{D}'}{\partial r} + \frac{1}{r^2}\frac{\partial \mathbf{E}}{\partial \theta} + \frac{\partial \mathbf{F}}{\partial z} + \mathbf{G} \tag{2.26}$$

where

$$\mathbf{U} = \begin{bmatrix} \rho r \\ \rho r u_r \\ \rho r u_\theta \\ \rho r u_z \\ \rho c_p r T_i \end{bmatrix} \quad \mathbf{A} = \begin{bmatrix} \rho r u_r \\ r(p + \rho u_r^2) \\ \rho r u_r u_\theta \\ \rho r u_r u_z \\ \rho c_p r u_r T_i \end{bmatrix} \quad \mathbf{B} = \begin{bmatrix} \rho u_\theta \\ \rho r u_r u_\theta \\ p + \rho u_\theta^2 \\ \rho r u_\theta u_z \\ \rho c_p r u_\theta T_i \end{bmatrix} \quad \mathbf{C} = \begin{bmatrix} \rho r u_z \\ \rho r u_r u_z \\ \rho r u_\theta u_z \\ r(p + \rho u_z^2) \\ \rho c_p r u_z T_i \end{bmatrix}$$

$$\mathbf{D} = \begin{bmatrix} 0 \\ \mu \frac{1}{r} \frac{\partial}{\partial r}(r u_r) \\ \mu \frac{1}{r} \frac{\partial}{\partial r}(r u_\theta) \\ 0 \\ 0 \end{bmatrix} \quad \mathbf{D}' = \begin{bmatrix} 0 \\ 0 \\ 0 \\ \mu r \frac{\partial u_z}{\partial r} \\ k_i r \frac{\partial T_i}{\partial r} \end{bmatrix} \quad \mathbf{E} = \begin{bmatrix} 0 \\ \mu(\frac{\partial u_r}{\partial \theta} - 2u_\theta) \\ \mu(\frac{\partial u_\theta}{\partial \theta} + 2u_r) \\ \mu \frac{\partial u_z}{\partial \theta} \\ k_i \frac{\partial T_i}{\partial \theta} \end{bmatrix}$$

$$\mathbf{F} = \begin{bmatrix} 0 \\ \mu \frac{\partial u_r}{\partial z} \\ \mu \frac{\partial u_\theta}{\partial z} \\ \mu \frac{\partial u_z}{\partial z} \\ k_i \frac{\partial T_i}{\partial z} \end{bmatrix} \quad \mathbf{G} = \begin{bmatrix} 0 \\ \rho(g_r + \frac{u_\theta^2}{r}) \\ \rho(g_\theta - \frac{u_r u_\theta}{r}) \\ \rho g_z \\ 0 \end{bmatrix}$$

where u_r, u_θ and u_z denote the velocity components in the radial, angular and axial directions respectively.

We write these forms of equations only for compactness rather than following strictly the conservative law as in [57].

2.4 Governing Equations In Axisymmetric Cylindrical Coordinates

For phase-change in a vertical cylindrical enclosure, we assume the system is axisymmetric. Consequently, $u_\theta = 0$ and all derivatives with respect to θ are zero. The governing equations (2.26) then reduce to

$$\frac{\partial \mathbf{U}}{\partial t} + \frac{\partial \mathbf{A}}{\partial r} + \frac{\partial \mathbf{C}}{\partial z} = \frac{\partial \mathbf{D}}{\partial r} + \frac{1}{r}\frac{\partial \mathbf{D}'}{\partial r} + \frac{\partial \mathbf{F}}{\partial z} + \mathbf{G} \tag{2.27}$$

where

$$\mathbf{U} = \begin{bmatrix} \rho r \\ \rho r u_r \\ \rho r u_z \\ \rho c_p r T_i \end{bmatrix} \quad \mathbf{A} = \begin{bmatrix} \rho r u_r \\ r(p + \rho u_r^2) \\ \rho r u_r u_z \\ \rho c_p r u_r T_i \end{bmatrix} \quad \mathbf{C} = \begin{bmatrix} \rho r u_z \\ \rho r u_r u_z \\ r(p + \rho u_z^2) \\ \rho c_p r u_z T_i \end{bmatrix}$$

$$\mathbf{D} = \begin{bmatrix} 0 \\ \mu \frac{1}{r}\frac{\partial}{\partial r}(r u_r) \\ 0 \\ 0 \end{bmatrix} \quad \mathbf{D}' = \begin{bmatrix} 0 \\ 0 \\ \mu r \frac{\partial u_z}{\partial r} \\ k_i r \frac{\partial T_i}{\partial r} \end{bmatrix} \quad \mathbf{F} = \begin{bmatrix} 0 \\ \mu \frac{\partial u_r}{\partial z} \\ \mu \frac{\partial u_z}{\partial z} \\ k_i \frac{\partial T_i}{\partial z} \end{bmatrix} \quad \mathbf{G} = \begin{bmatrix} 0 \\ 0 \\ \rho g_z \\ 0 \end{bmatrix}$$

where we assume that there is no centrifugal force in the cylinder.

2.5 Boundary Conditions

The above governing equations must be completed by the appropriate boundary conditions. In other words, a phase-change problem is not defined until the boundary conditions have been properly specified. We shall consider boundary conditions which occur in most problems of practical interest.

2.5.1 Hydrodynamic Boundary Conditions

There are two kinds of boundary conditions for fluid flows, namely a solid wall and a free surface. For a solid wall, the no-slip boundary condition is appropriate as a fluid particle does not move at a solid boundary. Mathematically we can set all the velocity components at the solid wall equal to zero.

For a free surface, fluid may flow along with the surface. In this case, a full-slip boundary condition can be imposed where velocities normal to the boundary and the gradients of velocity components tangent to the boundary can be set to zero. Instead of the Dirichlet condition for the no-slip boundary, the full-slip boundary condition implies both the Dirichlet and the Neumann type conditions.

2.5.2 Thermal Boundary Conditions

The most common thermal boundary condition at the heated wall is that of constant temperature. Physical meaning is that a phase-change process begins when a temperature, which is higher than the fusion temperature for melting, or lower than the freezing point for freezing, is imposed on the solid wall and remains constant throughout the process.

Another common thermal boundary condition is that of constant heat flux. In this instance, we do not know, or it is not necessary to know, the temperature of the boundary. Instead we know the imposed heat flux. A complete discussion on boundary conditions can be found in the book by Shah and London [58].

Chapter 3

COORDINATE TRANSFORMATION

The accuracy of the numerical solutions depends essentially on the grid system. The most convenient grid network is composed of rectangles. The application of this method is however limited to rectangular domains. To treat an irregular domain, interpolations have to be devised to overcome the difficulties encountered at the boundaries. In most partial differential systems, the boundary conditions have a dominant influence on the accuracy of the solution. When the interpolations between grid points do not fall on the boundaries, the inaccuracy of the interpolation may significantly affect the behavior of the solution, especially for a system with large gradients in the vicinity of the boundaries.

The best finite difference representation should be chosen such that the finite difference expression at, and close to the boundary only involves grid points on the intersections of coordinate lines *i.e.* without the need of any interpolation between grid points. In view of this, the transformation of an arbitrarily shaped domain to a new space where the boundaries coincide with a coordinate line has been brought out. Among all possible choices for the new space, a rectangular domain is the most convenient for the application of the classic finite difference technique. The solution procedure for a partial differential system is to transform all the spatial derivatives from the Cartesian or cylindrical coordinates to the new curvilinear coordinates. The transformed equations will be of the same type as the

original ones [59] except for the appearance of additional terms called scale factors. The boundary conditions are transformed in a similar way. Once transformed, the partial derivatives with the new independent variables are discretized as in a Cartesian space, since the grid system in the new space is rectangular. Therefore, all the conventional techniques of solving partial differential equations can be employed on the transformed plan.

3.1 Preliminary Theory of Coordinate Transformation

This section describes a general theory of transformation from a curvilinear coordinate system onto a canonical region R. The region R is usually chosen as a rectangular region, as mentioned, for convenience of using the finite difference techniques. As a matter of fact, this choice is quite arbitrary. One can, for example, choose a cylindrical region[61], or any two or three-dimensional region for which a natural coordinate system can be easily defined.

Suppose the curvilinear coordinates are related to the Cartesian coordinates by the transformation [62]

$$\xi^i = \xi^i(x_1, x_2, \ldots, x_n) \tag{3.1}$$

where ξ^i is at least twice differentiable.

The inverse of this transformation is then given by

$$x_i = x_i(\xi^i, \xi^i, \ldots, \xi^n) \tag{3.2}$$

The Laplacian of any set of curvilinear coordinates is given by

$$\nabla^2 \xi^i = -g^{jk}\Gamma^i_{jk} \tag{3.3}$$

where the Christoffel symbol Γ^l_{ij} is defined as

$$\Gamma^l_{ij} = \frac{1}{2}g^{kl}(\frac{\partial g_{ik}}{\partial x^j} + \frac{\partial g_{jk}}{\partial x^i} - \frac{\partial g_{ij}}{\partial x^k}) \tag{3.4}$$

The Cartesian coordinates are required to satisfy the following partial differential system in the above Laplacians

$$g^{jk}\frac{\partial^2 x_i}{\partial \xi^j \partial \xi^k} = -\frac{\partial x_i}{\partial \xi^r}\nabla^2 \xi^r \tag{3.5}$$

This equation may also be written as

$$\mathcal{D}x_i = -g\frac{\partial x_i}{\partial \xi^r}\nabla^2 \xi^r \tag{3.6}$$

with the operator $\mathcal{D}$ defined as

$$\mathcal{D} = g(g^{11}\frac{\partial^2}{\partial \xi^2} + g^{22}\frac{\partial^2}{\partial \eta^2} + g^{33}\frac{\partial^2}{\partial \zeta^2} + 2g^{12}\frac{\partial^2}{\partial \xi \partial \eta} + 2g^{13}\frac{\partial^2}{\partial \xi \partial \zeta} + 2g^{23}\frac{\partial^2}{\partial \eta \partial \zeta}) \tag{3.7}$$

where the coefficients g^{ij} are the contravariant components of the metric tensor which are related to the covariant components by the equation

$$g_{ij}g^{ik} = \delta^k_j \tag{3.8}$$

The covariant components of the metric tensor are given by

$$g_{jk} = \frac{\partial x_i}{\partial \xi^j}\frac{\partial x_i}{\partial \xi^k} \tag{3.9}$$

The other contravariant components are

$$g^{11} = (g_{22}g_{33} - g_{23}^2)/g \tag{3.10}$$

$$g^{22} = (g_{11}g_{33} - g_{13}^2)/g \tag{3.11}$$

$$g^{33} = (g_{11}g_{22} - g_{12}^2)/g \tag{3.12}$$

$$g^{12} = (g_{13}g_{23} - g_{12}g_{33})/g \tag{3.13}$$

$$g^{13} = (g_{12}g_{23} - g_{13}g_{22})/g \tag{3.14}$$

$$g^{23} = (g_{12}g_{13} - g_{11}g_{23})/g \tag{3.15}$$

$$g = g_{11}g_{22}g_{33} + 2g_{12}g_{13}g_{23} - g_{23}^2 g_{11} - g_{13}^2 g_{22} - g_{12}^2 g_{33} \tag{3.16}$$

where g is the determinant of g_{ij}.

For a two-dimensional system, the coefficients $g_{13} = g_{23} = 0, g_{33} = 1$ and all the derivatives with respect to ζ are zero. Then

$$g^{11} = g_{22}/g \tag{3.17}$$

$$g^{22} = g_{11}/g \tag{3.18}$$

$$g^{12} = -g_{12}/g \tag{3.19}$$

$$g = g_{11}g_{22} - g_{12}^2 \tag{3.20}$$

3.2 Grid Generation

There are several approaches to generating boundary fitted coordinates. The common ones are the algebraic transformation, the conformal mapping, and the numerical solution of a set partial differential equation proposed by Thompson et al [59]. The algebraic procedure is the simplest method and is commonly used in finite element methods. The drawback is that a lot of manual effort may be required to generate a smooth grid network, and the grid generated by this method is difficult to control. The conformal mapping technique is another method for constructing curvilinear coordinates in a two-dimensional region. Because of this limitation and its inherently ill-conditioned numerical problem, and the lack of control of the grid, the conformal mapping is not as attractive as the numerical solution of a general partial differential system.

So far, the most popular and flexible curvilinear coordinate generation method is based on an automated numerical generation by the solution of a set of elliptic quasilinear partial differential equations without the restriction of orthogonality or conformality.

The simplest elliptic partial differential equation is the Laplace equation

$$\nabla^2 \xi^i = 0 \tag{3.21}$$

subject to Dirichlet boundary conditions. With this generating system, Eq. (3.5) becomes

$$g^{jk} \frac{\partial^2 x_i}{\partial \xi^i \partial \xi^k} = 0 \tag{3.22}$$

and Eq. (3.6) becomes

$$\mathcal{D}x_i = 0 \tag{3.23}$$

The generating system (3.21) has a non-vanishing Jacobian for any simply or doubly connected region transformed to a rectangular plane [63]. In order to control the spacing of the grid lines, Thompson et al [59] put a source term $P^i(\xi^i)$ in the Laplace equation (3.21) as

$$\nabla^2 \xi^i = P^i(\xi^i) \tag{3.24}$$

Therefore, the system (3.5) becomes

$$g^{jk}\frac{\partial^2 x_i}{\partial \xi^j \partial \xi^k} = -P^r \frac{\partial x_i}{\partial \xi^r} \tag{3.25}$$

Furthermore,

$$\mathcal{D}x_i = -gP^r \frac{\partial x_i}{\partial \xi^r} \tag{3.26}$$

In the two-dimensional system, the latter system can be written as

$$g_{22}x_{\xi\xi} - 2g_{12}x_{\xi\eta} + g_{11}x_{\eta\eta} + g(Px_\xi + Qx_\eta) = 0 \tag{3.27}$$

$$g_{22}y_{\xi\xi} - 2g_{12}y_{\xi\eta} + g_{11}y_{\eta\eta} + g(Py_\xi + Qy_\eta) = 0 \tag{3.28}$$

3.2.1 Grid Control Functions

From a computational standpoint, we often require the physical grid points to be distributed as desired along the boundaries. This kind of grid system is especially important to obtain accurate solution in high gradient regions where the boundary layers require a locally refined grid.

To control the grid points in the interior region of the computational domain, Thompson [59] proposed a couple of grid control functions

$$\begin{aligned} P(\xi,\eta) &= -\sum_{i=1}^{n} a_i sgn(\xi-\xi_i) exp(-c_i|\xi-\xi_i|) \\ &\quad -\sum_{j=1}^{m} b_j sgn(\xi-\xi_j) exp(-d_j\sqrt{(\xi-\xi_j)^2+(\eta-\eta_j)^2}) \end{aligned} \tag{3.29}$$

$$\begin{aligned} Q(\xi,\eta) &= -\sum_{i=1}^{n} a_i sgn(\eta-\eta_i) exp(-c_i|\eta-\eta_i|) \\ &\quad -\sum_{j=1}^{m} b_j sgn(\eta-\eta_j) exp(-d_j\sqrt{(\xi-\xi_j)^2+(\eta-\eta_j)^2}) \end{aligned} \tag{3.30}$$

where the positive amplitudes and decay functions are not necessarily the same in the two equations. The first term has the effect of attracting the $\xi = constant$ line to the $\xi = \xi_i$ line in equation (3.30) and attracting $\eta = constant$ lines to the $\eta = \eta_i$ lines in equation(3.31). The second term causes $\xi = constant$ line to be attracted to the points (ξ, η) in (3.30), with similar effect on $\eta = constant$ line in (3.31).

As a matter of fact, the source terms P and Q are not exclusive. Although the forms of P and Q in Eqs. (3.30) and (3.31) have been used successfully in many applications [59], the values of the adjustable parameter in this *ad hoc* approach require an artful selection and are problem dependent.

In many cases, it is difficult to control the spacing between grid points and generate a smooth grid network within the computational domain. Thomas and Middlecoff [64] found that the influence of the boundary value which we set as a Dirichlet condition does not penetrate very deeply into the interior of the region. The interior grid is affected primarily by the generating systems, rather than by the boundary values. They provided a couple of control functions

$$P(\xi,\eta) = \varphi(\xi,\eta)(\xi_x^2 + \xi_y^2) \tag{3.31}$$

$$Q(\xi,\eta) = \psi(\xi,\eta)(\eta_x^2 + \eta_y^2) \tag{3.32}$$

where

$$\varphi(\xi,\eta) = -(x_\xi x_{\xi\xi} + y_\xi y_{\xi\xi})/g_{11} \tag{3.33}$$

$$\psi(\xi,\eta) = -(x_\eta x_{\eta\eta} + y_\eta y_{\eta\eta})/g_{22} \tag{3.34}$$

With these control functions, the generating system (3.5) becomes

$$g_{22}(x_{\xi\xi} + \varphi x_\xi) - 2g_{12}x_{\xi\eta} + g_{11}(x_{\eta\eta} + \psi x_\eta) = 0 \tag{3.35}$$

$$g_{22}(y_{\xi\xi} + \varphi y_\xi) - 2g_{12}y_{\xi\eta} + g_{11}(y_{\eta\eta} + \psi y_\eta) = 0 \tag{3.36}$$

This generating system has shown that the interior grid point distribution is controlled entirely by *a priori* selection of the grid point distribution along the boundaries of the physical domain. This method can also control the local angle of intersection between a transverse grid line and the boundary. Particularly, the

grid lines may be constrained to be locally orthogonal to the boundaries which is especially important for fluid flow and heat transfer problems.

3.2.2 Transformation Relations

In order to perform all the computations on the transformed plane (ξ, η), the physical variables have to be transformed into functions of the independent variables ξ and η. Here we are only concerned with a two-dimensional transformation. The extension to three dimensions is straightforward.

The general transformation relations were given in Section 2 of Chapter 2, where we have not discussed any grid transformation. Here we will take the resulting transformation relations for the two-dimension systems, and more transformation relations and scale factors will be provided.

3.2.2.1 Transformed Spatial and Transient Derivatives

From the last chapter, we have spatial derivative transformations as

$$f_x = \xi_x f_\xi + \eta_x f_\eta \tag{3.37}$$

$$f_y = \xi_y f_\xi + \eta_y f_\eta \tag{3.38}$$

$$(f_t)_{x,y} = (f_t)_{\xi,\eta} + \xi_t f_\xi + \eta_t f_\eta \tag{3.39}$$

Using the chain rule one can obtain

$$f_{xx} = \xi_x^2 f_{\xi\xi} + 2\xi_x\eta_x f_{\xi\eta} + \eta_x^2 f_{\eta\eta} + \xi_{xx} f_\xi + \eta_{xx} f_\eta \tag{3.40}$$

$$f_{yy} = \xi_y^2 f_{\xi\xi} + 2\xi_y\eta_y f_{\xi\eta} + \eta_y^2 f_{\eta\eta} + \xi_{yy} f_\xi + \eta_{yy} f_\eta \tag{3.41}$$

$$f_{xy} = \xi_x\xi_y f_{\xi\xi} + (\eta_x\xi_y + \eta_y\xi_x) f_{\xi\eta} + \eta_x\eta_y f_{\eta\eta} + \xi_{xy} f_\xi + \eta_{xy} f_\eta \tag{3.42}$$

The transformed Laplacian operator from the Cartesian coordinates then becomes

$$\nabla^2 f = g^{11} f_{\xi\xi} + 2g^{12} f_{\xi\eta} + g^{22} f_{\eta\eta} + \nabla^2\xi f_\xi + \nabla^2\eta f_\eta \tag{3.43}$$

where

$$\xi_x = y_\eta / J \tag{3.44}$$

$$\xi_y = -x_\eta / J \tag{3.45}$$

$$\eta_x = -y_\xi / J \tag{3.46}$$

$$\eta_y = x_\xi / J \tag{3.47}$$

$$g^{11} = \xi_x^2 + \xi_y^2 \tag{3.48}$$

$$g^{22} = \eta_x^2 + \eta_y^2 \tag{3.49}$$

$$g^{12} = \xi_x\eta_x + \xi_y\eta_y \tag{3.50}$$

$$J^{-1} = \xi_x\eta_y - \xi_y\eta_x \tag{3.51}$$

$$\nabla^2 \xi = P(\xi, \eta) \tag{3.52}$$

$$\nabla^2 \eta = Q(\xi, \eta) \tag{3.53}$$

$$\xi_t = -(\xi_x x_t + \xi_y y_t) \tag{3.54}$$

$$\eta_t = -(\eta_x x_t + \eta_y y_t) \tag{3.55}$$

Unlike many other authors[59], [60], [65], [66], [68] [69], all the transformation relations we used in this thesis are in the form of contravariant metric components. The reason for this is that using contravariant components to express the transformation relations is simpler than using the covariant metric components, easy to obtain from the chain rule, and less computational effort is needed in the program. Although the contravaraint components can not be obtained directly, after the grid system is generated, the contravariant components can be computed from the covariant components once and for all. A subroutine to compute the contravariant metric components is given in Appendix D.

Eq.(3.39) is the transformation relation of the transient term. The time derivative on the left side is at a fixed position in the physical plane and the time derivative on the right side is at a fixed position in the transformed plane. x_τ and y_τ are the grid point speeds. With that relation, the movement of the grid points in the physical plane is reflected only through the rate of change of x and y at the fixed grid points in the transformed plane. Thereby, only time derivatives at fixed points in the transformed plane will appear in the transformed equations, and all the computations may be thus performed on the fixed grid in the transformed field without any interpolation of the field variables.

3.2.2.2 Transformation of Vectors and Gradients

Since all the variables have been transformed onto the computational domain, the boundary conditions specified on the physical domain have to be transformed into the computational domain. The Dirichlet boundary conditions may be treated in the same way as on the physical plane. But the Neumann boundary conditions have to be transformed as follows.

For an arbitrary scalar function f in the contravariant scale factors, (for covariant scale factors, see Appendix A) we have

$$\nabla f = (f_\xi \xi_x + f_\eta \eta_x)\mathbf{i} + (f_\xi \xi_y + f_\eta \eta_y)\mathbf{j} \tag{3.56}$$

The unit vector normal to the $\xi = constant$ curve can be expressed in the contravariant form

$$\mathbf{n}^{(\xi)} = \frac{\nabla \xi}{\|\nabla \xi\|} = \frac{1}{\sqrt{g^{11}}}(\xi_x \mathbf{i} + \xi_y \mathbf{j}) \tag{3.57}$$

and for $\eta = constant$ curve, the unit vector is

$$\mathbf{n}^{(\eta)} = \frac{\nabla \eta}{\|\nabla \eta\|} = \frac{1}{\sqrt{g^{22}}}(\eta_x \mathbf{i} + \eta_y \mathbf{j}) \tag{3.58}$$

Therefore, any gradient at the boundaries of the transformed domain can be obtained by $\nabla f \cdot \mathbf{n}$,*i.e.*

$$\left.\frac{\partial f}{\partial n}\right|_{\xi = const.} = \frac{1}{\sqrt{g^{11}}}(g^{11} f_\xi + g^{12} f_\eta) \tag{3.59}$$

and

$$\left.\frac{\partial f}{\partial n}\right|_{\eta = const.} = \frac{1}{\sqrt{g^{22}}}(g^{12}f_\xi + g^{22}f_\eta) \tag{3.60}$$

3.2.2.3 Transformation of An Arc Element

To compute the heat transport coefficients, we have to deal with integrations along some coordinate line on the transformed plane. To find an arc length element, we begin with a general arc length increment in the curvilinear coordinates which can be expressed as

$$ds^2 = g_{ij}d\xi^i d\xi^j \tag{3.61}$$

To perform an integration along which ξ^i varies, the increment of an arc length is

$$ds^i = \sqrt{g_{ii}}d\xi^i \tag{3.62}$$

In particular, an increment of an arc length along ξ line becomes

$$d\xi^{(\xi)} = \sqrt{g_{11}}d\xi = J\sqrt{g^{22}}d\xi \tag{3.63}$$

while along η line, we have

$$d\xi^{(\eta)} = \sqrt{g_{22}}d\eta = J\sqrt{g^{11}}d\eta \tag{3.64}$$

3.3 Numerical Method of Grid Generation

3.3.1 Discrete Representation of Derivatives

Before solving the partial differential equations in the transformed domain, a grid network has to be constructed. Although the transformed domain can be arbitrary, a rectangular transformed plane is chosen as shown below

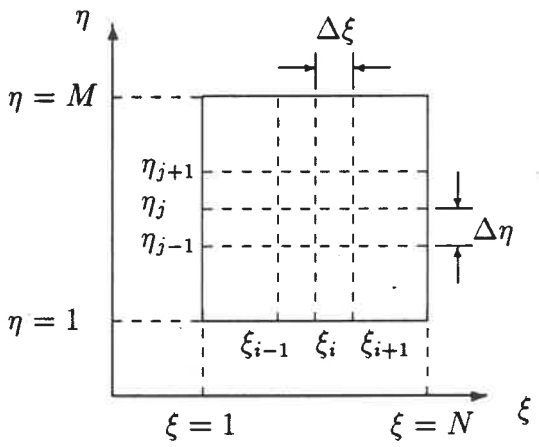

Figure 3.1: Computational grid system in the transformed plane

With this uniform grid, the conventional finite difference form can be easily constructed. The first, second and mixed partial derivatives with respect to the curvilinear coordinates ξ and η are ordinarily represented at an interior point (i, j) by central difference as

$$(f_\xi)_{ij} = \frac{1}{2}(f_{i+1,j} - f_{i-1,j}) \tag{3.65}$$

$$(f_\eta)_{ij} = \frac{1}{2}(f_{i,j+1} - f_{i,j-1}) \tag{3.66}$$

$$(f_{\xi\xi})_{ij} = f_{i+1,j} - 2f_{i,j} + f_{i-1,j} \tag{3.67}$$

$$(f_{\eta\eta})_{ij} = f_{i,j+1} - 2f_{i,j} + f_{i,j-1} \tag{3.68}$$

$$(f_{\xi\eta})_{i,j} = \frac{1}{4}(f_{i+1,j+1} - f_{i+1,j-1} - f_{i_1,j+1} + f_{i-1,j-1}) \tag{3.69}$$

For the derivatives at the boundaries, the second order forward and backward finite difference representations are respectively

$$(f_{\xi})_{\xi=1} = \frac{1}{2}(-3f_{1,j} + 4f_{2,j} - f_{3,j}) \tag{3.70}$$

$$(f_{\xi})_{\xi=N} = \frac{1}{2}(3f_{N,j} - 4f_{N-1,j} + f_{N-2,j}) \tag{3.71}$$

and

$$(f_{\eta})_{\eta=1} = \frac{1}{2}(-3f_{i,1} + 4f_{i,2} - f_{i,3}) \tag{3.72}$$

$$(f_{\eta})_{\eta=M} = \frac{1}{2}(3f_{i,M} - 4f_{i,M-1} + f_{i,M-2}) \tag{3.73}$$

3.3.2 Method of Solution of the Generating System

To develop the finite difference representation of the grid generating system, we rewrite the generating equations as

$$g_{22}(x_{\xi\xi} + \varphi x_{\xi}) - 2g_{12}x_{\xi\eta} + g_{11}(x_{\eta\eta} + \psi x_{\eta}) = 0$$

$$g_{22}(y_{\xi\xi} + \varphi y_{\xi}) - 2g_{12}y_{\xi\eta} + g_{11}(y_{\eta\eta} + \psi y_{\eta}) = 0$$

For the sake of simplicity we only present the finite difference expression of

the first equation. The second one can be treated in the same way as the first, by replacing x by y.

Using the classical finite difference technique, the finite difference representation of the first equation is

$$\begin{aligned}
&(g_{22})_{i,j}\left(\frac{x_{i+1,j}-2x_{i,j}+x_{i-1,j}}{\Delta\xi^2}+\varphi_{i,j}\frac{x_{i+1,j}-x_{i-1,j}}{2\Delta\xi}\right)\\
&-2(g_{12})_{i,j}\left(\frac{x_{i+1,j+1}-x_{i+1,j-1}+x_{i-1,j-1}-x_{i-1,j+1}}{4\Delta\xi\Delta\eta}\right)\\
&+(g_{11})_{i,j}\left(\frac{x_{i,j+1}-2x_{i,j}+x_{i,j-1}}{\Delta^2\eta}+\psi_{i,j}\frac{x_{i,j+1}-x_{i,j-1}}{2\Delta\eta}\right)=0
\end{aligned} \tag{3.74}$$

for $1 \leq \xi \leq N$ and $1 \leq \eta \leq M$

Because of the arbitrary choice of the transformed plane, we can choose $\Delta\xi = \Delta\eta = 1$ for simplicity.

This equation can be cast in a form suitable for an iterative method of solution as

$$Ax_{i-1,j} + Bx_{i,j} + Cx_{i+1,j} = D \tag{3.75}$$

where

$$A = -(g_{22})_{i,j} + \frac{1}{2}\varphi_{i,j} \tag{3.76}$$

$$B = 2((g_{11})_{i,j} + (g_{22})_{i,j}) \tag{3.77}$$

$$C = -(g_{22})_{i,j} - \frac{1}{2}\varphi_{i,j} \tag{3.78}$$

$$D = (g_{11})_{i,j}(x_{i,j+1} + x_{i,j-1} + \psi_{i,j}\frac{x_{i,j+1} - x_{i,j-1}}{2}) \tag{3.79}$$
$$-(g_{12})_{i,j}\frac{1}{2}(x_{i+1,j+1} - x_{i+1,j-1} + x_{i-1,j-1} - x_{i-1,j+1})$$

Similarly we can obtain the finite difference equation along the vertical lines

$$A'x_{i,j-1} + B'x_{i,j} + C'x_{i,j+1} = D' \tag{3.80}$$

where

$$A' = -(g_{11})_{i,j} + \frac{1}{2}\psi_{i,j} \tag{3.81}$$

$$B' = 2((g_{11})_{i,j} + (g_{22})_{i,j}) \tag{3.82}$$

$$C' = -(g_{11})_{i,j} - \frac{1}{2}\psi_{i,j} \tag{3.83}$$

$$D' = (g_{22})_{i,j}(x_{i+1,j} + x_{i-1,j} + \varphi_{i,j}\frac{x_{i+1,j} - x_{i-1,j}}{2}) \tag{3.84}$$
$$-(g_{12})_{i,j}\frac{1}{2}(x_{i+1,j+1} - x_{i+1,j-1} + x_{i-1,j-1} - x_{i-1,j+1})$$

and

$$(g_{11})_{i,j} = x_\xi^2 + y_\xi^2 \tag{3.85}$$
$$= \frac{1}{4}(x_{i+1,j} - x_{i-1,j})^2 + \frac{1}{4}(y_{i+1,j} - y_{i-1,j})^2$$

$$(g_{22})_{i,j} = x_\eta^2 + y_\eta^2 \tag{3.86}$$
$$= \frac{1}{4}(x_{i,j+1} - x_{i,j-1})^2 + \frac{1}{4}(y_{i,j+1} - y_{i,j-1})^2$$

$$(g_{12})_{i,j} = x_\xi x_\eta + y_\xi y_\eta \tag{3.87}$$

$$= \frac{1}{4}(x_{i+1,j} - x_{i-1,j})(x_{i,j+1} - x_{i,j-1}) + \frac{1}{4}(y_{i+1,j} - y_{i-1,j})(y_{i,j+1} - y_{i,j-1}) \tag{3.88}$$

When the physical domain is defined, the parameters φ and ψ can be evaluated from equations (3.33) and (3.34) at the boundaries by the finite difference representations. To begin the iteration, the initial interior values of φ and ψ can be obtained by interpolation between the boundaries. With equations (3.75), (3.80), and the two equations from the generating equation of y, one can use the ADI (Alternative Directional Implicit) technique proposed by Roache [71] to construct a smooth grid network as soon as a physical plane is defined. In order to accelerate the convergence, the successive over-relaxation (SOR) technique has been adopted. A subroutine to generate any two-dimensional grid system is given in Appendix D.

Chapter 4

NUMERICAL STUDY OF MELTING AROUND A VERTICAL CYLINDER WITH SIDE HEATING

Melting in a vertical cylindrical enclosure has been studied by a few investigators [24], [52] and [54]. Both analytical and experimental results show that natural convection plays an important role during the melting process. Among these studies, Sparrow *et al* [52] have adopted a numerical method to simulate the melting process. In their studies, the moving interface was mathematically immobilized by the Landau transformation. By using this transformation, an irregular melt domain can be mapped onto a rectangular one in the computational plane. Using this kind of transformation, many authors neglected the terms involving dr/dz and dr^2/dz^2 to make the transformed equations more tractable, under the assumption that the interface width varies slowly with height [38],[39],[52]. This assumption, however, is not valid near the top of the melt region, especially in convection-dominated cases. In our studies, a complete transformation, the so-called body-fitted transformation described in the previous chapters, has been used to deal with the irregular domain. The problem solved by Sparrow *et al* [52] has been recomputed by this method. The results indicate that the so-called "quasi-static" and "smooth interface" approximations used in most phase change analyses can significantly affect the solutions as the natural convection becomes

relatively important compared to the conduction.

To extend the studies, we have considered the inward melting for a fixed temperature boundary as well as the outward melting for constant heat flux condition. In the following sections, we shall first consider the problem of outward melting from an isothermal vertical cylinder. We consider next the case of melting around a cylinder subject to a constant heat flux. Finally, the problem of inward melting is considered for a cylinder maintained at a fixed temperature.

4.1 Outward Melting Around a Vertical Cylinder

4.1.1 Physical description and Mathematical Model

The physical problem is schematically pictured in Fig. 4:1.

A vertical cylinder of height H and radius r_0 is surrounded by a solid material at its fusion temperature T_f. At time $t = 0$, the temperature at the surface of the cylinder is raised, and maintained at a fixed value $T_w > T_f$. As a consequence, the solid material will melt around the cylinder. In order to describe the melting process, it is necessary to determine the evolution of the convective flow and heat transfer in the melt region. In fact, it should be noted that while the heat transfer is initially due to conduction, it is ultimately dominated by convection as the melt region becomes larger such that the melting front, almost vertical at early times, becomes more and more distorted under the effects of an upward convective flow along the heated cylinder and a downward flow along the melting front. The mathematical formulation of this problem is based on the following assumptions:

- The thermal properties of the materials are independent of temperature,

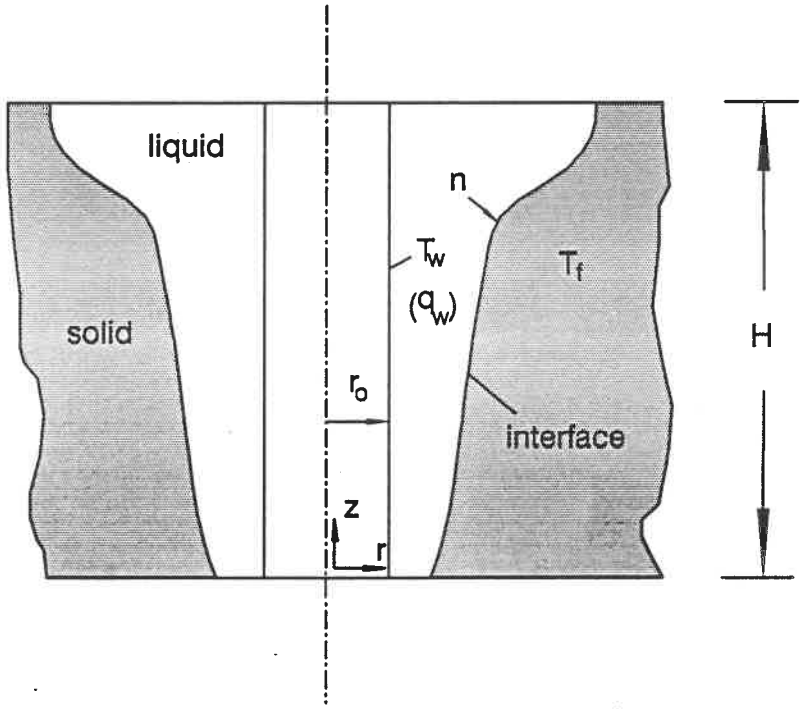

Figure 4.1: Schematic diagram of the physical problem

except for density in the buoyancy term, *i.e.* the Boussinesq approximation is valid.

- The process is two-dimensional because of axial symmetry.
- The volume changes during melting, and viscous dissipation are neglected.
- The flow in the liquid region is laminar.
- The melt is a Newtonian and incompressible fluid.

The general form of the governing equations for the phase-change problems in cylindrical coordinates were given in Chapter 2. For the convenience of the

discussion, we rewrite them explicitly in the following form

Continuity equation:

$$\frac{\partial(ru)}{\partial r} + \frac{\partial(rv)}{\partial z} = 0 \tag{4.1}$$

Momentum equations:

$$\frac{\partial u}{\partial t} + u\frac{\partial u}{\partial r} + v\frac{\partial u}{\partial z} = -\frac{1}{\rho}\frac{\partial p}{\partial r} + \nu(\frac{\partial^2 u}{\partial r^2} + \frac{1}{r}\frac{\partial u}{\partial r} + \frac{\partial^2 u}{\partial z^2} - \frac{u}{r^2}) \tag{4.2}$$

$$\frac{\partial v}{\partial t} + u\frac{\partial v}{\partial r} + v\frac{\partial v}{\partial z} = -\frac{1}{\rho}\frac{\partial p}{\partial z} + \nu(\frac{\partial^2 v}{\partial r^2} + \frac{1}{r}\frac{\partial v}{\partial r} + \frac{\partial^2 v}{\partial z^2}) + g\beta(T - T_f) \tag{4.3}$$

Energy equation:

$$\frac{\partial T}{\partial t} + u\frac{\partial T}{\partial r} + v\frac{\partial T}{\partial z} = \alpha(\frac{\partial^2 T}{\partial r^2} + \frac{1}{r}\frac{\partial T}{\partial r} + \frac{\partial^2 T}{\partial z^2}) \tag{4.4}$$

To simplify the physical model, it is assumed that the solid is kept at its fusion temperature i.e. there is no heat conduction in the solid, all the heat transferred to the interface is utilized for melting. With this assumption, the interface energy balance equation may be written as

$$-k\frac{\partial T}{\partial n} = \rho h\frac{\partial n}{\partial t} \tag{4.5}$$

4.1.2 Dimensionless Equations

Introducing a length scale r_0 , a time scale r_0^2/α and temperature scale $(T_w - T_f)$, with the reference temperature T_f, the dimensionless variables may be expressed as

$$R = \frac{r}{r_0} \qquad Z = \frac{z}{r_0} \qquad U = \frac{ur_0}{\alpha}$$

$$V = \frac{vr_0}{\alpha} \qquad P = \frac{p}{\alpha r_0 \rho} \qquad \theta = \frac{T - T_f}{T_w - T_f}$$

$$Pr = \frac{\nu}{\alpha} \qquad Ra = \frac{g\beta\Delta T r_0^3}{\alpha\nu} \qquad \tau = Ste \cdot Fo = \frac{C_p\Delta T}{h} \cdot \frac{\alpha t}{r_0^2}$$

To eliminate the pressure terms in the momentum equations, we introduce the stream function and vorticity defined by

$$U = \frac{1}{R}\frac{\partial\psi}{\partial Z} \tag{4.6}$$

$$V = -\frac{1}{R}\frac{\partial\psi}{\partial R} \tag{4.7}$$

$$\omega = \frac{\partial V}{\partial R} - \frac{\partial U}{\partial Z} \tag{4.8}$$

With the foregoing definition, we can eliminate the pressure derivatives from the momentum equations by subtracting Eq. (4.3) after deriving with respect to r from Eq. (4.2) after deriving with respect to z. The resulting equation called the vorticity transport equation, can be written as

$$Ste\frac{\partial\omega}{\partial\tau} + \frac{\partial(U\omega)}{\partial R} + \frac{\partial(V\omega)}{\partial Z} = Pr(\nabla^2\omega - \frac{\omega}{R^2}) + PrRa\frac{\partial\theta}{\partial R} \tag{4.9}$$

By substituting Eqs. (4.6),(4.7) into (4.8), we obtain the following equation for the stream function

$$\nabla^2\psi = \frac{2}{R}\frac{\partial\psi}{\partial R} - R\omega \tag{4.10}$$

The energy equation in dimensionless form reads

$$Ste\frac{\partial\theta}{\partial\tau} + U\frac{\partial\theta}{\partial R} + V\frac{\partial\theta}{\partial Z} = \nabla^2\theta \tag{4.11}$$

while the interface energy equation becomes

$$-\frac{\partial\theta}{\partial n} = \frac{\partial n}{\partial\tau} \tag{4.12}$$

The appropriate dimensionless boundary conditions are

$$\theta = 1 \quad \psi = 0 \quad at \quad r = 1$$

$$\theta = 0 \quad \psi = 0 \quad along \quad S_i$$

$$\frac{\partial\theta}{\partial z} = 0 \quad \psi = 0 \quad at \quad z = 0,\ A$$

where A is aspect ratio (height to radius) of the cylinder. The boundary condition for the vorticity is determined by Eq. (4.8). For a solid wall, the no-slip boundary is imposed. At the top and bottom of the cylinder, we assume adiabatic boundary conditions for temperature.

4.1.3 Transformed Governing Equations

Since all the computations will be performed in the transformed plane, the governing equations need to be transformed according to the relations provided in Chapter 3. After the transformation, the governing equations (4.2)-(4.4) become

$$Ste\frac{\partial \omega}{\partial \tau} + \tilde{U}\frac{\partial \omega}{\partial \xi} + \tilde{V}\frac{\partial \omega}{\partial \eta} = Pr\widetilde{\nabla}^2\omega + S_\omega \tag{4.13}$$

$$\widetilde{\nabla}^2\psi = S_\psi \tag{4.14}$$

$$Ste\frac{\partial \theta}{\partial \tau} + \tilde{U}\frac{\partial \theta}{\partial \xi} + \tilde{V}\frac{\partial \theta}{\partial \eta} = \widetilde{\nabla}^2\theta + S_\theta \tag{4.15}$$

the equations for the moving interface become

$$\frac{\partial x}{\partial \tau} = -\left(\xi_x\frac{\partial \theta}{\partial \xi} + \eta_x\frac{\partial \theta}{\partial \eta}\right) \tag{4.16}$$

$$\frac{\partial y}{\partial \tau} = -\left(\xi_y\frac{\partial \theta}{\partial \xi} + \eta_y\frac{\partial \theta}{\partial \eta}\right) \tag{4.17}$$

where $\tilde{U}$ and $\tilde{V}$ are contravariant velocities expressed as[1]

$$\tilde{U} = \xi_x U + \xi_y V \tag{4.18}$$

$$\tilde{V} = \eta_x U + \eta_y V \tag{4.19}$$

[1]The alternative expressions can be found as $\tilde{U} = \frac{1}{J}\frac{1}{R}\frac{\partial \psi}{\partial \eta}$ and $\tilde{V} = -\frac{1}{J}\frac{1}{R}\frac{\partial \psi}{\partial \xi}$.

and

$$
\begin{aligned}
U &= \frac{1}{x}(\xi_y \frac{\partial \psi}{\partial \xi} + \eta_y \frac{\partial \psi}{\partial \eta}) \\
V &= -\frac{1}{x}(\xi_x \frac{\partial \psi}{\partial \xi} + \eta_x \frac{\partial \psi}{\partial \eta}) \\
S_\omega &= -Ste(\xi_\tau \frac{\partial \omega}{\partial \xi} + \eta_\tau \frac{\partial \omega}{\partial \eta}) + (\frac{U}{x} - \frac{Pr}{x^2})\omega + PrRa(\xi_x \frac{\partial \theta}{\partial \xi} + \eta_x \frac{\partial \theta}{\partial \eta}) \\
S_\psi &= \frac{2}{x}(\xi_x \frac{\partial \psi}{\partial \xi} + \eta_x \frac{\partial \psi}{\partial \eta}) - x\omega \\
S_\theta &= -Ste(\xi_\tau \frac{\partial \theta}{\partial \xi} + \eta_\tau \frac{\partial \theta}{\partial \eta}) \\
\widetilde{\nabla}^2 &= g^{11}\frac{\partial^2}{\partial \xi^2} + 2g^{12}\frac{\partial^2}{\partial \xi \eta} + g^{22}\frac{\partial^2}{\partial \eta^2} + P\frac{\partial}{\partial \xi} + Q\frac{\partial}{\partial \eta} + \frac{1}{x}(\xi_x \frac{\partial}{\partial \xi} + \eta_x \frac{\partial}{\partial \eta})
\end{aligned}
$$

The last equation is the transformed Laplacian operator in cylindrical coordinates. It is worth noting that the last term is an extra term compared with the transformed Laplacian in Cartesian coordinates.

The transformed boundary conditions are

$$\xi = \xi_{min} \tag{4.20}$$

$$U = 0; \qquad V = 0;$$

$$\psi = 0; \qquad \theta = 1;$$

$$\omega = \xi_x V_\xi - \xi_y U_\xi$$

$$\xi = \xi_{max} \tag{4.21}$$

$$U = 0; \qquad V = 0;$$

$$\psi = 0; \qquad \theta = 0;$$

$$\omega = \xi_x V_\xi - \xi_y U_\xi$$

$$\eta = \eta_{min} \tag{4.22}$$

$$\eta = \eta_{max}$$

$$U = 0; \qquad V = 0;$$

$$\psi = 0;$$

$$\omega = \eta_x V_\eta - \eta_y U_\eta;$$

$$g^{22}\theta_\eta + g^{12}\theta_\xi = 0$$

4.1.4 Numerical Schemes

The governing equations (4.13)-(4.17) with the boundary conditions (4.20)-(4.22) have been solved numerically. A first order forward difference approximation is used for time derivatives. The diffusion terms are treated by the second-order central difference approximation. In the convection dominated flow, special attention has to be paid to the convection terms. It is well known that using the second-order central difference approximation to discretize the convective terms in the transport equations can produce wiggly solutions for high Peclet, or Rayleigh

numbers. Although the first-order upwind scheme can eliminate these wiggles, it may introduce significant truncation errors and produce large artificial diffusion. There exist higher order upwind schemes such as the second-order upwind scheme, the third-order upwind, and the QUICK scheme (Quadratic Upstream Interpolation for Convective Kinematics) [67].

Using the higher order upwind schemes, the discretized equations are no longer represented by a tri-diagonal matrix. Instead, the algebraic equations become a penta-diagonal matrix.

A general finite difference expression for an arbitrary scalar function in upwind schemes can be written as follows:

$$u\frac{\partial f}{\partial x}\Big|_i = A^u f_{i-2} + B^u f_{i-1} + C^u f_i + D^u f_{i+1} + E^u f_{i+2} \tag{4.23}$$

Where A^u, B^u, C^u, D^u and E^u are functions of u whose expressions for different upwind schemes are listed in Table 4.1: (details in Appendix B)

Table 4.1: *The coefficients of the different schemes*

Scheme	A^u	B^u	C^u	D^u	E^u
Central difference	0	$-\frac{u}{2\Delta x}$	0	$\frac{u}{2\Delta x}$	0
First − order upwind	0	$-\frac{\lvert u\rvert + u}{2\Delta x}$	$\frac{\lvert u\rvert}{\Delta x}$	$-\frac{\lvert u\rvert - u}{2\Delta x}$	0
Second − order upwind	$\frac{\lvert u\rvert + u}{4\Delta x}$	$-\frac{\lvert u\rvert + u}{\Delta x}$	$\frac{3\lvert u\rvert}{2\Delta x}$	$-\frac{\lvert u\rvert - u}{\Delta x}$	$\frac{\lvert u\rvert - u}{4\Delta x}$
Third − order upwind	$\frac{\lvert u\rvert + u}{12\Delta x}$	$-\frac{\lvert u\rvert + 2u}{3\Delta x}$	$\frac{\lvert u\rvert}{2\Delta x}$	$-\frac{\lvert u\rvert - 2u}{3\Delta x}$	$\frac{\lvert u\rvert - u}{12\Delta x}$
QUICK	$\frac{\lvert u\rvert + u}{16\Delta x}$	$-\frac{2\lvert u\rvert + 5u}{8\Delta x}$	$\frac{3\lvert u\rvert}{8\Delta x}$	$-\frac{2\lvert u\rvert - 5u}{8\Delta x}$	$\frac{\lvert u\rvert - u}{16\Delta x}$

Similar formulas for $v\left.\frac{\partial f}{\partial x}\right|_i$, $u\left.\frac{\partial f}{\partial y}\right|_j$ and $v\left.\frac{\partial f}{\partial y}\right|_j$ can be obtained by interchanging u, x and v, y accordingly.

As shown in Table 4.1, the coefficients A^u and E^u of the central difference and the first-order upwind schemes are equal to zero. The remaining coefficients B^u, C^u and D^u of f_{i-1}, f_i and f_{i+1} (for central difference the f_i terms come from the Laplacian terms), form a tri-diagonal matrix. Higher-order schemes always introduce a penta-diagonal matrix which can be solved by a procedure similar to the TDMA (Tri-Diagonal Matrix Algorithm), called PDMA (Penta-Diagonal Matrix Algorithm), the details of which are given in Appendix C. Subroutines for TDMA and PDMA methods are provided in Appendix D.

The different schemes have been tested in a cavity with one moving wall at the top to evaluate their accuracy. It was found that the second-order upwind scheme gives the most accurate results. A comprehensive discussion can be found in [66].

Throughout our studies, convection terms in the transport equation have been treated by the second-order upwind scheme. The resulting algebraic finite difference equations were solved by the PDMA. For the stream function equation, the central difference technique can be readily employed as no convection term is present. The resulting algebraic finite difference equation was solved by the TDMA. The global sweeping is performed according to the alternating direction implicit (ADI) procedure proposed by Roache [71].

4.1.5 Discretized Equations

4.1.5.1 Discretized Governing Equations

For numerical computations, the governing differential equations (4.13)-(4.17) have to be cast in a discretized form. All the convection terms in the equations are discretized by the secondary upwind scheme, and the diffusive terms are discretized by the central differential scheme. For the time derivatives, the first order backward finite difference scheme is adopted. The discretization procedure is developed as follows.

For the vorticity equation, the discretized representation is

$$\begin{aligned} Ste\frac{\omega_{i,j}^{k+1}-\omega_{i,j}^{k}}{\Delta\tau} &+ A^u\omega_{i-2,j}^{k+1} + B^u\omega_{i-1,j}^{k+1} + C^u\omega_{i,j}^{k+1} + D^u\omega_{i+1,j}^{k+1} + E^u\omega_{i+2,j}^{k+1} \quad (4.24)\\ &+A^v\omega_{i,j-2}^{k+1} + B^v\omega_{i,j-1}^{k+1} + C^v\omega_{i,j}^{k+1} + D^v\omega_{i,j+1}^{k+1} + E^v\omega_{i,j+2}^{k+1}\\ &= Pr\left(g_{i,j}^{11}\frac{\omega_{i+1,j}^{k+1}-2\omega_{i,j}^{k+1}+\omega_{i-1,j}^{k+1}}{\Delta\eta^2} + g_{i,j}^{22}\frac{\omega_{i,j+1}^{k+1}-2\omega_{i,j}^{k+1}+\omega_{i,j-1}^{k+1}}{\Delta\xi^2}\right.\\ &\quad\left.+2g_{i,j}^{12}\frac{\omega_{i+1,j+1}^{k+1}-\omega_{i+1,j-1}^{k+1}+\omega_{i-1,j-1}^{k+1}-\omega_{i-1,j+1}^{k+1}}{4\Delta\xi\Delta\eta}\right.\\ &+\left.\left(P+\frac{\xi_x}{x}\right)_{i,j}\frac{\omega_{i+1,j}^{k+1}-\omega_{i-1,j}^{k+1}}{2\Delta\xi} + \left(Q+\frac{\eta_x}{x}\right)_{i,j}\frac{\omega_{i,j+1}^{k+1}-\omega_{i,j-1}^{k+1}}{2\Delta\eta}\right) + (S_\omega)_{i,j} \end{aligned}$$

for $2 \le i \le N-1$ and $2 \le j \le M-1$

To use the iteration technique, it is better to cast the discretized equation in the form

$$A_i^\omega\omega_{i,j-2}^{k+1} + B_i^\omega\omega_{i,j-1}^{k+1} + C_i^\omega\omega_{i,j}^{k+1} + D_i^\omega\omega_{i,j+1}^{k+1} + E_i^\omega\omega_{i,j+2}^{k+1} = F_i^\omega \qquad (4.25)$$

where

$$
\begin{aligned}
A_i^\omega &= A^v \\
B_i^\omega &= B^v - Prg_{i,j}^{22} \\
C_i^\omega &= 2Pr(g_{i,j}^{11} + g_{i,j}^{22}) + \frac{Ste}{\Delta\tau} \\
D_i^\omega &= D^v - Prg_{i,j}^{22} \\
E_i^\omega &= E^v \\
F_i^\omega &= A^u\omega_{i-2,j}^{k+1} + B^u\omega_{i-1,j}^{k+1} + D^u\omega_{i+1,j} + E^u\omega_{i+2,j}^{k+1} \\
&+ Prg_{i,j}^{11}(\omega_{i+1,j}^{k+1} + \omega_{i-1,j}^{k+1}) \\
&+ \frac{1}{2}Prg_{i,j}^{12}(\omega_{i+1,j+1}^{k+1} - \omega_{i+1,j-1}^{k+1} + \omega_{i-1,j-1}^{k+1} - \omega_{i-1,j+1}^{k+1}) \\
&+ \frac{1}{2}Pr\left(P + \frac{\xi_x}{x}\right)_{i,j}(\omega_{i+1,j}^{k+1} - \omega_{i-1,j}^{k+1}) \\
&+ \frac{1}{2}Pr\left(Q + \frac{\eta_x}{x}\right)_{i,j}(\omega_{i,j+1}^{k+1} - \omega_{i,j-1}^{k+1}) + (S_\omega)_{i,j} + \frac{Ste}{\Delta\tau}\omega_{i,j}^k
\end{aligned}
$$

At the grid points adjacent to the boundaries, no $j-2$ and $j+2$ points can be reached. Therefore, we set A_i^ω and E_i^ω equal to zero locally according to the first order upwind scheme. Similarly, for the j direction

$$A_j^\omega\omega_{i-2,j}^{k+1} + B_j^\omega\omega_{i-1,j}^{k+1} + C_j^\omega\omega_{i,j}^{k+1} + D_j^\omega\omega_{i+1,j}^{k+1} + E_j^\omega\omega_{i+2,j}^{k+1} = F_j^\omega \tag{4.26}$$

$$A_j^\omega = A^u$$

$$
\begin{aligned}
B_j^{\omega} &= B^u - Prg_{i,j}^{11} \\
C_j^{\omega} &= 2Pr(g_{i,j}^{11} + g_{i,j}^{22}) + \frac{Ste}{\Delta\tau} \\
D_j^{\omega} &= D^u - Prg_{i,j}^{11} \\
E_j^{\omega} &= E^u \\
F_j^{\omega} &= A^v\omega_{i,j-2}^{k+1} + B^v\omega_{i,j-1}^{k+1} + D^v\omega_{i,j+1} + E^v\omega_{i,j+2}^{k+1} \\
&+ Prg_{i,j}^{22}(\omega_{i,j+1}^{k+1} + \omega_{i,j-1}^{k+1}) \\
&+ \frac{1}{2}Prg_{i,j}^{12}(\omega_{i+1,j+1}^{k+1} - \omega_{i+1,j-1}^{k+1} + \omega_{i-1,j-1}^{k+1} - \omega_{i-1,j+1}^{k+1}) \\
&+ \frac{1}{2}Pr\left(P + \frac{\xi_x}{x}\right)_{i,j}(\omega_{i+1,j}^{k+1} - \omega_{i-1,j}^{k+1}) \\
&+ \frac{1}{2}Pr\left(Q + \frac{\eta_x}{x}\right)_{i,j}(\omega_{i,j+1}^{k+1} - \omega_{i,j-1}^{k+1}) + (S_\omega)_{i,j} + \frac{Ste}{\Delta\tau}\omega_{i,j}^{k}
\end{aligned}
$$

where

$$
\begin{aligned}
(S_\omega)_{i,j} &= -Ste\left((\xi_\tau)_{i,j}\frac{\omega_{i+1,j} - \omega_{i-1,j}}{2\Delta\xi} + (\eta_\tau)_{i,j}\frac{\omega_{i,j+1} - \omega_{i,j-1}}{2\Delta\eta}\right) \\
&+ \left(\frac{U}{x} - \frac{Pr}{x^2}\right)_{i,j}\omega_{i,j} + PrRa\left((\xi_x)_{i,j}\frac{\theta_{i+1,j} - \theta_{i-1,j}}{2\Delta\xi} + (\eta_x)_{i,j}\frac{\theta_{i,j+1} - \theta_{i,j-1}}{2\Delta\xi}\right)
\end{aligned}
$$

Again, at the grid points adjacent to the boundary, A_i^{ω} and E_i^{ω} are equal to zero. The equations (4.25) and (4.26) can be solved by the PDMA technique as discussed in Appendix C. With these two equations, the ADI technique can be used to sweep alternatively in the i and j directions.

For the stream function equation, the conventional central difference scheme has been used.

$$g^{11}_{i,j}\frac{\psi_{i+1,j}-2\psi_{i,j}+\psi_{i-1,j}}{\Delta\eta^2}+g^{22}_{i,j}\frac{\psi_{i,j+1}-2\psi_{i,j}+\psi_{i,j-1}}{\Delta\xi^2} \tag{4.27}$$

$$+2g^{12}_{i,j}\frac{\psi_{i+1,j+1}-\psi_{i+1,j-1}+\psi_{i-1,j-1}-\psi_{i-1,j+1}}{4\Delta\xi\Delta\eta}$$

$$+\left(P+\frac{\xi_x}{x}\right)_{i,j}\frac{\psi_{i+1,j}-\psi_{i-1,j}}{2\Delta\xi}+\left(Q+\frac{\eta_x}{x}\right)_{i,j}\frac{\psi_{i,j+1}-\psi_{i,j-1}}{2\Delta\eta}=(S_\psi)_{i,j}$$

$$A^\psi_i\psi_{i,j-1}+B^\psi_i\psi_{i,j}+C^\psi_i\psi_{i,j+1}=D^\psi_i \tag{4.28}$$

$$\begin{aligned}
A^\psi_i &= -g^{22}_{i,j}\\
B^\psi_i &= 2(g^{11}_{i,j}+g^{22}_{i,j})\\
C^\psi_i &= -g^{22}_{i,j}\\
D^\psi_i &= g^{11}_{i,j}(\psi_{i+1,j}+\psi_{i-1,j})\\
&+ \frac{1}{2}g^{12}_{i,j}(\psi_{i+1,j+1}-\psi_{i+1,j-1}+\psi_{i-1,j-1}-\psi_{i-1,j+1})\\
&+ \frac{1}{2}\left(P+\frac{\xi_x}{x}\right)_{i,j}(\psi_{i+1,j}-\psi_{i-1,j})+\frac{1}{2}\left(Q+\frac{\eta_x}{x}\right)_{i,j}(\psi_{i,j+1}-\psi_{i,j-1})+(S_\psi)_{i,j}
\end{aligned}$$

Similarly for the j direction

$$A^\psi_j\psi_{i-1,j}+B^\psi_j\psi_{i,j}+C^\psi_j\psi_{i+1,j}=D^\psi_j \tag{4.29}$$

$$A^\psi_j = -g^{11}_{i,j}$$

$$
\begin{aligned}
B_j^{\psi} &= 2(g_{i,j}^{11} + g_{i,j}^{22}) \\
C_j^{\psi} &= -g_{i,j}^{11} \\
D_j^{\psi} &= g_{i,j}^{22}(\psi_{i,j+1} + \psi_{i,j-1}) \\
&+ \frac{1}{2} g_{i,j}^{12}(\psi_{i+1,j+1} - \psi_{i+1,j-1} + \psi_{i-1,j-1} - \psi_{i-1,j+1}) \\
&+ \frac{1}{2}\left(P + \frac{\xi_x}{x}\right)_{i,j}(\psi_{i+1,j} - \psi_{i-1,j}) + \frac{1}{2}\left(Q + \frac{\eta_x}{x}\right)_{i,j}(\psi_{i,j+1} - \psi_{i,j-1}) + (S_\psi)_{i,j}
\end{aligned}
$$

where

$$
(S_\psi)_{i,j} = \frac{2}{x}_{i,j}\left((\xi_x)_{i,j}\frac{\psi_{i+1,j} - \psi_{i-1,j}}{2\Delta\xi} + (\eta_x)_{i,j}\frac{\psi_{i,j+1} - \psi_{i,j-1}}{2\Delta\eta}\right) - x_{i,j}\omega_{i,j}
$$

Eqs. (4.28) and (4.29) can be rewritten in the form below for the iteration procedure, and solved by the TDMA method.

The energy equation can be discretized as

$$
\begin{aligned}
&Ste\frac{\theta_{i,j}^{k+1} - \theta_{i,j}^{k}}{\Delta\tau} + A^u\theta_{i-2,j}^{k+1} + B^u\theta_{i-1,j}^{k+1} + C^u\theta_{i,j}^{k+1} + D^u\theta_{i+1,j}^{k+1} + E^u\theta_{i+2,j}^{k+1} \quad (4.30) \\
&+A^v\theta_{i,j-2}^{k+1} + B^v\theta_{i,j-1}^{k+1} + C^v\theta_{i,j}^{k+1} + D^v\theta_{i,j+1}^{k+1} + E^v\theta_{i,j+2}^{k+1} \\
&= g_{i,j}^{11}\frac{\theta_{i+1,j}^{k+1} - 2\theta_{i,j}^{k+1} + \theta_{i-1,j}^{k+1}}{\Delta\eta^2} + g_{i,j}^{22}\frac{\theta_{i,j+1}^{k+1} - 2\theta_{i,j}^{k+1} + \theta_{i,j-1}^{k+1}}{\Delta\xi^2} \\
&+2g_{i,j}^{12}\frac{\theta_{i+1,j+1}^{k+1} - \theta_{i+1,j-1}^{k+1} + \theta_{i-1,j-1}^{k+1} - \theta_{i-1,j+1}^{k+1}}{4\Delta\xi\Delta\eta} \\
&+\left(P + \frac{\xi_x}{x}\right)_{i,j}\frac{\theta_{i+1,j}^{k+1} - \theta_{i-1,j}^{k+1}}{2\Delta\xi} + \left(Q + \frac{\eta_x}{x}\right)_{i,j}\frac{\theta_{i,j+1}^{k+1} - \theta_{i,j-1}^{k+1}}{2\Delta\eta} + (S_\theta)_{i,j}
\end{aligned}
$$

yielding

$$A_i^\theta \theta_{i,j-2}^{k+1} + B_i^\theta \theta_{i,j-1}^{k+1} + C_i^\theta \theta_{i,j}^{k+1} + D_i^\theta \theta_{i,j+1}^{k+1} + E_i^\theta \theta_{i,j+2}^{k+1} = F_i^\theta \qquad (4.31)$$

where

$$\begin{aligned}
A_i^\theta &= A^v \\
B_i^\theta &= B^v - g_{i,j}^{22} \\
C_i^\theta &= 2(g_{i,j}^{11} + g_{i,j}^{22}) + \frac{Ste}{\Delta\tau} \\
D_i^\theta &= D^v - g_{i,j}^{22} \\
E_i^\theta &= E^v \\
F_i^\theta &= A^u \theta_{i-2,j}^{k+1} + B^u \theta_{i-1,j}^{k+1} + D^u \theta_{i+1,j} + E^u \theta_{i+2,j}^{k+1} \\
&+ g_{i,j}^{11}(\theta_{i+1,j}^{k+1} + \theta_{i-1,j}^{k+1}) \\
&+ \frac{1}{2} g_{i,j}^{12}(\theta_{i+1,j+1}^{k+1} - \theta_{i+1,j-1}^{k+1} + \theta_{i-1,j-1}^{k+1} - \theta_{i-1,j+1}^{k+1}) \\
&+ \frac{1}{2}\left(P + \frac{\xi_x}{x}\right)_{i,j} (\theta_{i+1,j}^{k+1} - \theta_{i-1,j}^{k+1}) \\
&+ \frac{1}{2}\left(Q + \frac{\eta_x}{x}\right)_{i,j} (\theta_{i,j+1}^{k+1} - \theta_{i,j-1}^{k+1}) + (S_\theta)_{i,j} + \frac{Ste}{\Delta\tau}\theta_{i,j}^k
\end{aligned}$$

Similarly, for the j direction, one gets

$$A_j^\theta \theta_{i-2,j}^{k+1} + B_j^\theta \theta_{i-1,j}^{k+1} + C_j^\theta \theta_{i,j}^{k+1} + D_j^\theta \theta_{i+1,j}^{k+1} + E_j^\theta \theta_{i+2,j}^{k+1} = F_j^\theta \qquad (4.32)$$

with

$$
\begin{aligned}
A_j^\theta &= A^u \\
B_j^\theta &= B^u - g_{i,j}^{11} \\
C_j^\theta &= 2(g_{i,j}^{11} + g_{i,j}^{22}) + \frac{Ste}{\Delta\tau} \\
D_j^\theta &= D^u - g_{i,j}^{11} \\
E_j^\theta &= E^u \\
F_j^\theta &= A^v\theta_{i,j-2}^{k+1} + B^v\theta_{i,j-1}^{k+1} + D^v\theta_{i,j+1} + E^v\theta_{i,j+2}^{k+1} \\
&+ g_{i,j}^{22}(\theta_{i,j+1}^{k+1} + \theta_{i,j-1}^{k+1}) \\
&+ \frac{1}{2}g_{i,j}^{12}(\theta_{i+1,j+1}^{k+1} - \theta_{i+1,j-1}^{k+1} + \theta_{i-1,j-1}^{k+1} - \theta_{i-1,j+1}^{k+1}) \\
&+ \frac{1}{2}\left(P + \frac{\xi_x}{x}\right)_{i,j}(\theta_{i+1,j}^{k+1} - \theta_{i-1,j}^{k+1}) \\
&+ \frac{1}{2}\left(Q + \frac{\eta_x}{x}\right)_{i,j}(\theta_{i,j+1}^{k+1} - \theta_{i,j-1}^{k+1}) + (S_\theta)_{i,j} + \frac{Ste}{\Delta\tau}\theta_{i,j}^k
\end{aligned}
$$

where

$$
(S_\theta)_{i,j} = -Ste\left((\xi_\tau)_{i,j}\frac{\theta_{i+1,j} - \theta_{i-1,j}}{2\Delta\xi} + (\eta_\tau)_{i,j}\frac{\theta_{i,j+1} - \theta_{i,j-1}}{2\Delta\eta}\right)
$$

The same iteration technique can be used to solve for solving the energy equation.

4.1.5.2 Discretized Boundary Conditions

Since the no-slip boundary condition is imposed on the discretized solid wall, the velocity components and stream function are set to zero. The boundary conditions for the vorticity are therefore

$$\begin{aligned}\omega_{1,j} &= \frac{1}{2}\left((\xi_x)_{1,j}(-3V_{1,j}+4V_{2,j}-V_{3,j})\right. \\ &\quad \left.-(\xi_y)_{1,j}(-3U_{1,j}+4U_{2,j}-U_{3,j})\right)\end{aligned} \tag{4.33}$$

$$\begin{aligned}\omega_{N,j} &= \frac{1}{2}\left((\xi_x)_{N,j}(3V_{N,j}-4V_{N-1,j}-V_{N-2,j})\right. \\ &\quad \left.-(\xi_y)_{N,j}(3U_{N,j}-4U_{N-1,j}-U_{N-2,j})\right)\end{aligned} \tag{4.34}$$

$$2 \le j \le M-1$$

$$\begin{aligned}\omega_{i,1} &= \frac{1}{2}\left((\eta_x)_{i,1}(-3V_{i,1}+4V_{i,2}-V_{i,3})\right. \\ &\quad \left.-(\eta_y)_{i,1}(-3U_{i,1}+4U_{i,2}-U_{i,3})\right)\end{aligned} \tag{4.35}$$

$$\begin{aligned}\omega_{i,M} &= \frac{1}{2}\left((\eta_x)_{i,M}(3V_{i,M}+4V_{i,M-1}-V_{i,M-2})\right. \\ &\quad \left.-(\eta_y)_{i,M}(3U_{i,M}+4U_{i,M-1}-U_{i,M-2})\right)\end{aligned} \tag{4.36}$$

$$2 \le i \le N-1$$

The boundary conditions for the energy equation are the following: at the heated wall and interface, the dimensionless temperature are equal to 1 and 0, respectively. The adiabatic boundary conditions at the top and bottom of the cylinder can be expressed as

$$g^{22}\frac{\partial\theta}{\partial\eta} + g^{12}\frac{\partial\theta}{\partial\xi} = 0$$

The discretized forms are

$$\theta_{i,1} = \frac{1}{3}\left(g^{12}_{i,1}/g^{22}_{i,1}(\theta_{i+1,1} - \theta_{i-1,1}) - \theta_{i,3} + 4\theta_{i,2})\right) \tag{4.37}$$

$$\theta_{i,M} = \frac{1}{3}\left(g^{12}_{i,M}/g^{22}_{i,M}(\theta_{i+1,M} - \theta_{i-1,M}) - \theta_{i,M-2} + 4\theta_{i,M-1})\right) \tag{4.38}$$

$$2 \leq i \leq N-1$$

where the forward and backward difference formulae are used.

4.1.5.3 Discretized Interface Equations

There are two possibilities to describe the interface moving on the computation domain, either moving from $\xi = const.$ line or moving form $\eta = const.$ line. If the interface is chosen on the $\xi = \alpha$ line, the discretized interface moving equations are

$$x_{\alpha,j} = (x_0)_{\alpha,j} - \left(\xi_x\frac{\partial\theta}{\partial\xi} + \eta_x\frac{\partial\theta}{\partial\eta}\right)_{\alpha,j}\Delta\tau \tag{4.39}$$

$$y_{\alpha,j} = (y_0)_{\alpha,j} - \left(\xi_y\frac{\partial\theta}{\partial\xi} + \eta_y\frac{\partial\theta}{\partial\eta}\right)_{\alpha,j}\Delta\tau \tag{4.40}$$

where x_0 and y_0 are the coordinates on the physical domain before the motion begins and $\Delta\tau$ is the time step. In our study, $\alpha = N$ for the outward melting and $\alpha = 1$ for the inward melting.

If the interface is chosen to be on the $\eta = \gamma$ line, the discretized interface moving equations become

$$x_{i,\gamma} = (x_0)_{i,\gamma} - \Delta\tau \left(\xi_x \frac{\partial\theta}{\partial\xi} + \eta_x \frac{\partial\theta}{\partial\eta} \right)_{i,\gamma} \tag{4.41}$$

$$y_{i,\gamma} = (y_0)_{i,\gamma} - \Delta\tau \left(\xi_y \frac{\partial\theta}{\partial\xi} + \eta_y \frac{\partial\theta}{\partial\eta} \right)_{i,\gamma} \tag{4.42}$$

The temperature gradients $\partial\theta/\partial\xi$ and $\partial\theta/\partial\eta$ should be discretized according to the forward or backward difference formula depending on whether α or γ is the lowest bound or the highest bound.

4.1.6 Numerical Procedure

The general solution procedure, as described by the flow chart in Fig 4.2, consists of the following steps.

1. Set initial values of all the variables $U_{i,j}, V_{i,j}, \omega_{i,j}$ and $\psi_{i,j}$ equal to zero. The initial temperature field is set such that it is equal to zero everywhere except at the heated boundary where the nodal temperatures are all equal to 1.

2. Set the initial boundary grid points of the physical domain to be transformed.

3. Call the grid generator to generate grid points on the physical domain.

4. Calculate all the transformation factors which will be used in the solution of the transformed equations.

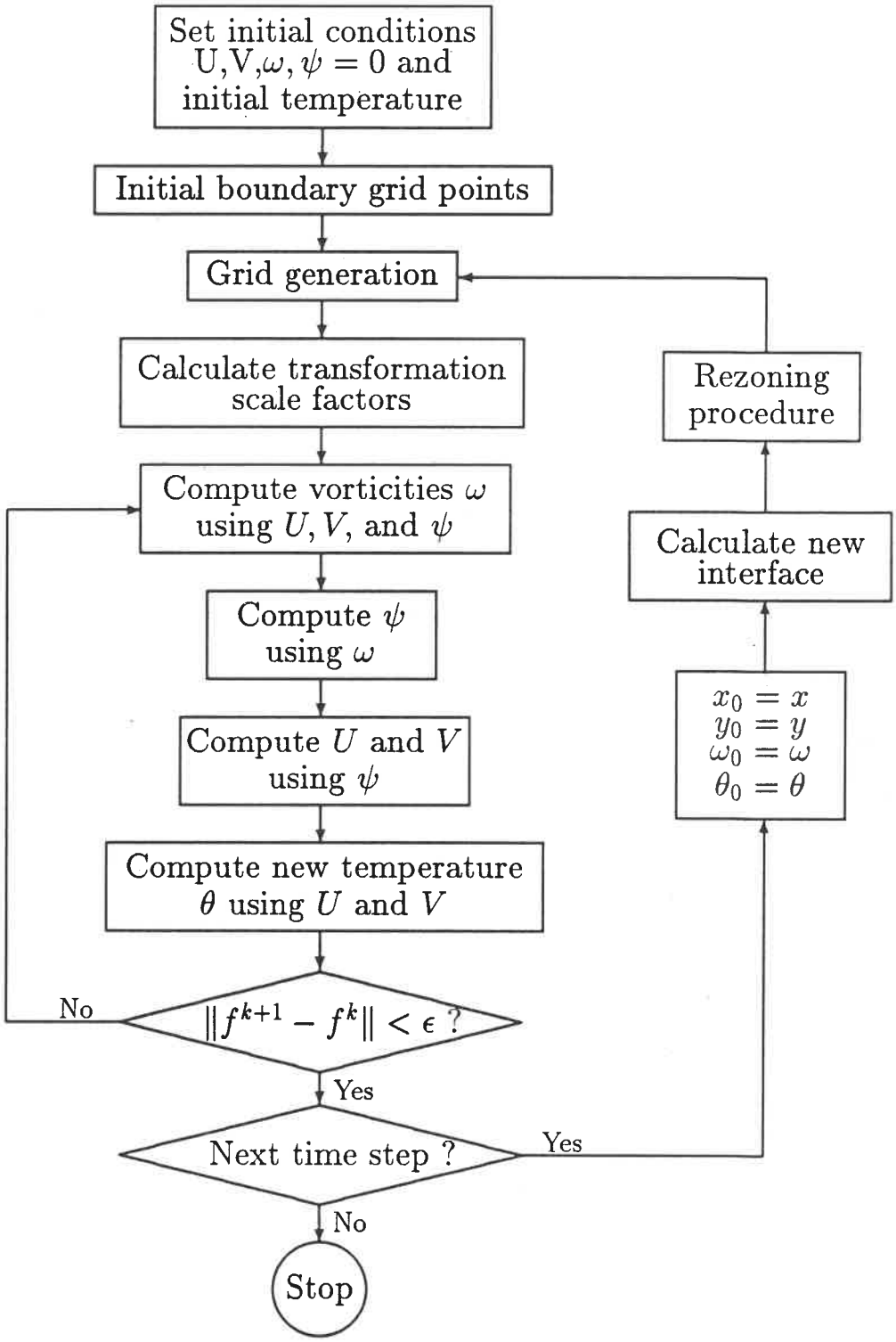

Figure 4.2: Flow chart of computation procedure

5. Compute vorticities by using $U_{i,j}, V_{i,j}, \psi_{i,j}$ and $\theta_{i,j}$. The computation is performed by alternatively sweeping in the i and j directions.

6. Compute the stream functions by using the updated vorticities $\omega_{i,j}$.

7. Compute $U_{i,j}, V_{i,j}$ by using the updated $\psi_{i,j}$ and velocity boundary conditions.

8. Compute the new temperatures $\theta_{i,j}$ by using $U_{i,j}, V_{i,j}$.

9. Check convergence. In the iteration, we only check the vorticity and energy equations since the other equations converge much faster than these two. There are two checkers. One checks the residue of the continuity equation on the all grid points

$$\sum_{i}^{N}\sum_{j}^{M} Residue \leq 10^{-4} \tag{4.43}$$

The other checker is

$$\|f_{i,j}^{k+1} - f_{i,j}^{k}\| \leq 10^{-4} \tag{4.44}$$

where f denotes vorticities and temperature.

10. If the convergence criteria are satisfied, go to step 11. Otherwise go back to step 4, for further iteration.

11. Check whether the maximum time step has been reached. If so, go to step 16. If not, go to step 12.

12. Update x_0, y_0, ω_0 and θ_0 for the next time step.

13. Calculate the new interface position from the moving interface equations.

14. After obtaining the new interface, call a rezoning procedure (to be discussed below).

15. Go to step 3 to begin the next time step computation.

16. Stop the program.

4.1.7 Rezoning Procedure

According to the energy balance equation, the local velocity of the interface should be locally orthogonal to the interface. Generally, the melting is nonuniform along the interface because of the natural convection. Therefore, the interface can become curved as the boundary is moving. If the interface becomes locally convex, all the moving interface grid points have tendencies to move towards their reflex center. As the melting proceeds, sooner or later, the generated grids could be distorted or even overlapped under some circumstances.

To overcome these difficulties, an implicit rezoning procedure is employed. Once the interface is determined at time level $\tau + \Delta\tau$, a spline interpolation is used to redistribute the boundary grid points at equal arc length interval along the interface. Thereby, a proper grid network system can be created by the generator.

4.1.8 Results and Discussion

The computation is started by assuming the existence of a very thin melt layer around the cylinder. The molten volume is assumed to be sufficiently small for the results to be unaffected. The melting process begins from the cylinder wall into the environment where the solid is assumed to be at its fusion temperature.

Advance in time is made with a step of $O(10^{-3})$. The number of grid points is chosen to be 11×31. The typical case of melting of the sodium nitrate-sodium hydroxide eutectic is presented here to compare with the previous results [52] obtained by a different approach.

Fig. 4.3 and 4.4 show the isotherms and streamlines in the melt region at various times. The values of the governing parameters are $Ra = 7\times^4, Pr = 7.0, Ste = 0.15$ and $A = 4$.

Fig. 4.3(a) shows the isotherms and flow pattern at time $\tau = 0.03$: one can note from this figure that the melting profile is almost a vertical line, and isotherms are almost parallel, reflecting the fact that conduction is the dominant mechanism of heat transfer at this very early time.

Fig. 4.3(b) shows the isotherms and flow pattern at time $\tau = 0.09$: as the melt layer becomes thicker, the convective motion becomes stronger and its effects on the heat transfer are revealed by the distorted isotherms and melting profiles near the top region. All these effects are enhanced as the melting progresses, as can be seen from figures 4.4(c) and 4.4(d), corresponding to $\tau = 0.20$ and $\tau = 0.28$ at which the thickness of the melt in the upper part is almost twice that in the lower part.

An overview of the progression of the melting process is given in Fig. 4.5 which shows the positions of the solid-liquid interface at successive times $\tau = 0.03$, 0.09, 0.20, 0.28. Also shown in this figure are the positions of the interface obtained by Sparrow *et al* [52] in a previous study. One can readily notice that our results and those of Sparrow et al [52] only agree during the early times ($\tau < 0.05$) when the convective flow is still relatively weak. As convection becomes important, the discrepancies become larger in the two aspects. The melt profiles are quite

different between the two groups of results. In our predictions, the melt profiles near the top boundary appear as curved and normal up to the boundary where an adiabatic condition is encountered, instead of straight lines inclining to the upper boundary under the same boundary conditions. The latter results may be caused by the approximations used in the study of Sparrow et al [52], namely:

- The quasi-static approximation which neglected the "pseudo-convection" terms that appeared in the set of transformed equations.
- The "smooth interface" approximations which neglected all terms involving the first and second order derivatives of the radial interface position with respect to the vertical coordinate.

The curvatures of melting profiles can be seen in the experimental investigation by Hale and Viskanta[35] shown in Fig.4.6.

The heat transfer rates are presented in Fig. 4.7. The average Nusselt number along the cylinder wall is defined as

$$Nu = \frac{1}{A}\int_0^A -\frac{\partial\theta}{\partial r}\Big|_{r=1} dz \tag{4.45}$$

The results are compared with [52]. For the early stage of melting, the Nusselt numbers agree very well ($\tau < 0.08$). But for later times, our results are larger than those predicted in [52]. These discrepancies may be explained by the same reasons mentioned above.

4.2 Melting Around A Cylinder Subject To A Constant Heat Flux

In many industry practices, the temperature of the heated wall may not be known or not readily be controlled. Instead one may know the heat flux imputed into the system. For a constant heat flux boundary condition, we can change the boundary condition $\theta = 1$ at the heated wall by

$$\frac{\partial \theta}{\partial \xi} = const. \tag{4.46}$$

The computations have also been carried out with the boundary condition of constant heat flux corresponding to three different Rayleigh numbers, $Ra = 7\times10^6, 7\times10^7, 7\times10^8$. The isotherms and flow pattern for the case of $Ra = 7\times10^8$ are presented in Fig. 4.8. The Nusselt numbers for a constant heat flux is defined as

$$Nu = \frac{1}{A}\int_0^A \frac{1}{\theta}\Big|_{\tau=1} dz \tag{4.47}$$

The Nusselt numbers for the three cases are plotted in Fig. 4.9. As shown, the heat transfer rates are dramatically decreased at the very beginning of the melting process. After reaching a minimum, the heat transfer rates increase as natural convection grows stronger. The larger the Rayleigh number, the stronger the heat transport. As the Rayleigh number increases, the time at which convection becomes dominant decreases. For $Ra = 7 \times 10^4$, the convection becomes dominant for $\tau = 0.05$, and for $Ra = 7 \times 10^8$, $\tau = 0.03$. For the larger time scale, when the boundary layer regime is established, the Nusselt number reaches

a constant value. The correlation between the average Nusselt number and the Raleigh number is

$$Nu = 0.175 Ra^{1/4} \tag{4.48}$$

The variations of molten volume fractions are plotted in Fig. 4.10

4.3 Inward Melting of A Vertical Cylinder

Using the same governing equations as in the previous section, we have considered the problem of inward melting of a vertical cylinder heated at a fixed temperature. The boundary conditions appear for this case are

For $R > 0$

$$\xi = \xi_{min} \tag{4.49}$$

$$U = 0; \qquad V = 0;$$

$$\psi = 0; \qquad \theta = 0;$$

$$\omega = \xi_x V_\xi - \xi_y U_\xi$$

For $R = 0$

$$\xi = \xi_{min} \tag{4.50}$$

$$U = 0; \quad \frac{\partial V}{\partial \xi} = 0;$$

$$\frac{\partial \psi}{\partial \xi} = 0; \quad \frac{\partial \theta}{\partial x} = 0;$$

$$\omega = 0$$

The other boundaries at the top and bottom of the cylinder are assigned the same conditions as before. The control parameters considered are $Pr = 7.0$, $Ste = 0.15$, $A = 2.0$, $Ra = 7 \times 10^4$, $Ra = 7 \times 10^5$ and $Ra = 7 \times 10^6$. The isotherms and flow patterns are presented in Fig. (4.11)-(4.16). From these figures, one can see that at the very beginning of the melting, heat conduction is predominant, which is reflected in the vertical melting profiles in Fig. 4.11(a) and 4.11(b). After a while, the convective heat transfer becomes stronger and the melting profiles become distorted. When the melting profiles reach the symmetry axis, an adiabatic-like boundary is encountered. Therefore, the isotherms are normal to the symmetry axis.

The melting profiles are plotted in Fig. 4.17, which shows that at the early stage, the three cases have almost the same vertical profiles except for the top region. After convection becomes important, the larger the Rayleigh number, the faster the melting velocities are. This can also be seen from the molten volume fraction plotted in Fig. 4.18. The Nusselt numbers for the three cases are plotted in Fig. 4.19(a,b,c). For the case of $Ra = 7 \times 10^4$, the Nusselt number decreases monotonically; for the other cases, the Nusselt numbers decrease at first; and after reaching their minimum values, they increase and then decrease again. The variations of the Nusselt number with time can be explained as follows: at the very beginning of the melting, conduction is dominant and the heat transfer rate decreases with time. After the natural convection begins, the heat transfer rate increases. As the melt region thickens, the boundary layer are formed, as illustrated by the isotherms, the heat transfer rate is delayed, and the Nusselt number decreases thereafter. During this period, heat is transported by both conduction and convection.

From Fig. 4.19(c), one can find oscillations of the Nusselt number that may

be caused by the strong natural convection.

4.4 SUMMARY

The melting of a solid material surrounding a heated vertical cylinder has been numerically investigated. The technique of boundary-fitted coordinates has been effectively applied to treat an irregular domain. The nonlinear Navier-Stockes and energy equations were solved numerically. The convective terms in the transport equations were treated by the second-order upwind scheme. Results have been obtained for the convective flow and temperature fields at various times during the melting process. A comparison with the results obtained previously by Sparrow *et al* [52] shows that the "quasi-static" and "smooth interface" approximations can significantly affect the form and the velocity of the melting profile, especially at later times when natural convection becomes important compared to conduction.

The melting process with a constant heat flux was also studied, for Rayleigh numbers from 7×10^6 to 7×10^8. The variations of Nusselt number with time clearly describe the strong influence of Rayleigh number during the melting process.

Inward melting in a cylindrical enclosure was also investigated. The flow pattern and isotherms as well as the Nusselt numbers were presented. For Rayleigh number varying between 7×10^4 and 7×10^6, the Nusselt number shows an oscillating behavior.

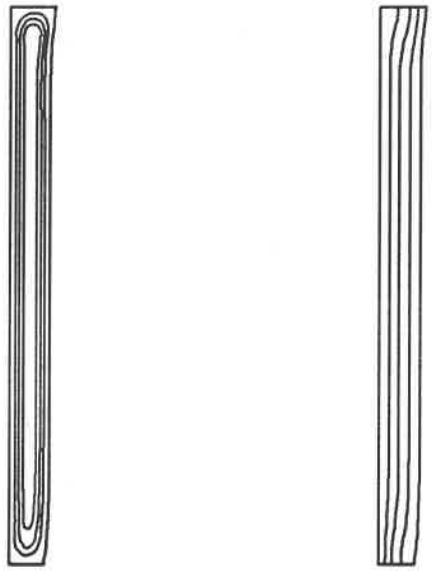

$\tau = 0.03$

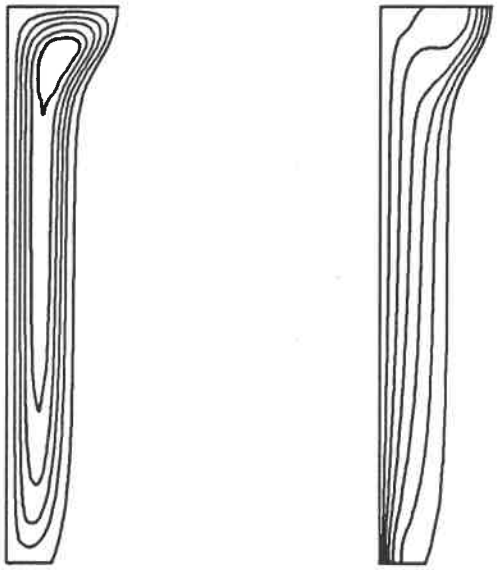

$\tau = 0.09$

Figure 4.3: Isotherms and flow pattern for outward melting of a cylinder at $Pr = 7, Ra = 7 \times 10^4$ and $Ste = 0.15$ and $\tau = 0.03 \sim 0.09$.

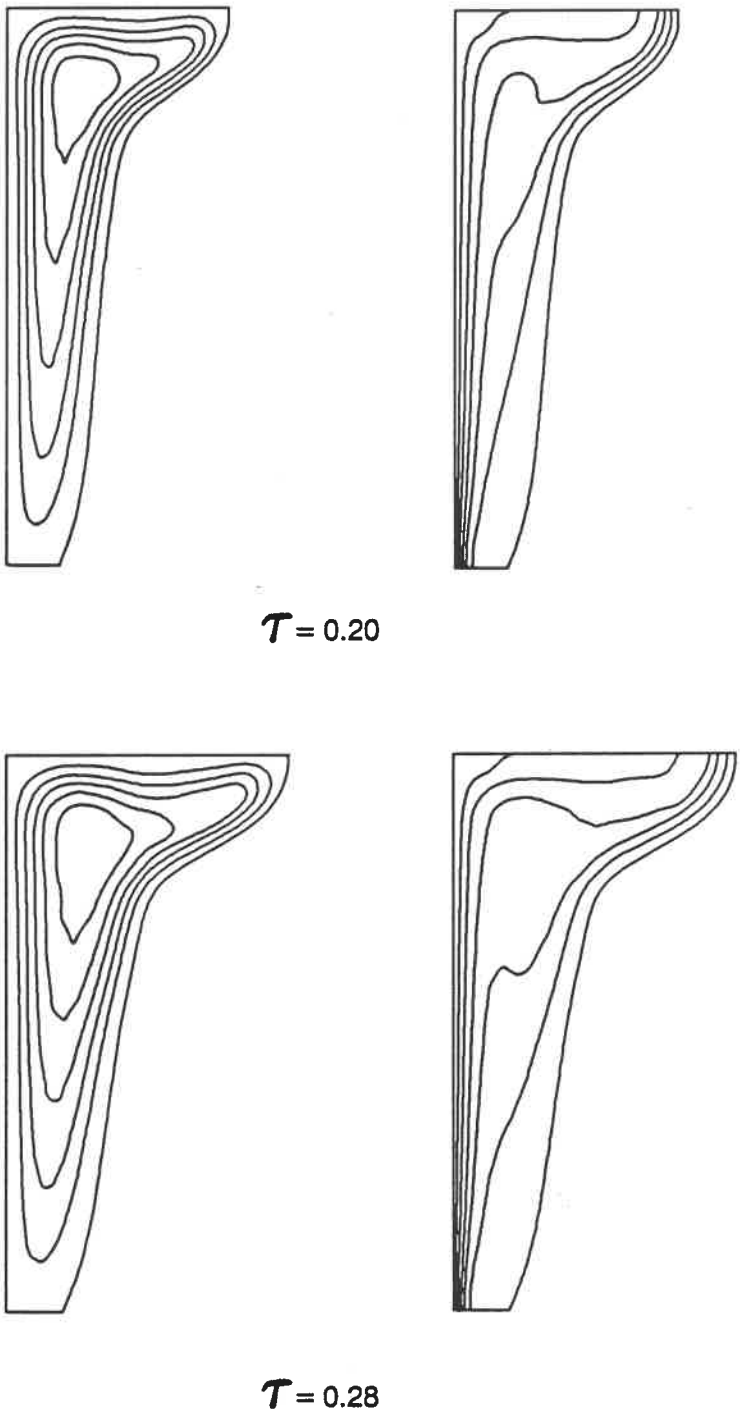

Figure 4.4: Isotherms and flow pattern for outward melting of a cylinder at $Pr = 7, Ra = 7 \times 10^4$ and $Ste = 0.15$ and $\tau = 0.20 \sim 0.28$.

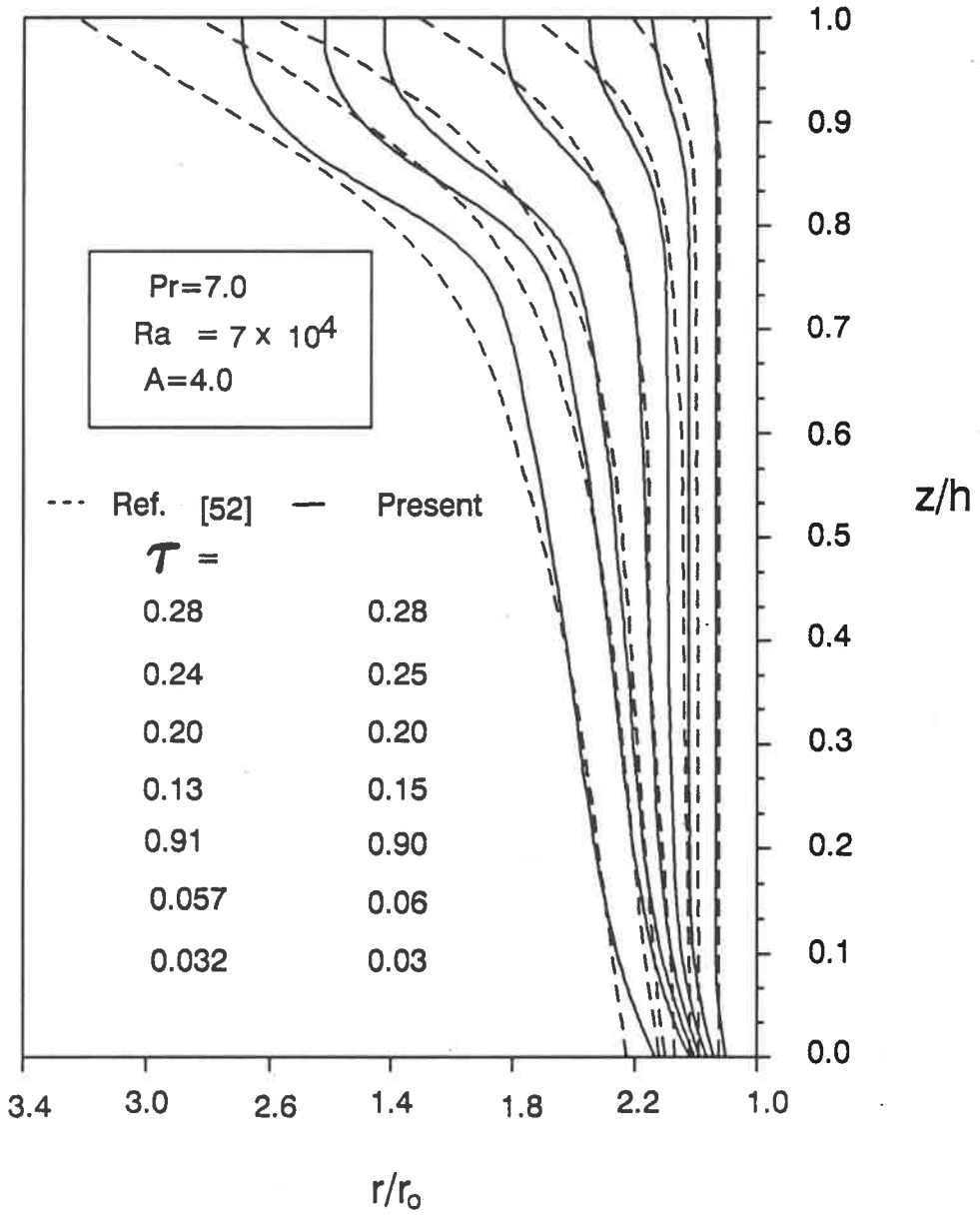

Figure 4.5: Comparison of the predicted melting front profiles with Sparrow *et al* [52].

Figure 4.6: Photographs illustrating the melting front by Hale and Viskanta [34].

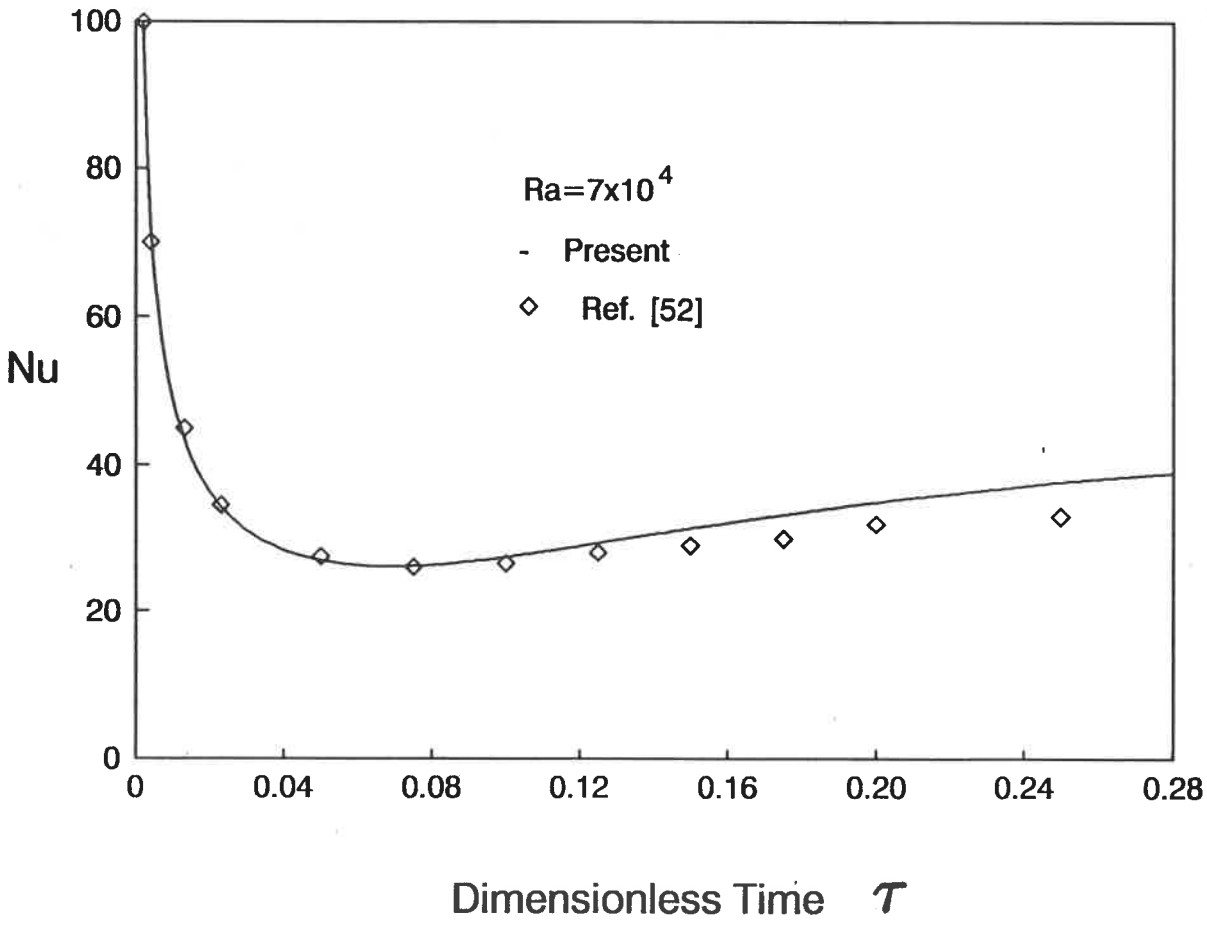

Figure 4.7: Comparison of the predicted Nusselt numbers as function of time with Sparrow *et al*[52].

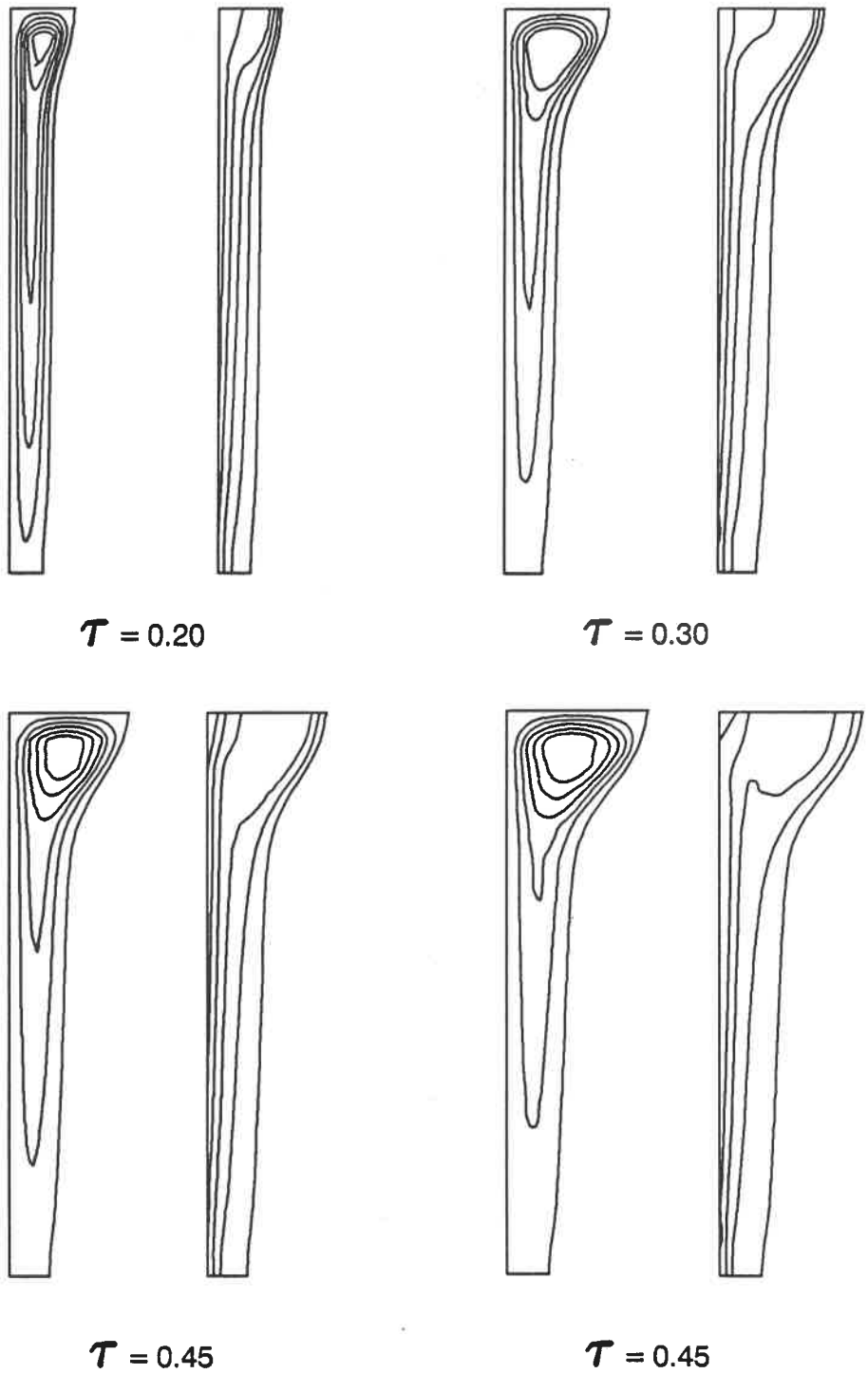

Figure 4.8: Predicted isotherms and flow patterns for $Ra = 7 \times 10^8$ at various times with a constant flux boundary condition.

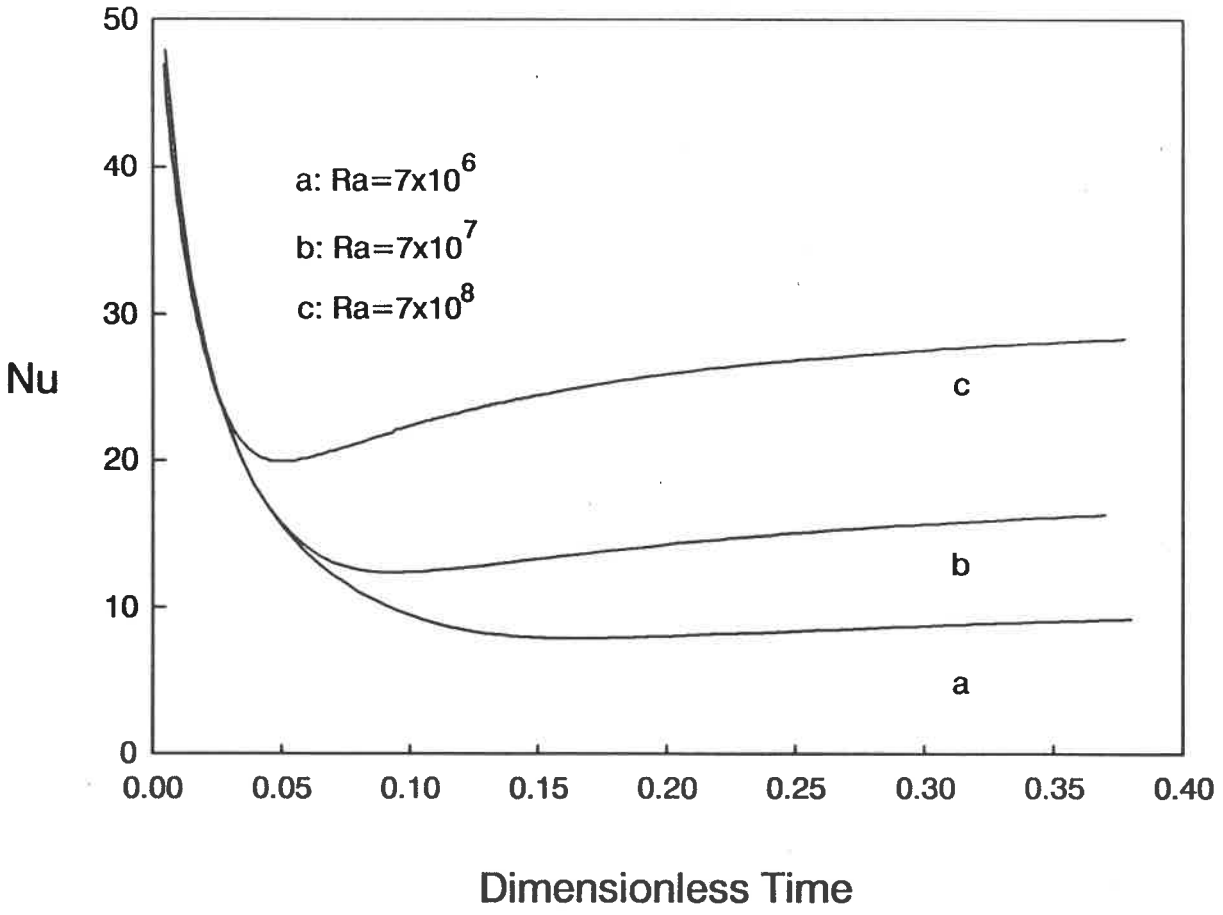

Figure 4.9: Average Nusselt numbers at the cylinder wall as function of time with a constant heat flux boundary condition, $Ra = 7 \times 10^6$, $Ra = 7 \times 10^7$ and $Ra = 7 \times 10^8$.

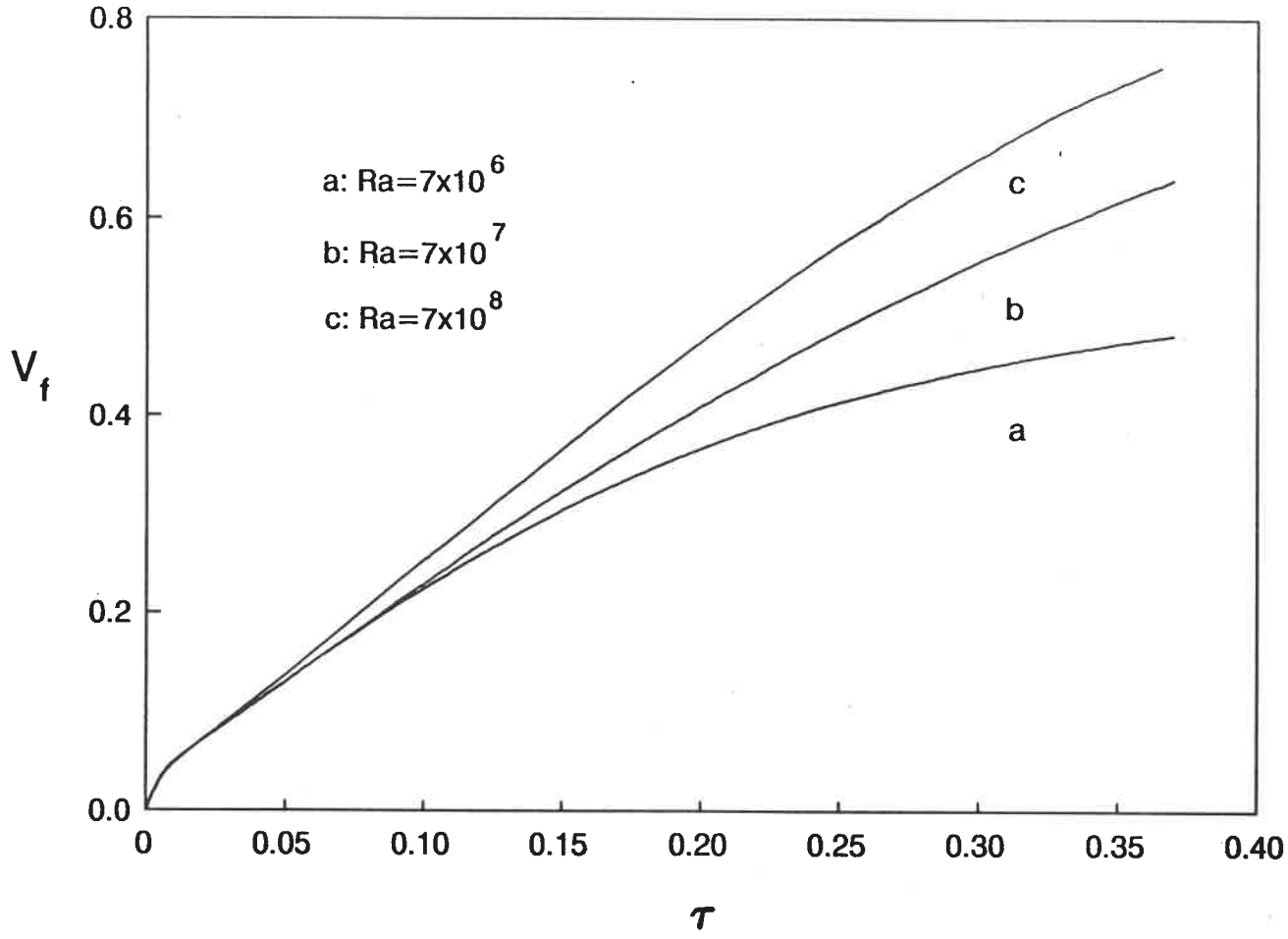

Figure 4.10: Molten volume fractions as function of time with a constant heat flux boundary condition, $Ra = 7 \times 10^6$, $Ra = 7 \times 10^7$ and $Ra = 7 \times 10^8$.

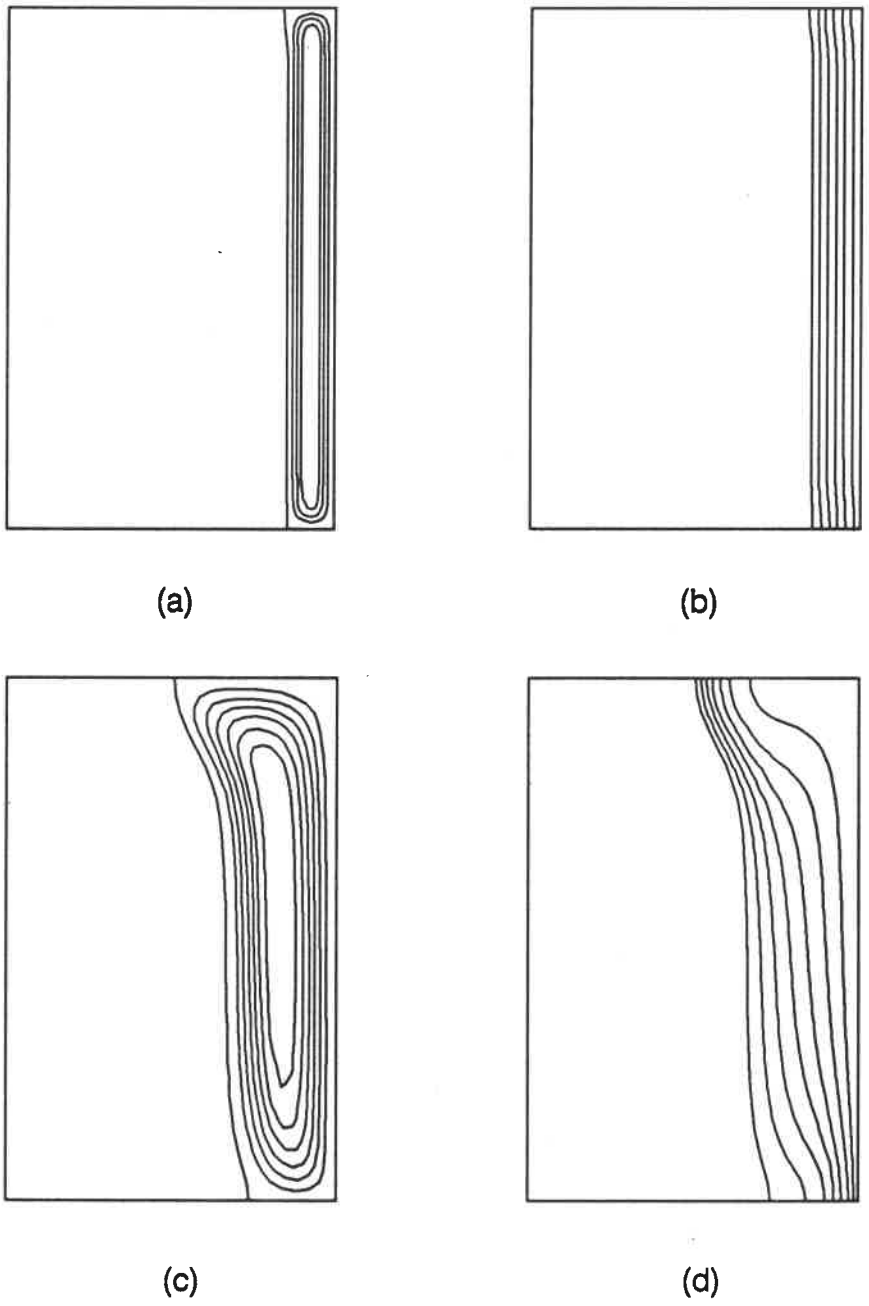

Figure 4.11: Isotherms and flow pattern for inward melting of a cylinder at $Ra = 7 \times 10^4$, $Ste = 0.15$ and $\tau = 0.01 \sim \tau = 0.05$.

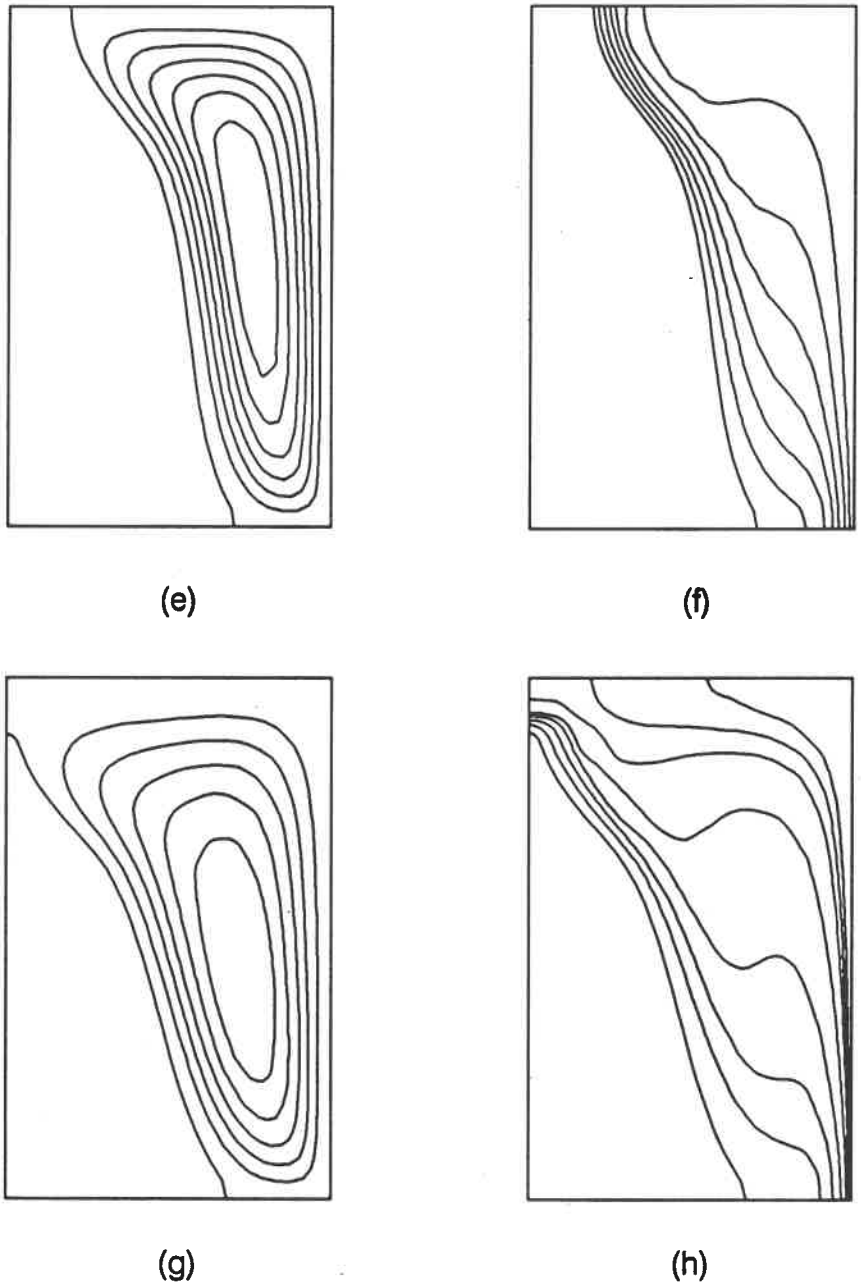

Figure 4.12: Isotherms and flow pattern for inward melting of a cylinder at $Ra = 7 \times 10^4$, $Ste = 0.15$ and $\tau = 0.08 \sim \tau = 0.10$.

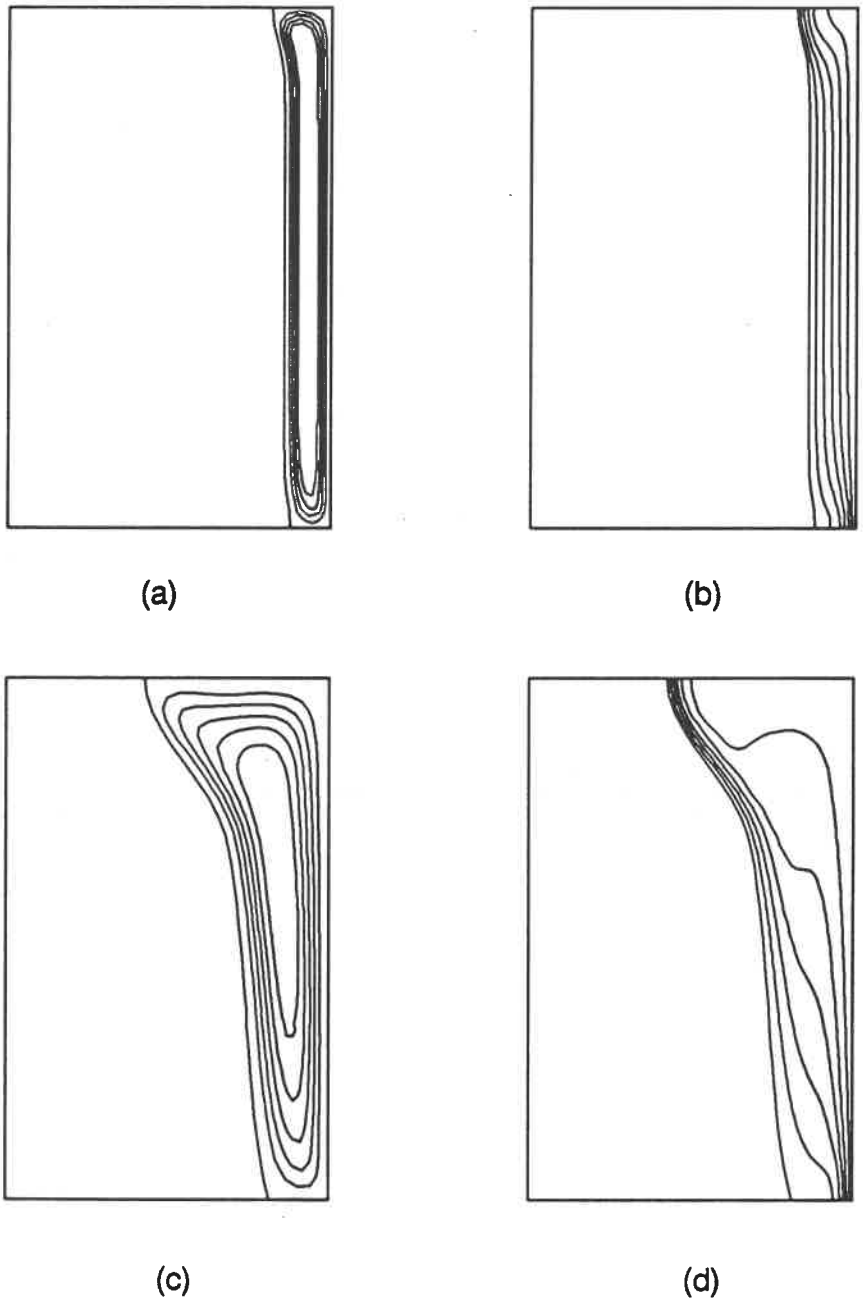

Figure 4.13: Isotherms and flow pattern for inward melting of a cylinder at $Ra = 7 \times 10^5$, $Ste = 0.15$ and $\tau = 0.01 \sim \tau = 0.03$.

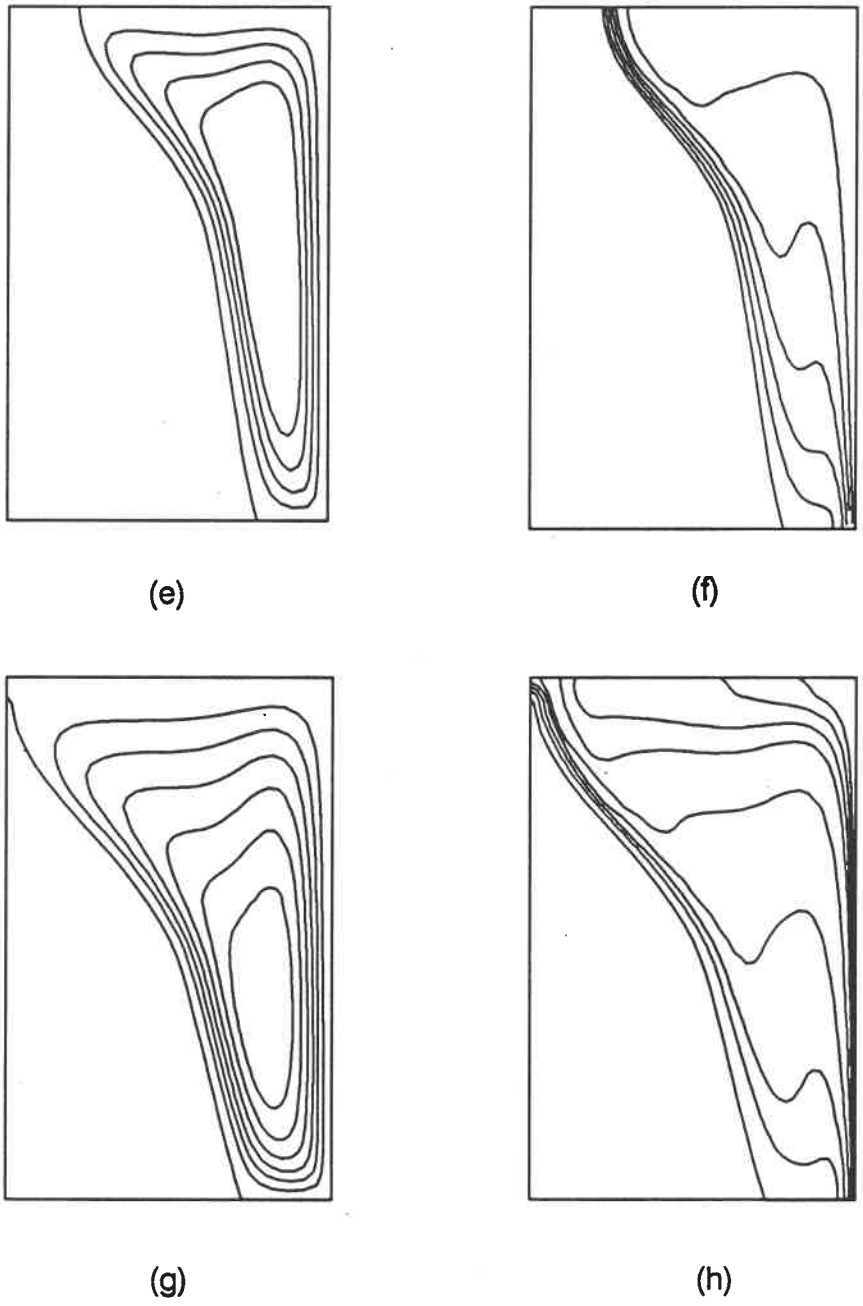

Figure 4.14: Isotherms and flow pattern for inward melting of a cylinder at $Ra = 7 \times 10^5$, $Ste = 0.15$ and $\tau = 0.04 \sim \tau = 0.05$.

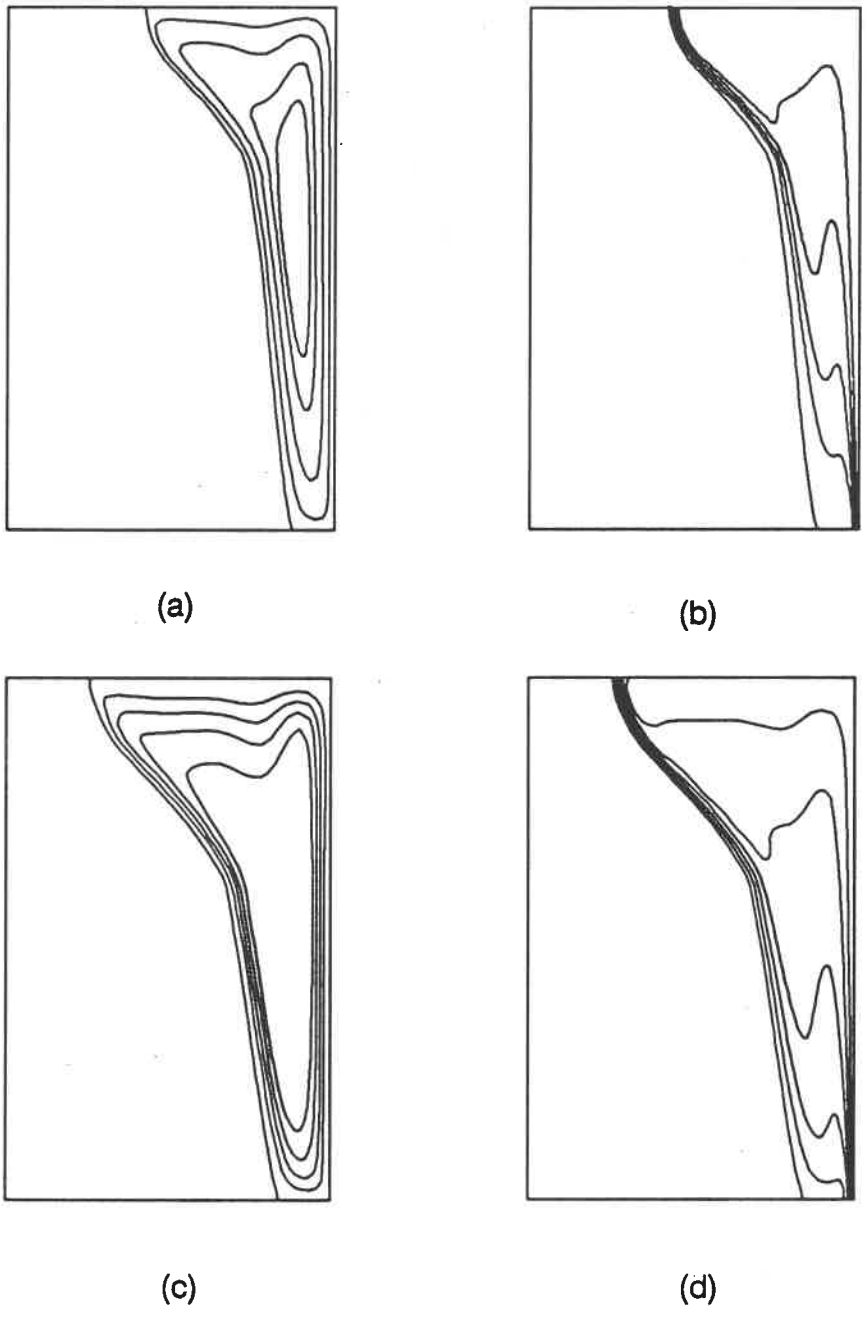

Figure 4.15: Isotherms and flow pattern for inward melting of a cylinder at $Ra = 7 \times 10^6$, $Ste = 0.15$ and $\tau = 0.01 \sim \tau = 0.02$.

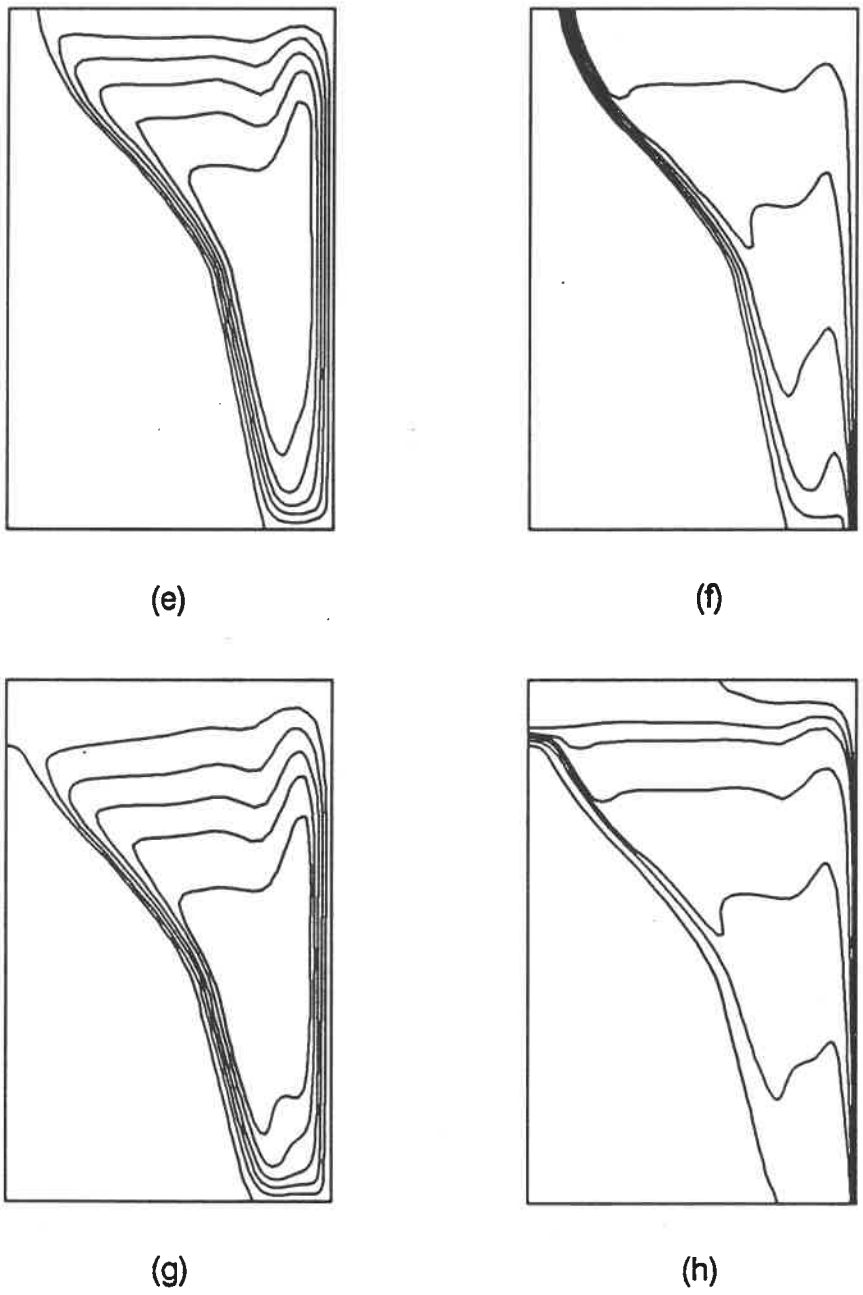

Figure 4.16: Isotherms and flow pattern for inward melting of a cylinder at $Ra = 7 \times 10^6$, $Ste = 0.15$ and $\tau = 0.025 \sim \tau = 0.03$.

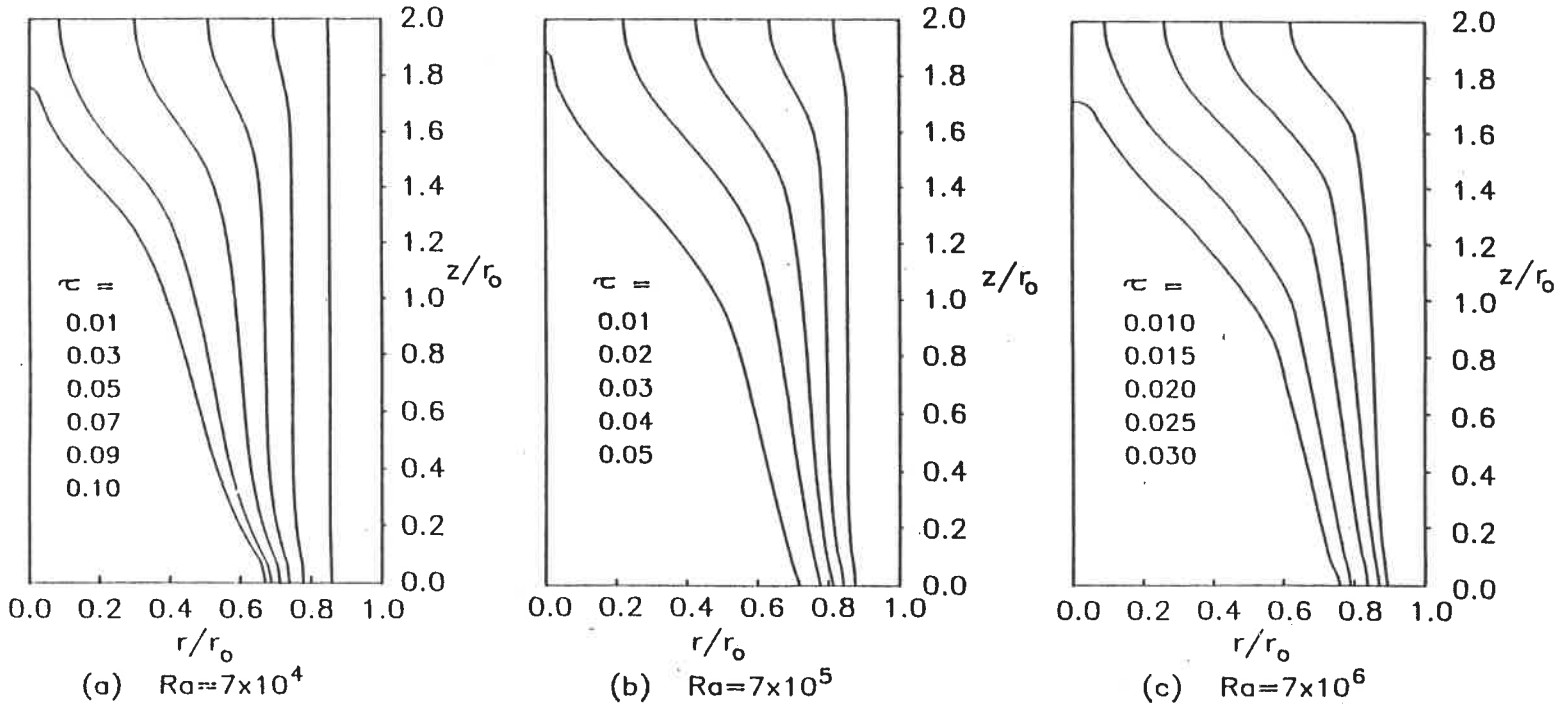

Figure 4.17: Predicted melting profiles for the cases of $Ra = 7 \times 10^4$, $Ra = 7 \times 10^5$ and $Ra = 7 \times 10^6$.

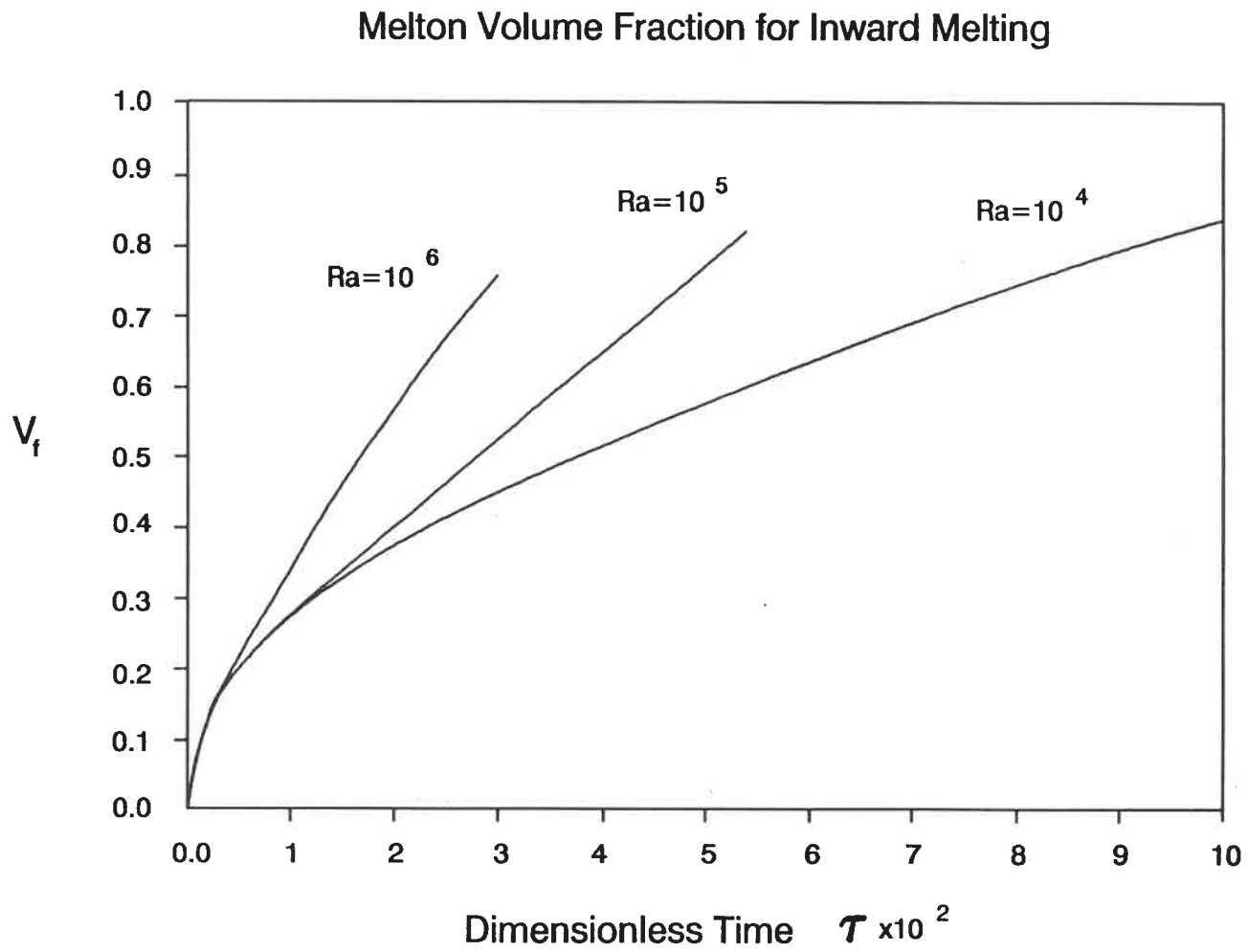

Figure 4.18: Molten volume fractions for the cases of $Ra = 7 \times 10^4$, $Ra = 7 \times 10^5$ and $Ra = 7 \times 10^6$.

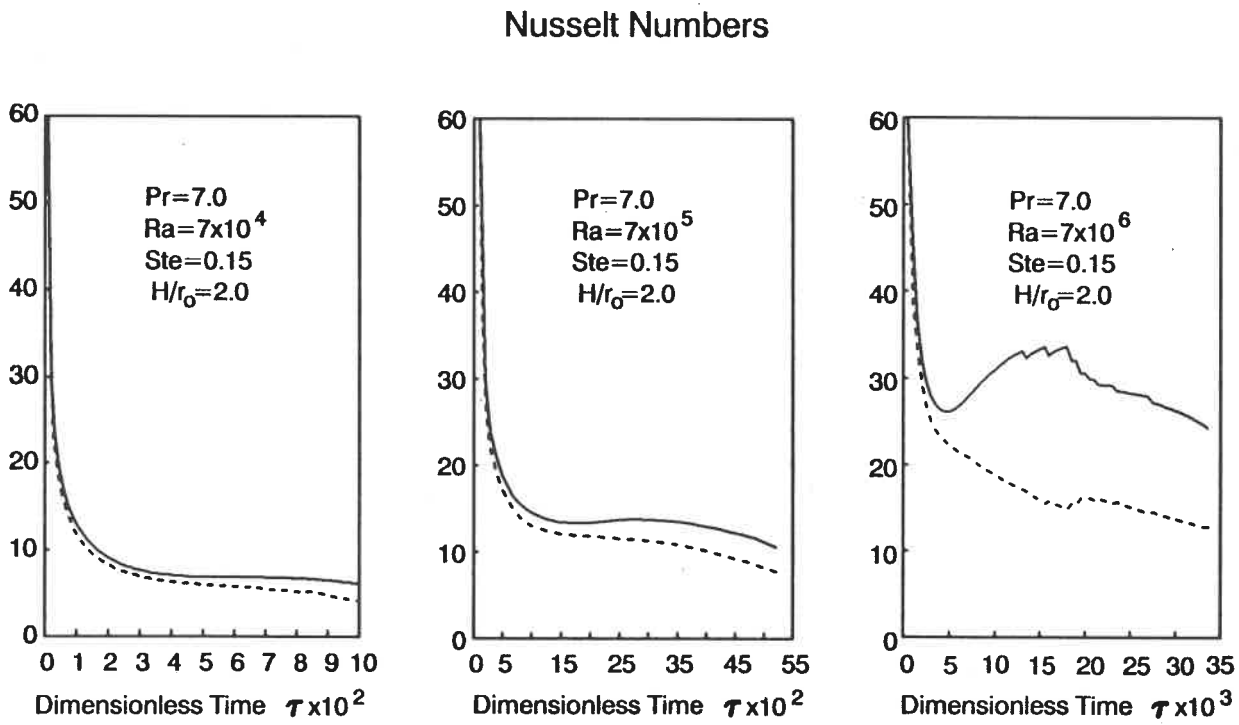

Figure 4.19: Average Nusselt numbers of inward melting for the cases of $Ra = 7 \times 10^4$, $Ra = 7 \times 10^5$ and $Ra = 7 \times 10^6$.

Chapter 5

MELTING OF A VERTICAL CYLINDER HEATED FROM BELOW

Melting in and around a vertical cylinder with side heating is always accompanied by natural convection because of the fact that the hot fluid, adjacent to the heating wall has a tendency to move upwards and the cold fluid near the interface has a tendency to move downwards. Natural convection can therefore arise as soon as a difference of temperatures between the heated wall and the solid-liquid interface exists. Mathematically, the driving force in the vorticity equation, $PrRa\frac{\partial \theta}{\partial x}$, is always effective as long as $\frac{\partial \theta}{\partial x}$ does not vanish, and the fluid motion occurs as soon as the heating starts.

The melting from below, however, represents a different phenomenon. As the melting proceeds, the melt layer thickness increases with time, with the hot, light melt adjacent to the heating surface of the bottom, and the cold, heavier melt near the solid-liquid interface at the top of the layer, which is a potentially unstable equilibrium. The only mode of the heat transfer in this case is conduction, because the uniform heating from the bottom does not generate any horizontal temperature gradient and the buoyancy force is therefore zero.

The state of rest of the melt described above is potentially unstable however. As the melting proceeds, some random disturbance, or noise may destroy the

balance and then the fluid motion is triggered. This instability is usually called the Bénard convection.

5.1 Previous Works

The Bénard problem has received considerable attention in studies of natural convection between two horizontal plates [77]-[82]. The critical Rayleigh number for the onset of natural convection is 1720. Tien and Yen [33] studied the melting of a semi infinite solid heated from below. Using a one-dimensional approximation they found a critical Rayleigh number for the onset of instability of 1720, which implies that the critical Rayleigh number is not affected by the phase-change. A comprehensive study of the effect of buoyancy on the phase-change, melting and freezing, between two horizontal plates was made by Boger and Westwater [34]. Their experimental results agreed very well with those of Tien and Yen [33]. They found that natural convection occurs for Rayleigh numbers above 1700, and the melting exhibited oscillations after the Rayleigh number exceeded 10^5. Ice-water melting was studied by Yen [83]. His picture shows that before the critical Rayleigh number is reached, the interface is flat and the melting front varies with time only. After the setting in of convection, the interface has a wavy form. In addition, Yen found that for the ice-water system the critical Rayleigh number depends on the heating temperature, and is not a universal value as in the case of a normal fluid. The same conclusion was made by Seki et al [84], who studied the same system with melting from the top.

Using linear stability theory, Sparrow *et al* [85] studied convective instability in a melt layer heated from below. Two boundary conditions were considered, either a convective heat transfer from an adjacent fluid medium or a step wise

change in the wall temperature. They found that the critical Rayleigh number is significantly affected by the convective boundary condition, *i.e.* by the value of the Biot number. At large Biot numbers, the results for the convective heating case approach those for the step wise wall temperature.

5.2 Physical Description and Control Parameters

The physical description of the problem considered is shown in the following figure.

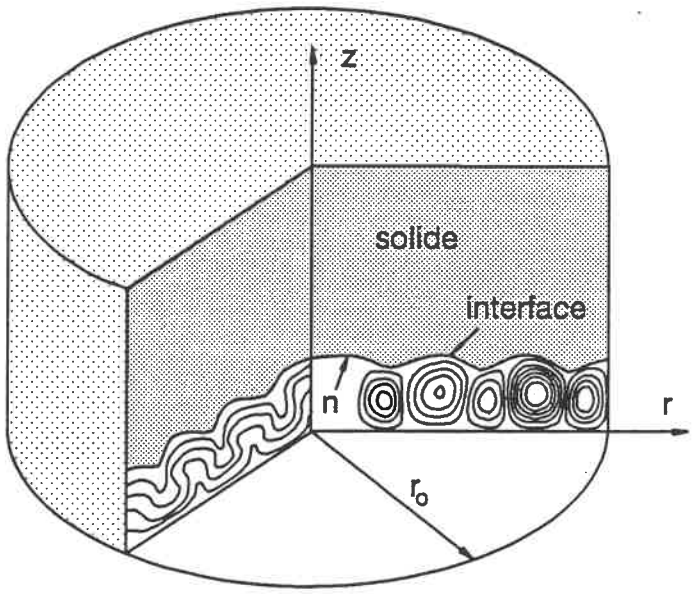

Figure 5.1: Physical diagram of melting by heating from below

Originally the solid cylinder is at its fusion temperature. The melting begins at time $t = 0$ at the lower boundary surface as the wall temperature is raised to a value T_w. The cylindrical wall is kept adiabatic throughout the process.

The governing equations have been provided in previous chapters. The only

differences are the boundary conditions, which now become

$$\xi = \xi_{min}: \quad U = 0; \qquad \frac{\partial V}{\partial \xi} = 0;$$
$$\frac{\partial \psi}{\partial \xi} = 0; \qquad \omega = 0;$$
$$\frac{\partial \theta}{\partial \xi} = 0$$

$$\xi = \xi_{max}: \quad U = 0; \qquad V = 0;$$
$$\psi = 0; \qquad \frac{\partial \theta}{\partial \xi} = 0$$
$$\omega = \xi_x V_\xi - \xi_y U_\xi$$

$$\eta = \eta_{min}: \quad U = 0; \qquad V = 0;$$
$$\psi = 0; \qquad \theta = 1;$$
$$\omega = \eta_x V_\eta - \eta_y U_\eta$$

$$\eta = \eta_{max}: \quad U = 0; \qquad V = 0;$$
$$\psi = 0; \qquad \theta = 0$$
$$\omega = \eta_x V_\eta - \eta_y U_\eta$$

To describe the hydrodynamic instability in the melting process, two Rayleigh numbers are defined. One of these is the internal Rayleigh number, based on the instantaneous thickness and a constant temperature difference across the melt layer, which is

$$Ra_i = \frac{g\beta\delta^3(T_w - T_f)}{\alpha\nu} \tag{5.1}$$

where δ is the melt thickness. It should be noted that the internal Rayleigh number is not an *a priori* prescribable quantity because of the unknown melt thickness δ.

Another Rayleigh number, called the external Rayleigh number, is defined as

$$Ra_e = \frac{g\beta r_0^3(T_w - T_f)}{\alpha\nu} \tag{5.2}$$

This Rayleigh number in fact is the same one we have already used in the previous chapters. Contrarily to the internal one, the external Rayleigh number is a priori prescribable. The relationship between the two Rayleigh number is given by

$$Ra_i = \left(\frac{\delta}{r_0}\right)^3 Ra_e \tag{5.3}$$

5.3 Results and Discussion

The computations were carried out for the set of parameters $Ste = 0.1, Pr = 7.0$ and $Ra_e = 10^6$. The variations of the melting front, temperature distribution and flow pattern with time are plotted on figures (5.2)-(5.8)

The melting begins when a temperature higher than the fusion temperature is imposed on the bottom. In the early stage of the melting, heat is transferred

uniformly from the bottom wall. As shown in Fig. 5.2(a), the isotherms are straight lines and the interface is flat. No flow motion exists at this stage. Although one can see the stream lines in the flow pattern, they are quite weak, about $O(10^{-8})$. In a numerical sense, they are zero.

As the melting proceeds, the interface moves upwards uniformly with time. In the meantime, the internal Rayleigh number increases as the melt layer becomes thicker. When the melt layer is thick enough for the internal Rayleigh number to reach a critical value, the fluid motion in the melt layer is activated. As shown in Fig. 5.2(b), the isotherms become curved after the critical Rayleigh number is exceeded, and the Bénard cells are observable. We mark the internal Rayleigh number at this time as the critical Rayleigh number. Converting the internal Rayleigh number from the external one by Eq. (5.3), we find $Ra_c = Ra_i = 2197$. Notice that the interface at this time is still flat, because we are just at the onset of natural convection. As the melting continues, the interface becomes curved due to the stronger natural convection. As seen in Fig. 5.3(c), the isotherms are distorted by upward and downward fluid motion between the two Bénard cells. In Fig. 5.3(d), some interesting phenomenon can be noticed: at $\tau = 0.01$, there are 7 cells in the melt layer; at time $\tau = 0.015$, only 6 remain, *i.e.* one cell has disappeared. Comparing the two figures 5.3(c) and 5.3(d), we find that it is the first vortex adjacent to the symmetry axis which has disappeared.

From the flow patterns in the following figures (5.4) to (5.8), one can check that the cells at left side are weaker than those at the right side Thus, the cell adjacent to the symmetry axis is always pushed out by its "neighbour". At time $\tau = 0.02$, the number of cells decreases to four; at time $\tau = 0.025$, there are three; and at time $\tau = 0.03$, there remain only two cells. Finally, only one cell can survive.

During the evolution of the convection flow, the shape of the ice-water interface changes continuously according to the number of developing vortices.

The variation of the local Nusselt number vs. time and radius are plotted in Fig. 5.9. In the early stage of the melting, the local Nusselt number decreases sharply. After the critical Rayleigh number is exceeded, the local Nusselt number exhibits oscillations. For a more precise appreciation, the variation of the local Nusselt number at the bottom wall with dimensionless time is shown in Fig. 5.10, for various positions along the radius. After the critical Rayleigh number is reached, at about $\tau = 0.007$, the local Nusselt number begins to oscillate. At $R = 1$, the local Nusselt number decreases almost monotonically, as the flow pattern does not change much at that position. The closer to the symmetry axis, the stronger the oscillation. This is because the flow pattern changes dramatically when a cell disappears near the symmetry axis For large times, the local Nusselt numbers remain almost constant since the flow pattern becomes stable.

The variation of the Nusselt number with radius is plotted in Fig. 5.11. At $\tau = 0.07$, just about the onset of natural convection, the local Nusselt number shows a damped oscillation. As times increases, the amplitude of the oscillations increase due to the stronger natural convection while the peaks of the oscillations move leftwards.

Fig. 5.12 shows the evolution of the average Nusselt number with time. At the beginning of the melting, the heat transfer is due to the conduction so that the Nusselt number decreases dramatically. After the onset of natural convection, the heat transfer rate increases as the Bénard cells are developed. As the melt layer becomes larger, the boundary layer is formed and the heat transfer rate begins to decrease. The heat transfer rate tends to a constant as the Bénard convection

reaches a unicellular flow regime.

5.4 SUMMARY

The melting of a vertical cylinder with bottom heating has been simulated. The resulting isotherms and flow patterns exhibit the Bénard phenomenon. The critical Rayleigh number for the onset of natural convection was found to be 2197.

Unlike a liquid between two parallel fixed plates, the Bénard cells decease in number as the melt layer increases. In a cylindrical geometry, the cell nearest to the symmetry axis is found to disappear. Only one cell remains at the end. Because of this transition phenomenon, the local Nusselt number oscillates both in time and space. The average Nusselt number tends to a constant value after the flow in the liquid region becomes unicellular.

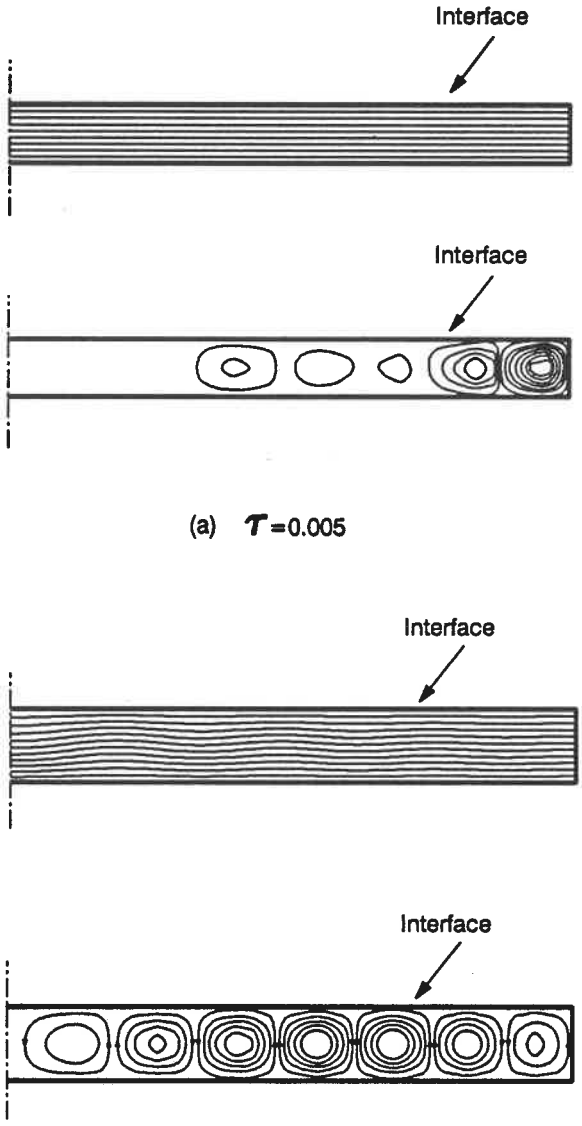

Figure 5.2: Isotherms and flow pattern of melting at different times from $\tau = 0.005 \sim 0.007$.

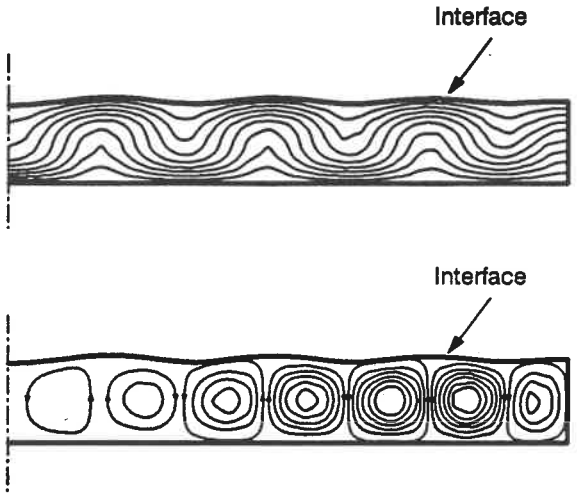

(c) τ=0.01

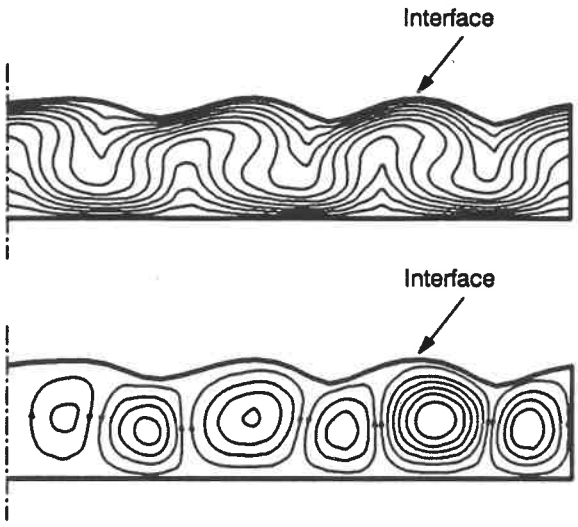

(d) τ=0.015

Figure 5.3: Isotherms and flow pattern of melting at different times from $\tau = 0.010 \sim 0.015$.

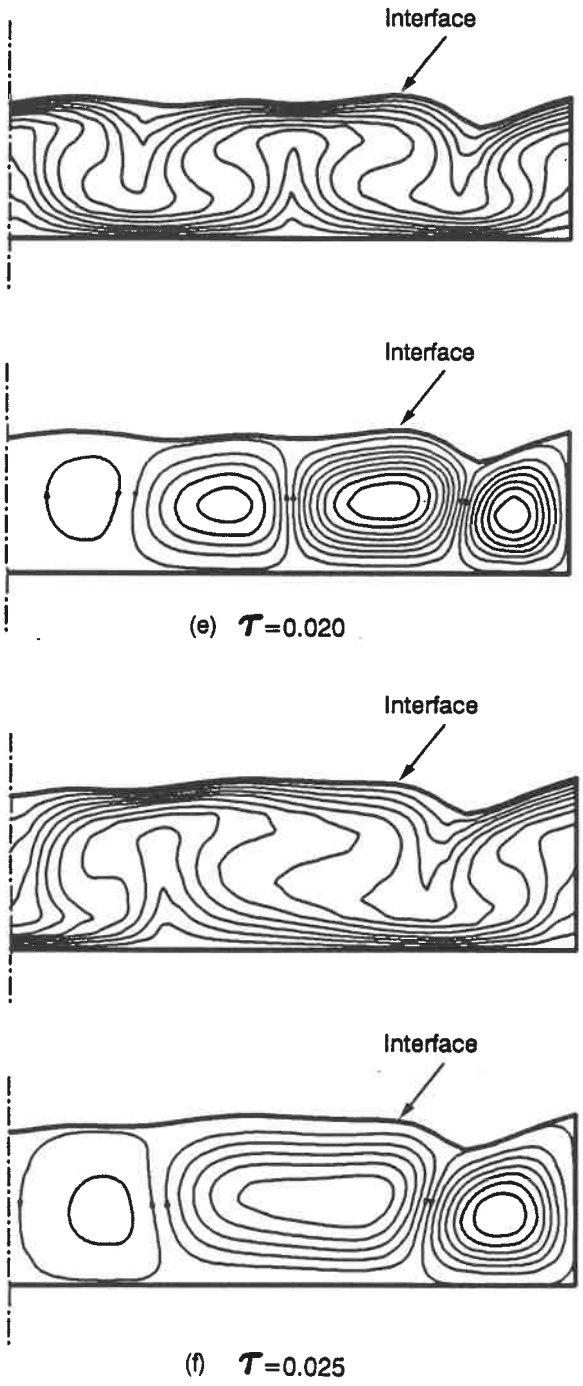

Figure 5.4: Isotherms and flow pattern of melting at different times from $\tau = 0.020 \sim 0.025$.

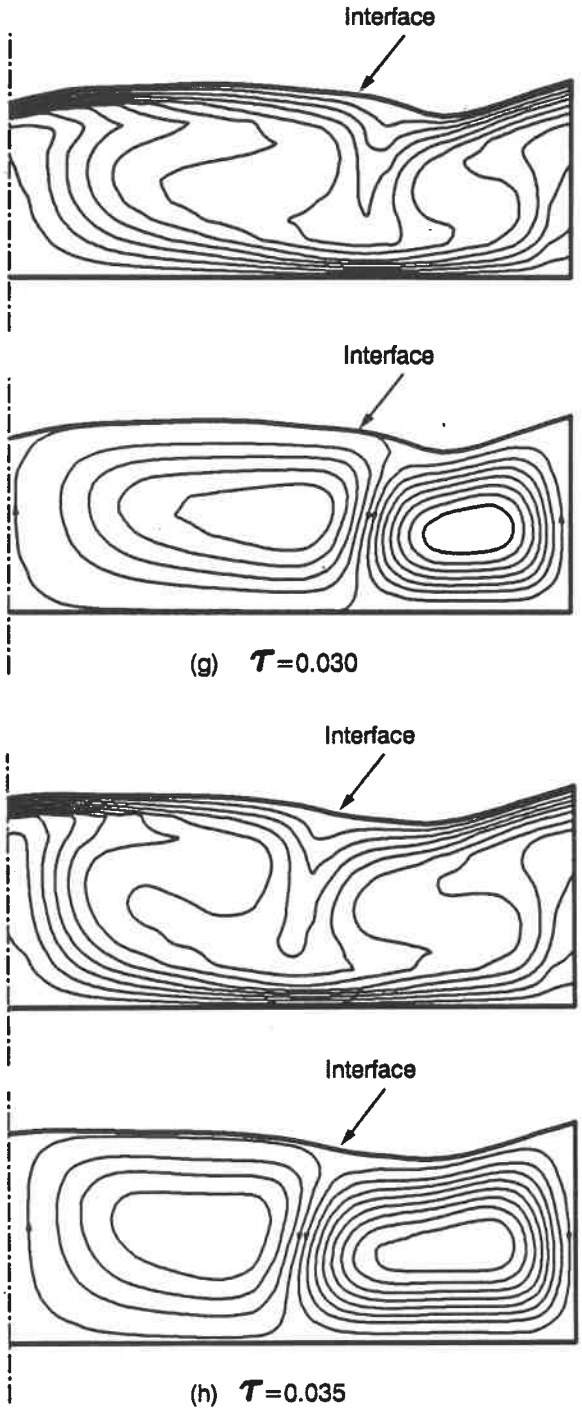

Figure 5.5: Isotherms and flow pattern of melting at different times $\tau = 0.030 \sim 0.035$.

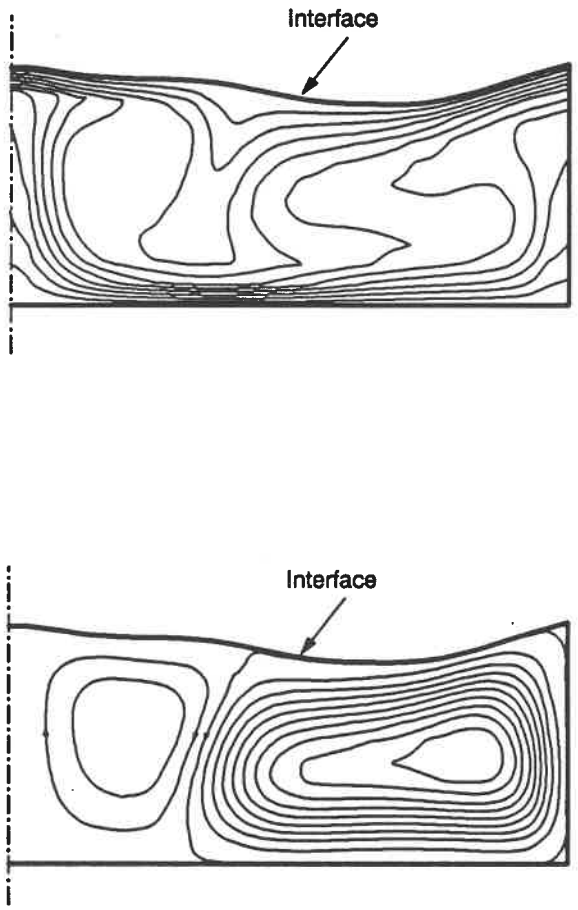

Figure 5.6: Isotherms and flow pattern of melting at different times $\tau = 0.04$.

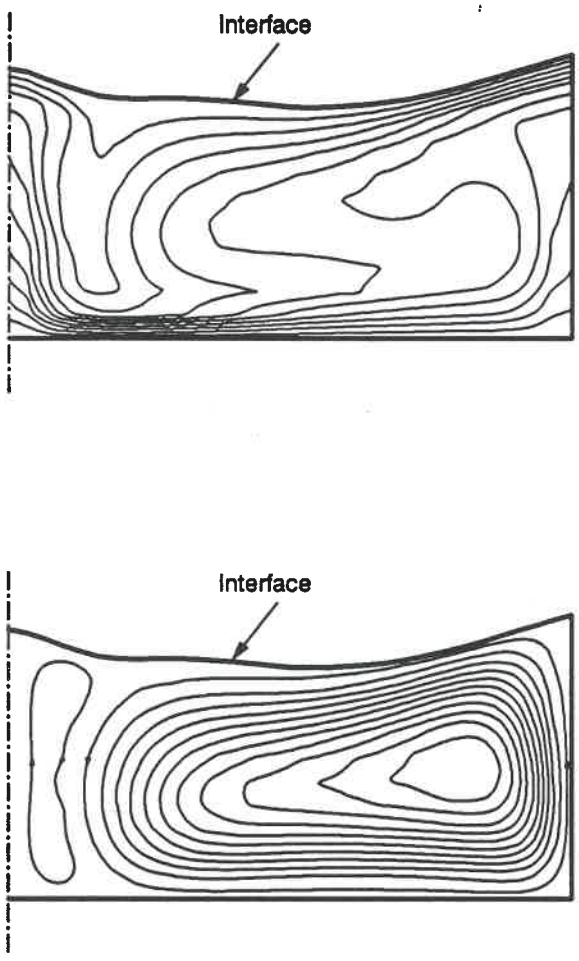

Figure 5.7: Isotherms and flow pattern of melting at different times $\tau = 0.05$.

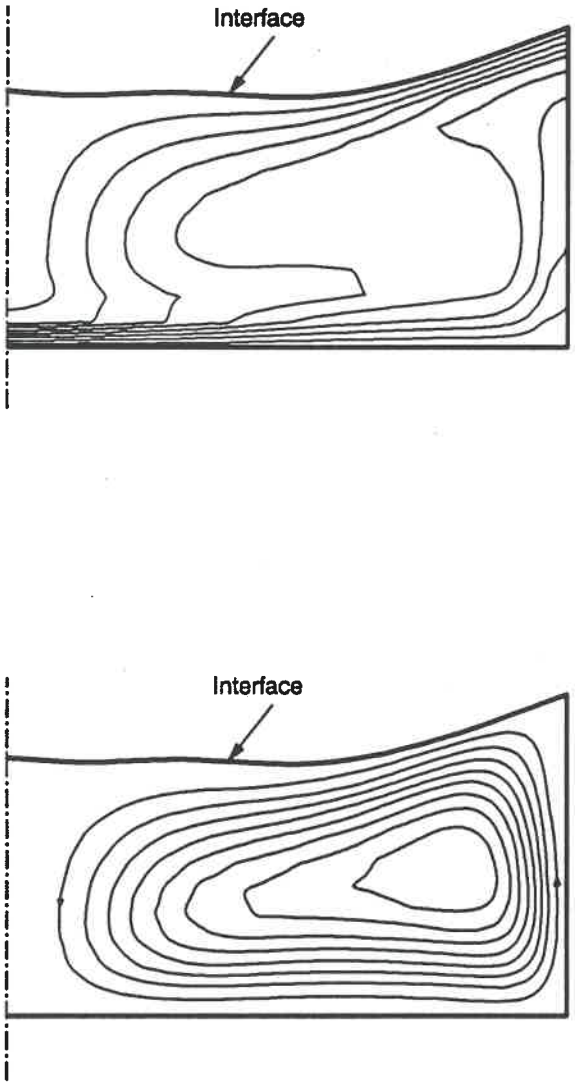

Figure 5.8: Isotherms and flow pattern of melting at different times $\tau = 0.06$.

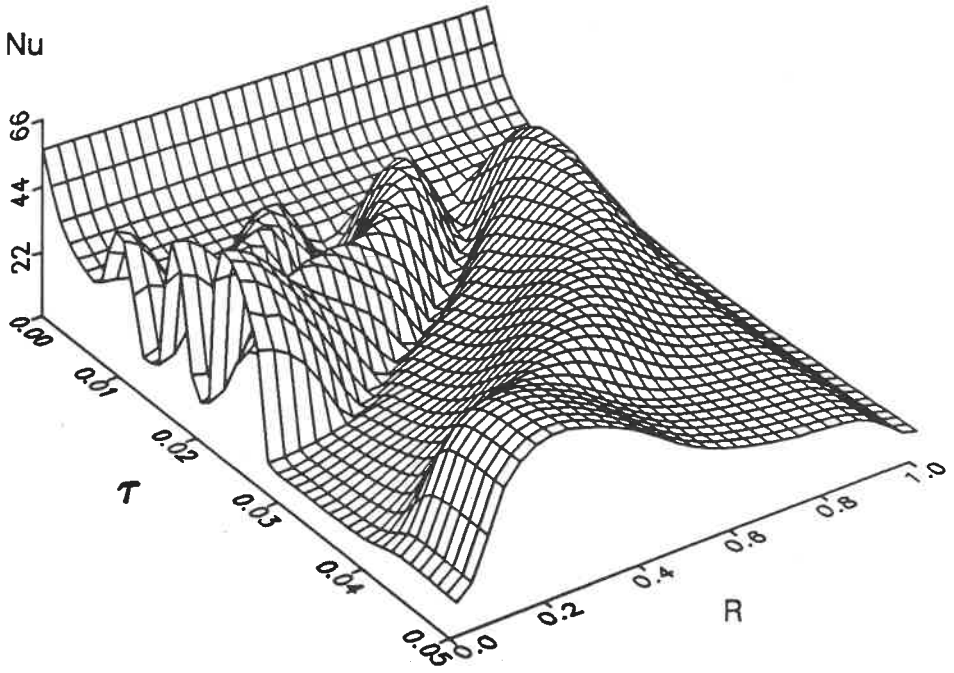

Local Nusselt number along the hot surface

Figure 5.9: Variations of the local Nusselt number with time and radius.

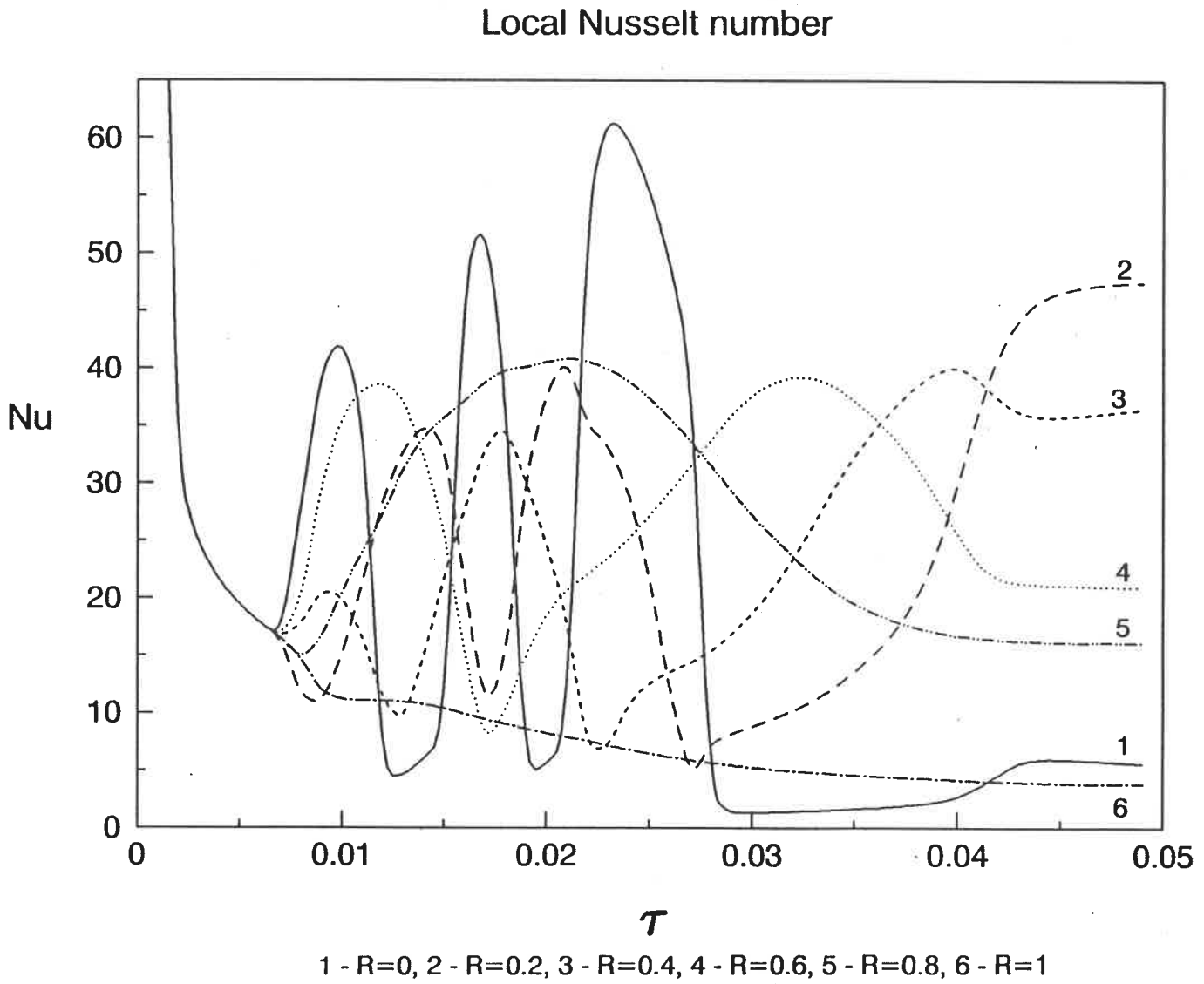

Figure 5.10: Variations of the local Nusselt number with time.

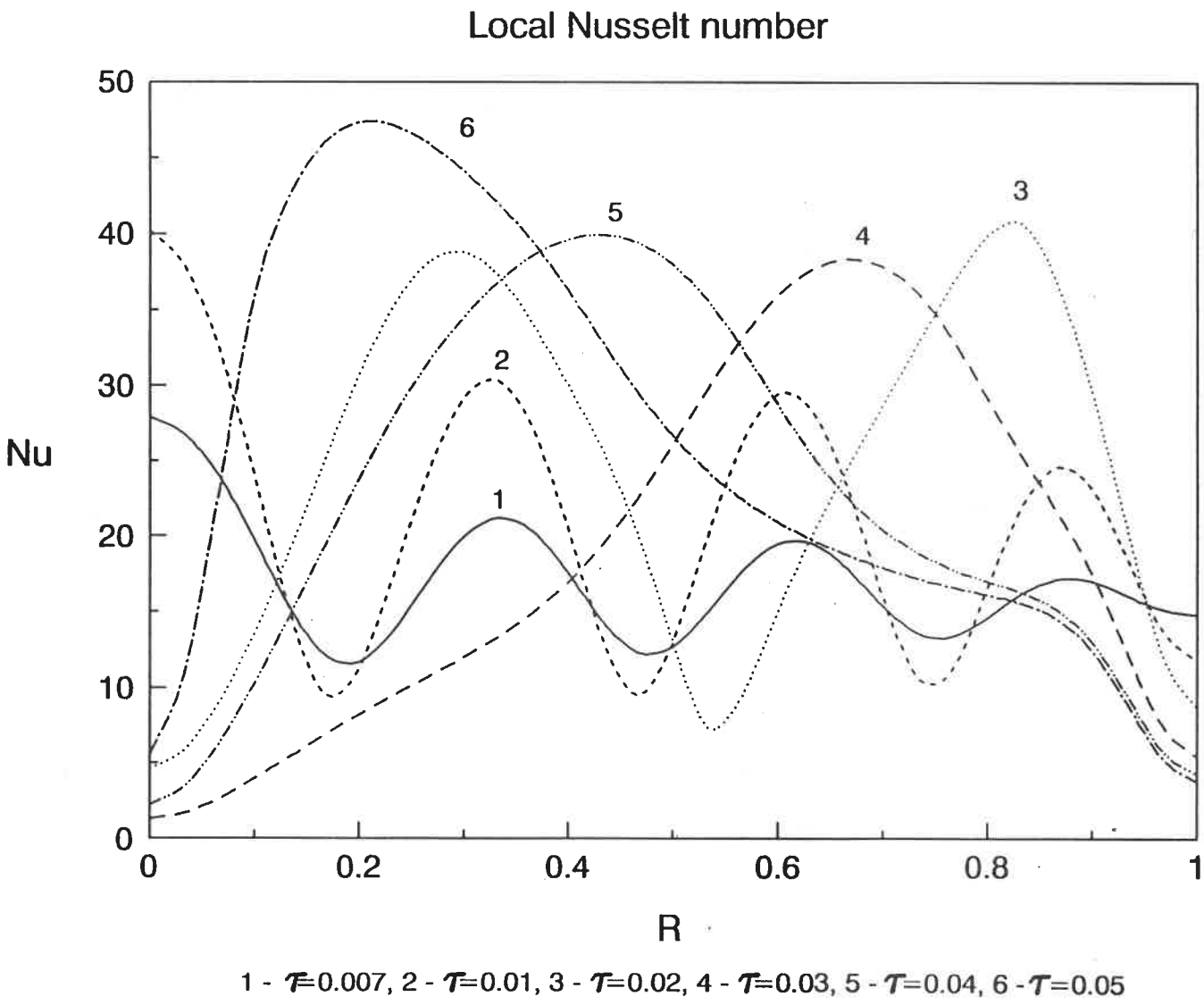

Figure 5.11: Variations of the local Nusselt number with radius.

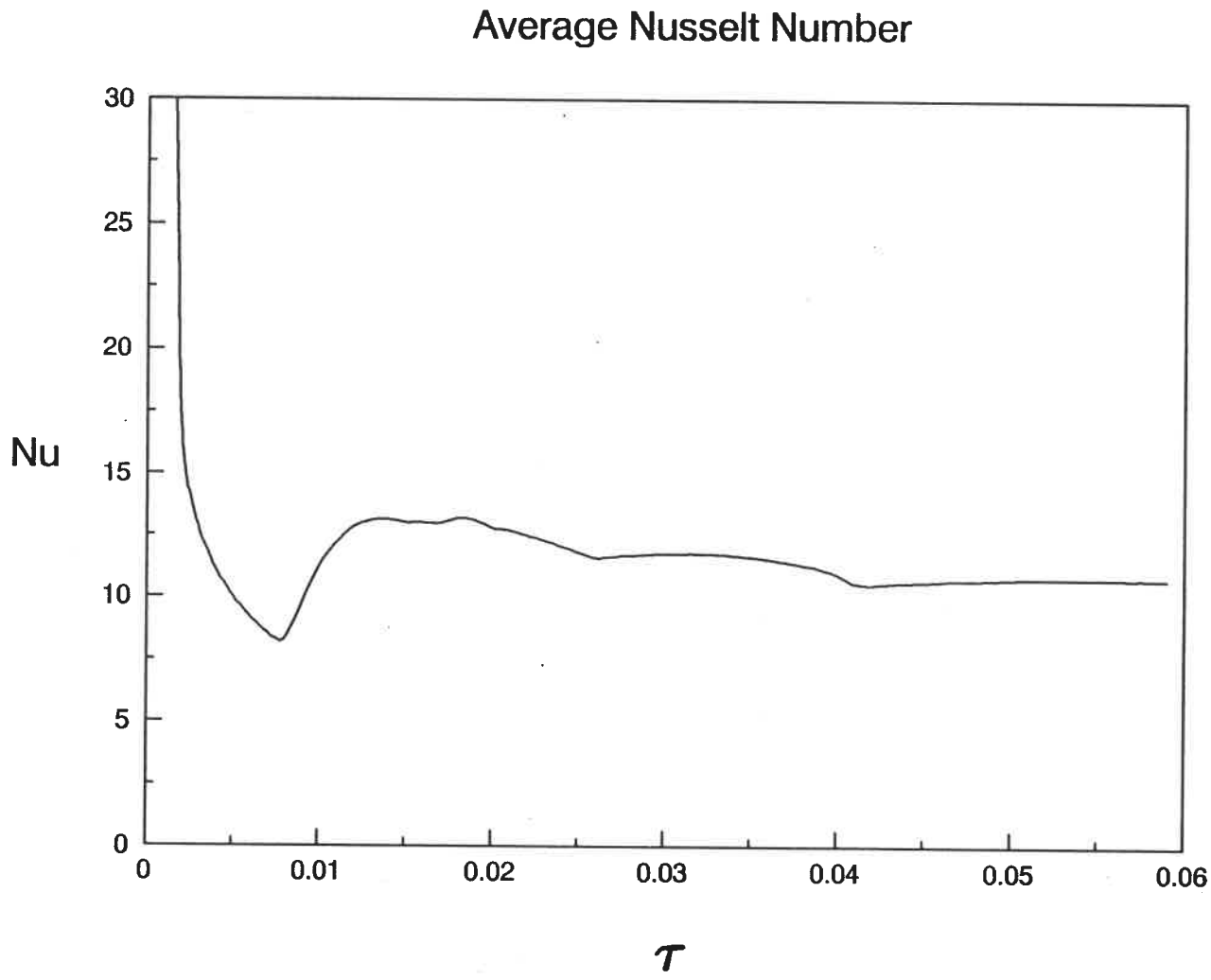

Figure 5.12: Variations of the average Nusselt number with time.

Chapter 6

MELTING WITHIN AN ISOTHERMAL VERTICAL CYLINDER

In the previous chapters, we have studied melting in a vertical cylinder with two kinds of boundary conditions; heating from the peripheral wall with a top and bottom adiabatic conditions and heating from the bottom with peripheral adiabatic condition. Both of them can find their application in practice. In this chapter, we will incorporate the two cases into a melting of vertical cylinder heated by an isothermal enclosure, which may be found in the chemical, metallurgical and also in the food industry.

6.1 Physical Description

The physical schematic diagram for melting heated by an isothermal enclosure is shown in Fig 6.1

A vertical cylindrical enclosure of height H and radius r_o contains a phase change material. The solid material is assumed to be initially at its fusion temperature T_f. At time $t = 0$, the temperature at the surface of the whole enclosure is raised to a value T_w, which is higher than the fusion temperature. As a consequence, the solid material begins melting inwards from the surface of the cylinder.

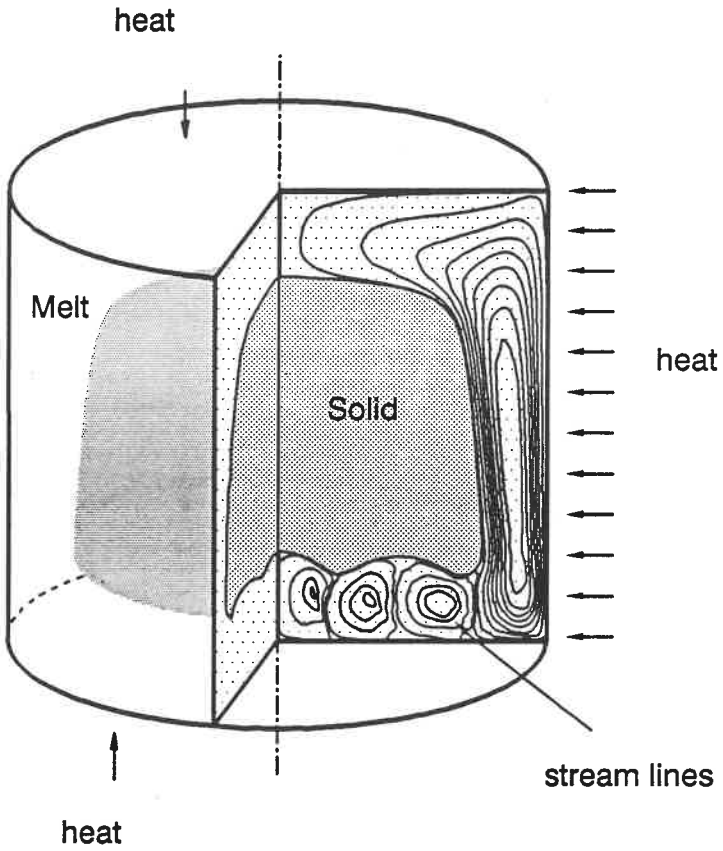

Figure 6.1: Physical diagram of a melting within an isothermal cylinder

At the top of the solid cylinder, the melting happens downwards, where the heat is transported from the top of the melt layer. The temperature increases from the bottom of the melt layer to the top surface of the enclosure. Therefore, the most-dense melt is located at the bottom of the melt layer and the least-dense melt is located at the top of the melt. The fluid flow in this region is stable, which is quite similar to what is found for convection between two plates with top heating.

At the side of the cylinder, the melting proceeds as in the cases studied in

Chapter 4, where convection always exist due to the difference of temperature across the melt layer.

At the bottom of the cylinder, the melting occurs upwards. Heating is imposed on the bottom surface of the enclosure. The most-dense melt is located at the top of the melt layer and the least-dense melt is at the bottom of the melt layer, which forms a potentially unstable layer. As the melt layer becomes thicker, a critical Rayleigh number will be reached and then convection begins, which is similar to the case we have discussed in the previous chapter.

6.2 Grid System

In view of the transformation, any two dimensional geometry, either a simply connected region or multi-connected region, can be transformed onto a rectangular [59]. In the previous study, we transformed the irregular domain onto a rectangular one, where the domain to be transformed is quite simple; three sides of the domain, one heated and two adiabatic walls, remain the same between the physical and computational plane. In addition, the domain to be transformed is rectangular-based. The four sides of the plane are very easy to choose.

For the case of a melting within an isothermal cylindrical enclosure, the melt region is around the whole cylinder. Taking advantage of the symmetry, we chose the four sides as follows, the first side is the half outer enclosure from the symmetric axis, the second side is the connection form the top surface of the enclosure to top of the interface at the axis, the third side is the half solid-liquid interface and the fourth one is the connection form the bottom surface of the enclosure to the bottom of the interface at the axis. With this arrangement, the

grid transformation is schematically shown in Fig. 6.2

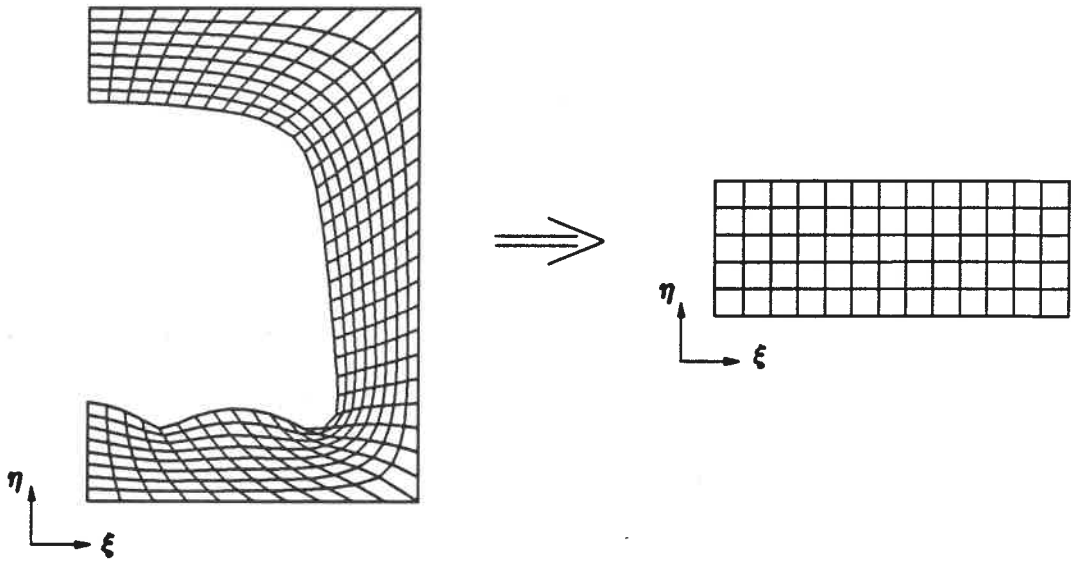

Figure 6.2: Grid system for a melting within an isothermal cylinder

Considering the transformed plane, one can easily define the boundary conditions, the two vertical sides are adiabatic, the bottom is isothermal and the top is the moving interface.

6.3 Mathematical Model and Boundary Conditions

The governing equations for the melting of a vertical cylinder within the isothermal enclosure are the same as those we have discussed in the previous chapters. We need not repeat them here. The only differences are again the boundary conditions.

According to the grid system shown in Fig. 6.2, the transformed boundary

conditions in the transformed plane are

$$\xi = \xi_{min} \quad \text{and} \quad \xi = \xi_{max}$$

$$U = 0; \qquad \frac{\partial V}{\partial \xi} = 0;$$

$$\frac{\partial \psi}{\partial \xi} = 0; \quad \frac{\partial \theta}{\partial \xi} = 0;$$

$$\omega = 0$$

$$\eta = \eta_{min}$$

$$U = 0; \qquad V = 0;$$

$$\psi = 0; \qquad \theta = 1$$

$$\omega = \eta_x V_\eta - \eta_y U_\eta;$$

$$\eta = \eta_{max}$$

$$U = 0; \qquad V = 0;$$

$$\psi = 0; \qquad \theta = 0$$

$$\omega = \eta_x V_\eta - \eta_y U_\eta;$$

where the no-slip boundary condition is imposed on the surface of the enclosure and the interface. A full slip boundary condition is imposed on the symmetry axis.

6.4 Results and Discussion

The computation is started assuming that there exits a very thin melt layer around the cylinder inside of the enclosure. After $\tau \geq 0$, the melting front begins moving inwards from the surface of the enclosure. Fig. 6.3(a) shows that at the early time, $\tau = 0.01$, the melting is in the conduction mode. The melting front moves uniformly inward from the surface of the enclosure. The isotherms at the top and bottom of the cavity are horizontally parallel to the heated surface of the enclosure, no flow convection exists. In the melt layer near the vertical wall of the cylinder, there exists a flow motion because of the nonuniformity of the temperature distribution between the heated wall and the solid-liquid interface. The isotherms in the region are still parallel to the heated surface due to the conduction dominated situation.

As the melt layer becomes thicker as in Fig. 6.3(b), the Bénard convection appears. Because the flow motion in the side region always exists, the onset of the convection at the bottom region is activated quite early by the convection in the side region. As a consequence, the Rayleigh number for the onset of convection is much smaller than for the melting with bottom heating alone. Here, we found that the internal critical Rayleigh number, defined in the previous chapter, is about 830.

At the later time $\tau = 0.03$, the convection becomes stronger and two Bénard cells are formed in the bottom region as shown in Fig. 6.4(c). As the melt continues, the Bénard cell at the right grows faster and stronger than the left one. Therefore, the left cell is pushed leftwards and shrinks until it disappears. The whole procedure can be seen from Fig. 6.4(c) $\sim$ Fig. 6.5(f). This phenomenon has been observed in the melting of a vertical cylinder heated from the bottom.

In order to observe the heat transfer rate from each side, we plot the average Nusselt numbers in Fig. 6.6, where Nu_b denotes the Nusselt number at the bottom of the cylinder, Nu_s, at the side wall and Nu_T, at the top. From Fig. 6.6, we can find that the average Nusselt numbers on all the surface decrease at the beginning when the conduction is dominant. After some time, the variations of the Nusselt numbers become different. The Nusselt number at the top of the cylinder decreases monotonically to zero. This is because the convection flow moves upwards from the bottom, along the side wall where the fluid is heated and the temperature gradient decreases. As the melt liquid region becomes larger, the melt region at the top of the cylinder becomes an isothermal zone as shown by the isotherms in Fig. 6.5(f). The fluid is cooled when it flows downwards along the interface. Therefore, the Nusselt number tends to zero as the temperature gradients vanish. The Nusselt number at the bottom surface increases after the onset of the convection in the bottom region. The variation of the Nusselt number at the side wall is between those at the top and the bottom wall.

The computation is also performed at the higher Rayleigh number $Ra = 10^6$. From Fig. 6.7(a), we find that the Bénard cell already appears. The corresponding internal Rayleigh number is about 1000. Because of the stronger convection in the side region, the convection mechanism is activated and begins the convection motion much earlier than in the previous case. Fig. 6.7(a) $\sim$ 6.9(f) describe the whole process of melting. One can clearly observe how the Bénard cells grow, shrink and disappear. The average Nusselt numbers are plotted on Fig. 6.10. The Nusselt number at the top surface decreases to zero much faster than for the case $Ra = 10^5$, due to the stronger convection. The Nusselt numbers at the bottom surface show the influence of the strong convection. For the beginning, the usual decrease is observed. After the onset of the convection, the Nusselt

numbers increase until they reach their maximum values and then decrease again. The oscillation of the Nusselt number at about $\tau = 0.025$ may be caused by the reorganization of the cell configuration a sudden change of the Bénard cell, as shown from Fig. 6.8(c) to Fig. 6.8(d). Typically, the variation of the molten volume fraction with time has been plotted in Fig. 6.11.

6.5 SUMMARY

The melting within an isothermal cylindrical enclosure incorporates the phenomena of the top heating, the side heating and the bottom heating problem. The heat transport from the top surface is essentially due to conduction. The Nusselt number at the top surface decreases monotonically to zero as the melt region increases, which means no vertical heat exchange at the top region after the convection is fully developed. The highest heat transfer rate is formed at the bottom. The melting at the bottom region developed almost the same way as that of a vertical cylinder heated from the bottom.

The onset of the convection in the bottom occurs much earlier than that in the standard case due to the induction by the convection of the side region.

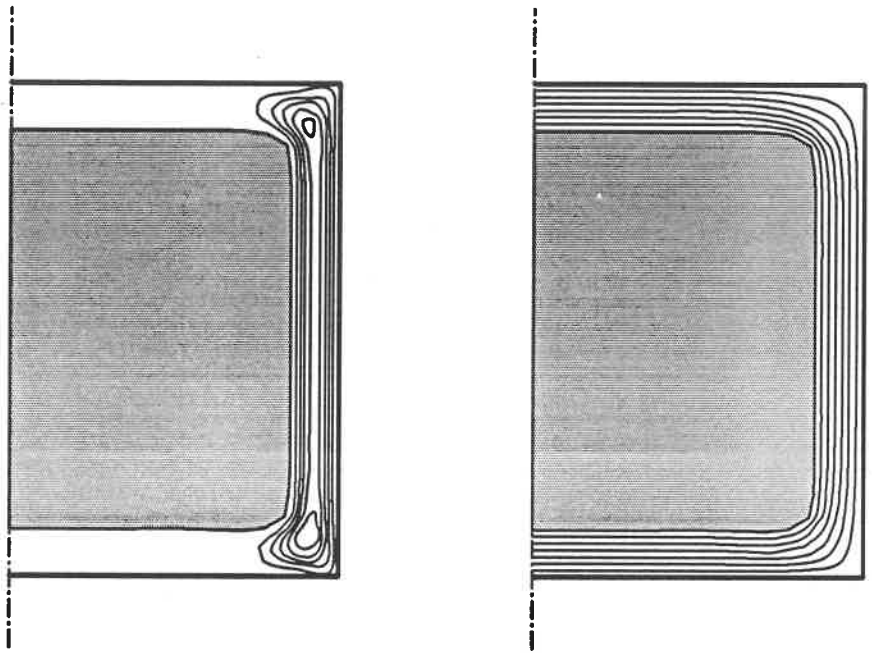

(a) τ=0.01

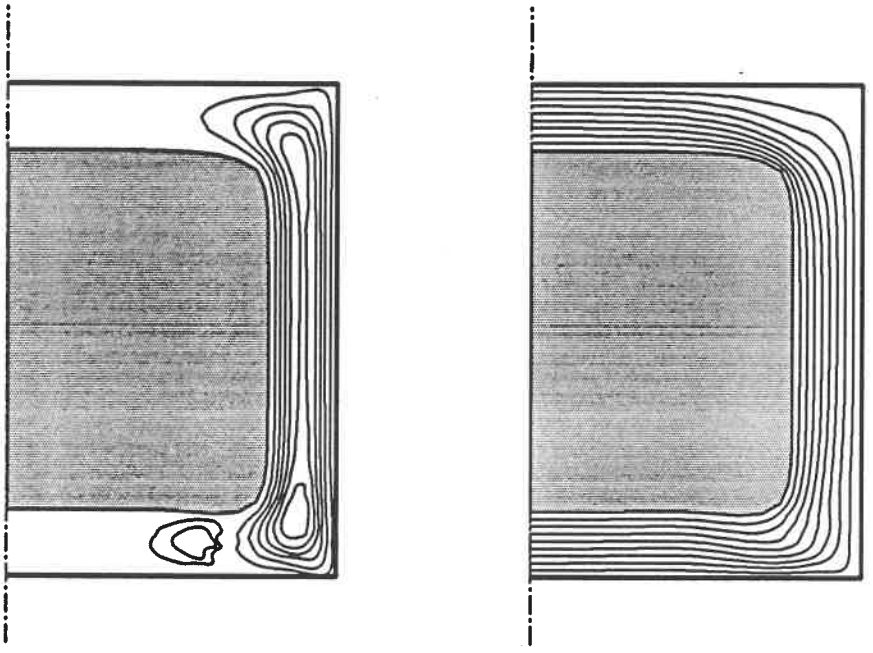

(b) τ=0.02

Figure 6.3: Isotherms and flow pattern of melting with $Ra = 1 \times 10^5$ at $\tau = 0.01$ and 0.02.

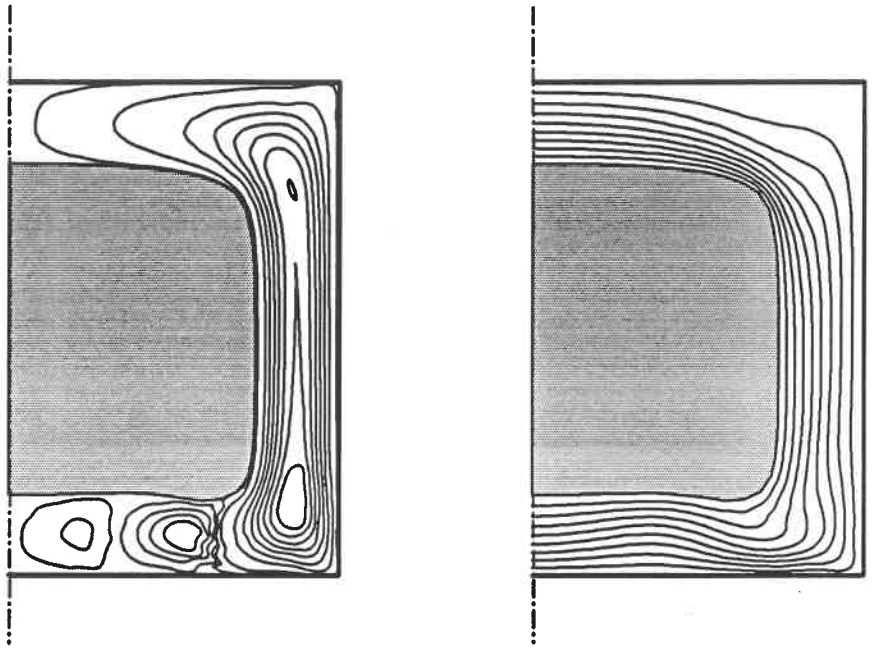

(c) τ=0.03

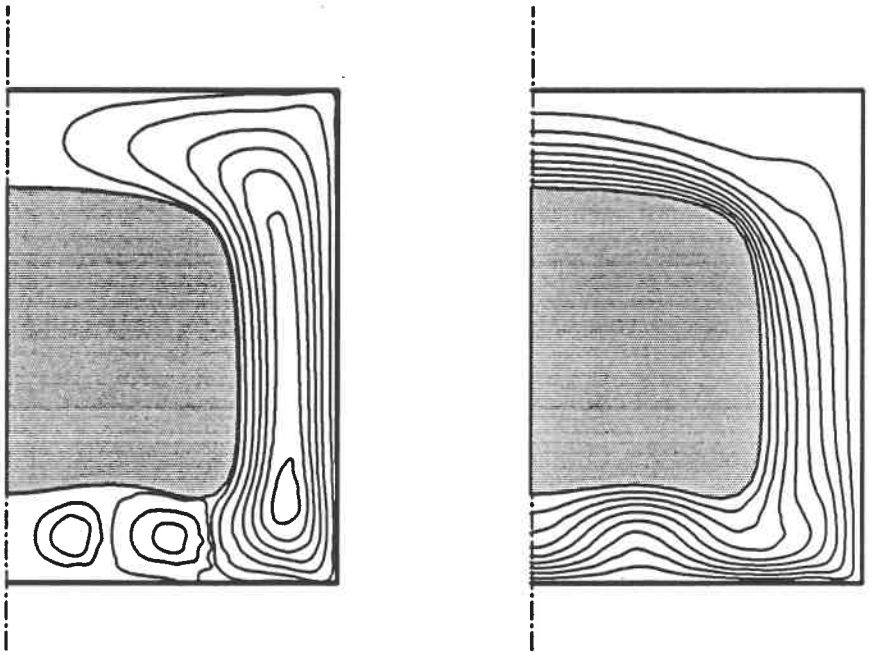

(d) τ=0.04

Figure 6.4: Isotherms and flow pattern of melting with $Ra = 1 \times 10^5$ at $\tau = 0.03$ and 0.04

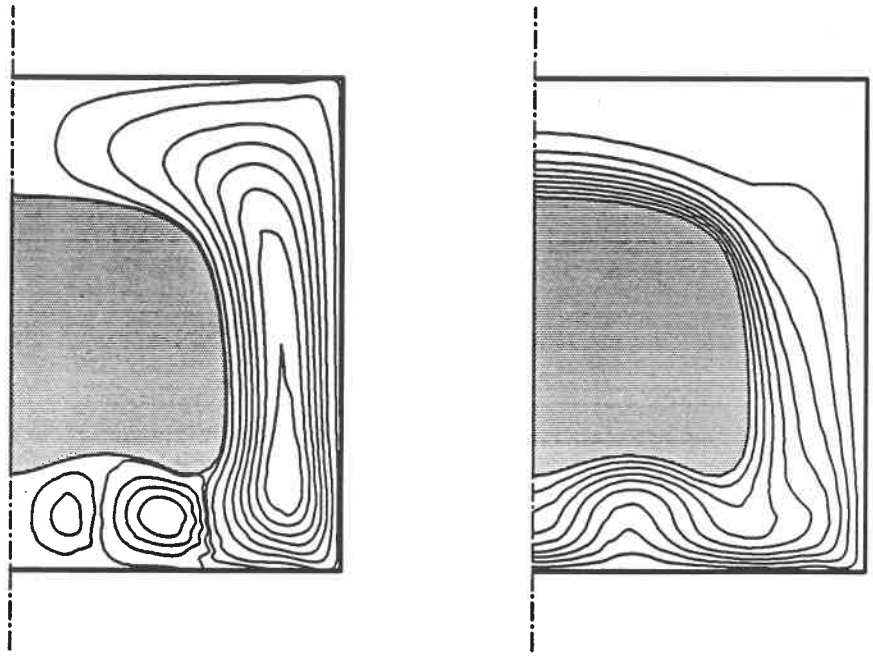

(e) τ=0.05

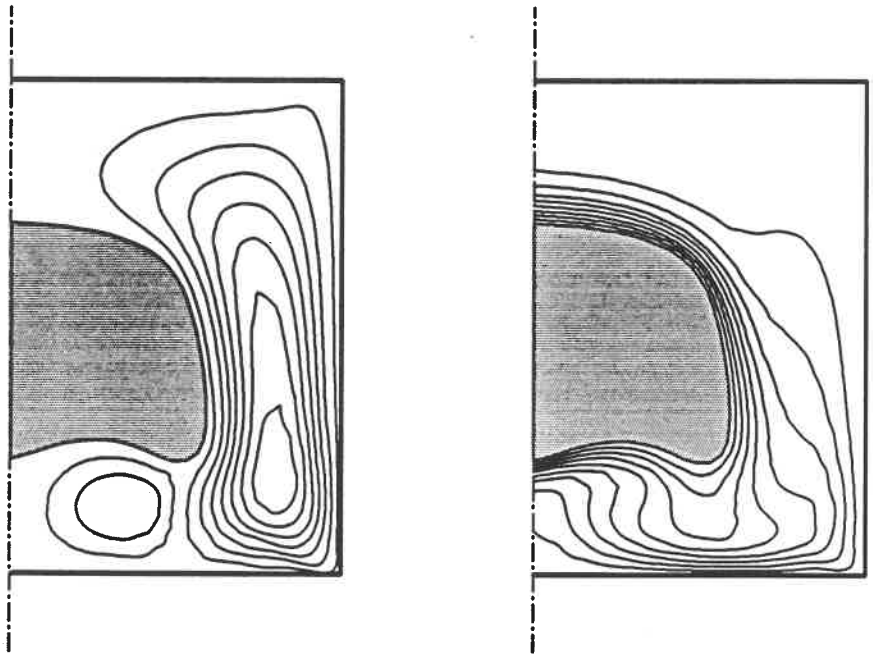

(f) τ=0.06

Figure 6.5: Isotherms and flow pattern of melting with $Ra = 1 \times 10^5$ at $\tau = 0.05$ and 0.06.

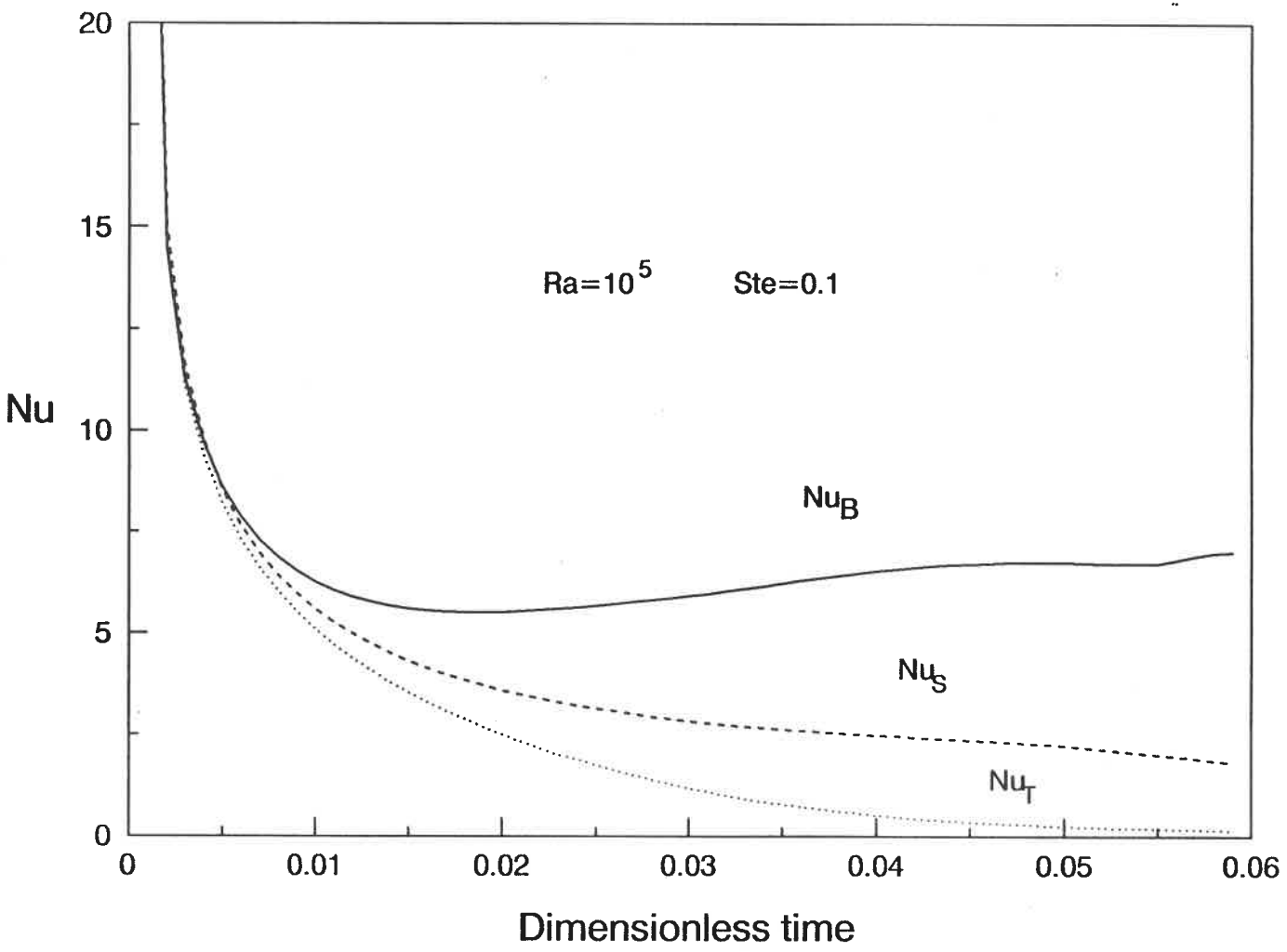

Figure 6.6: Variations of the average Nusselt number with time

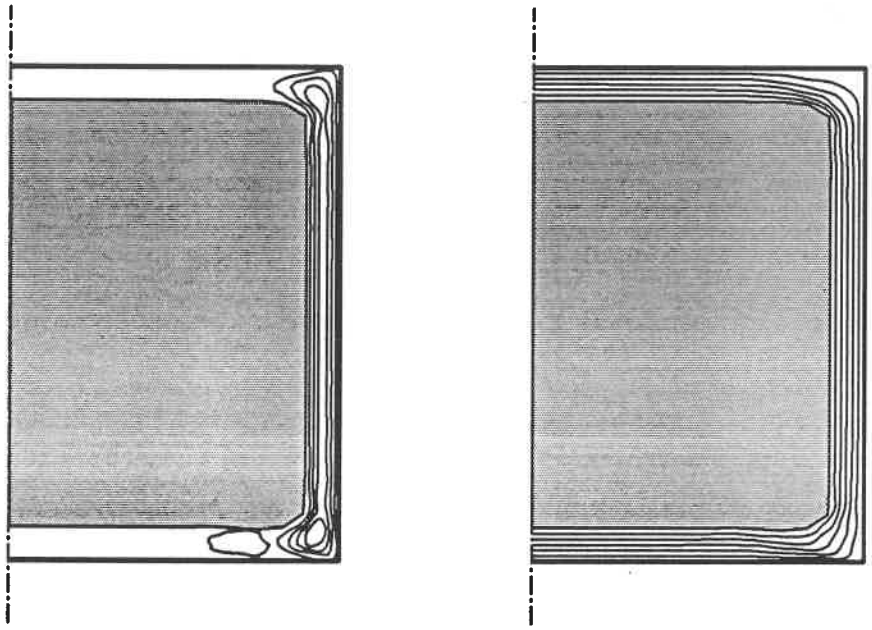

(a) τ=0.004

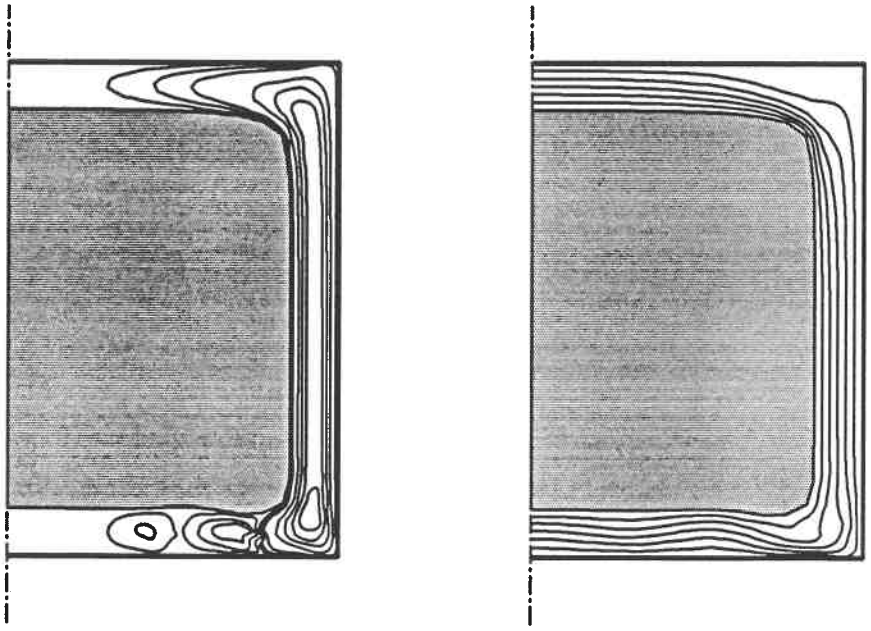

(b) τ=0.01

Figure 6.7: Isotherms and flow pattern of melting with $Ra = 1 \times 10^6$ at $\tau = 0.004$ and 0.01.

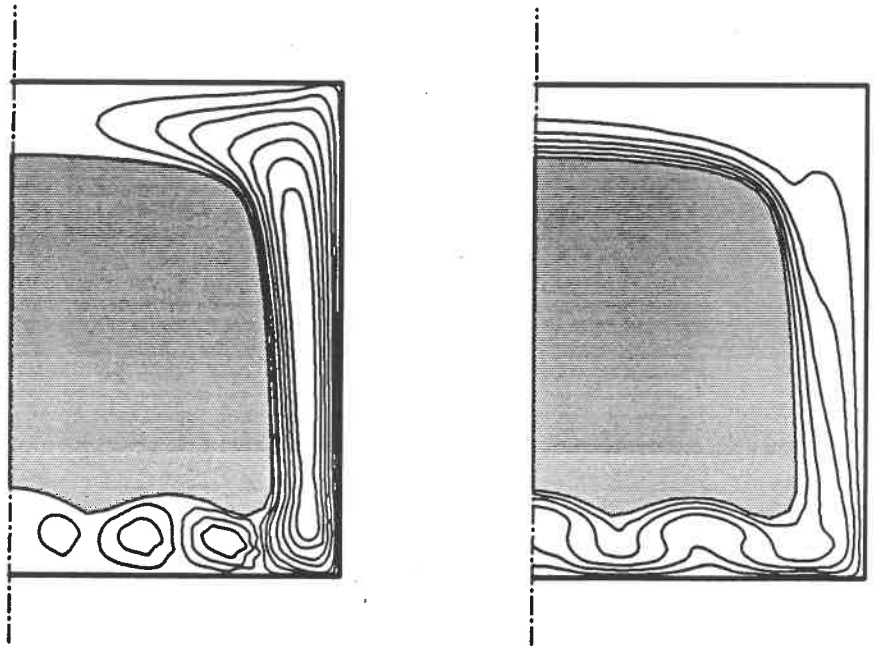

(c) τ=0.02

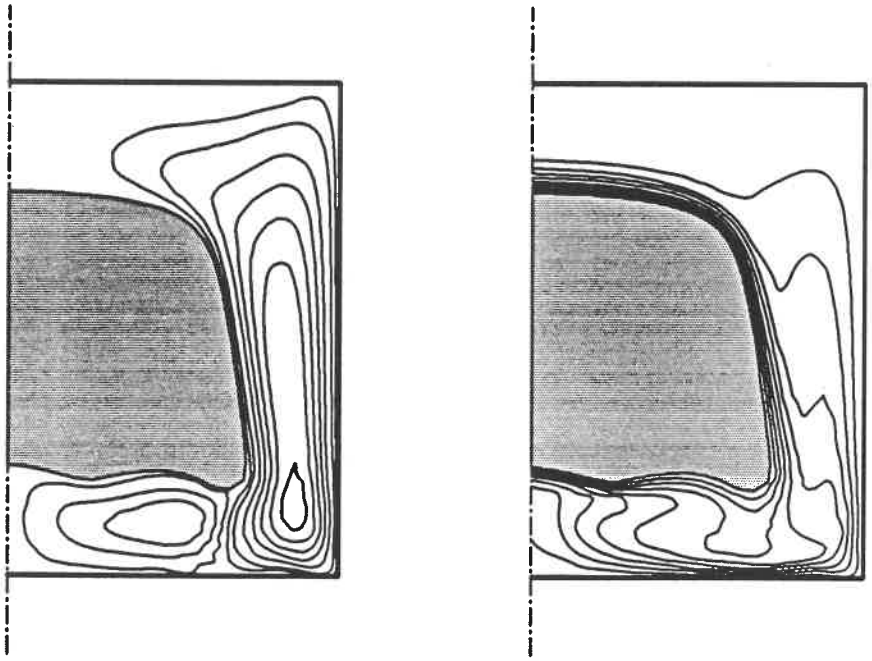

(d) τ=0.03

Figure 6.8: Isotherms and flow pattern of melting with $Ra = 1 \times 10^6$ at $\tau = 0.02$ and 0.03

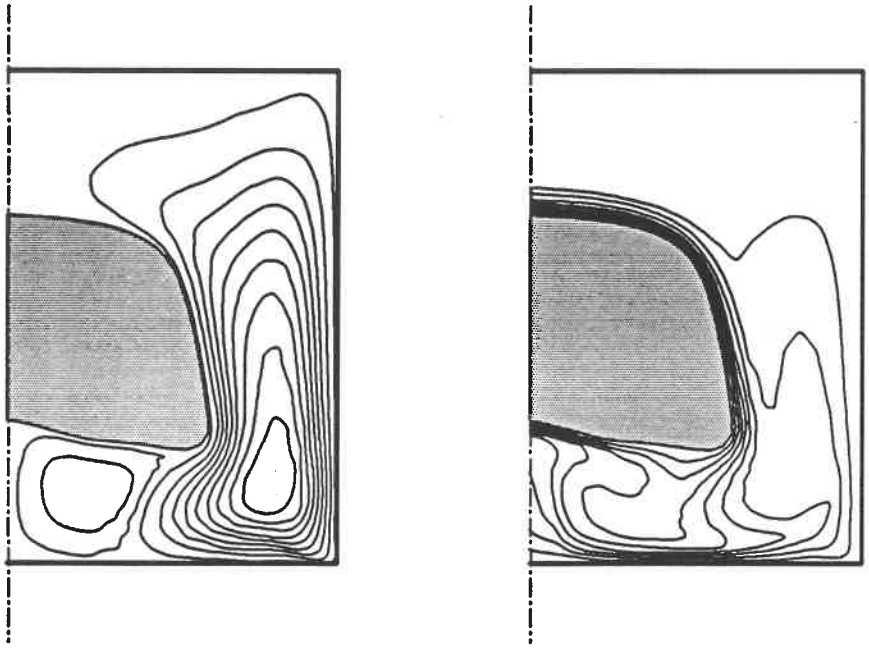

(e) τ=0.04

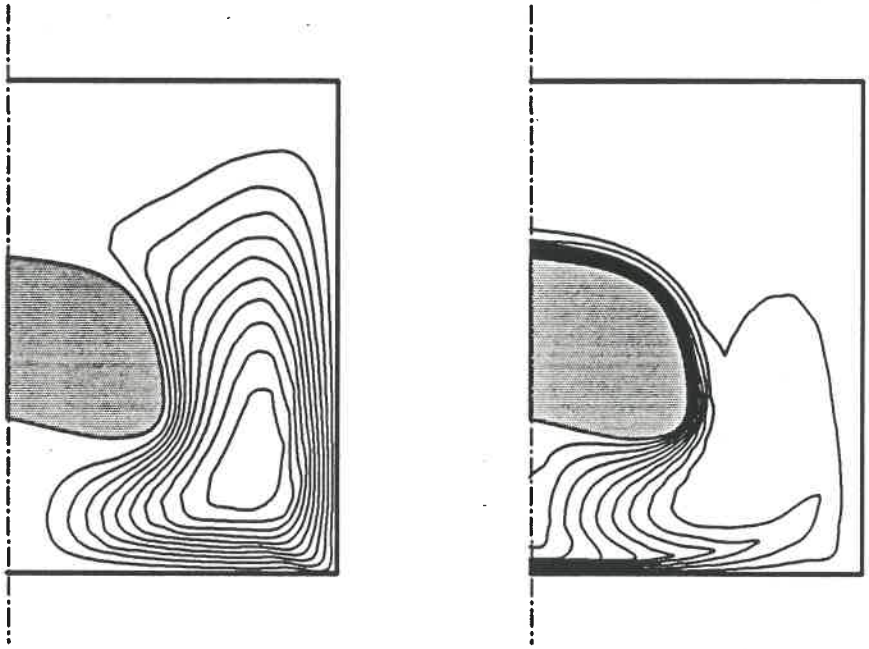

(f) τ=0.05

Figure 6.9: Isotherms and flow pattern of melting with $Ra = 1 \times 10^6$ at $\tau = 0.04$ and 0.05.

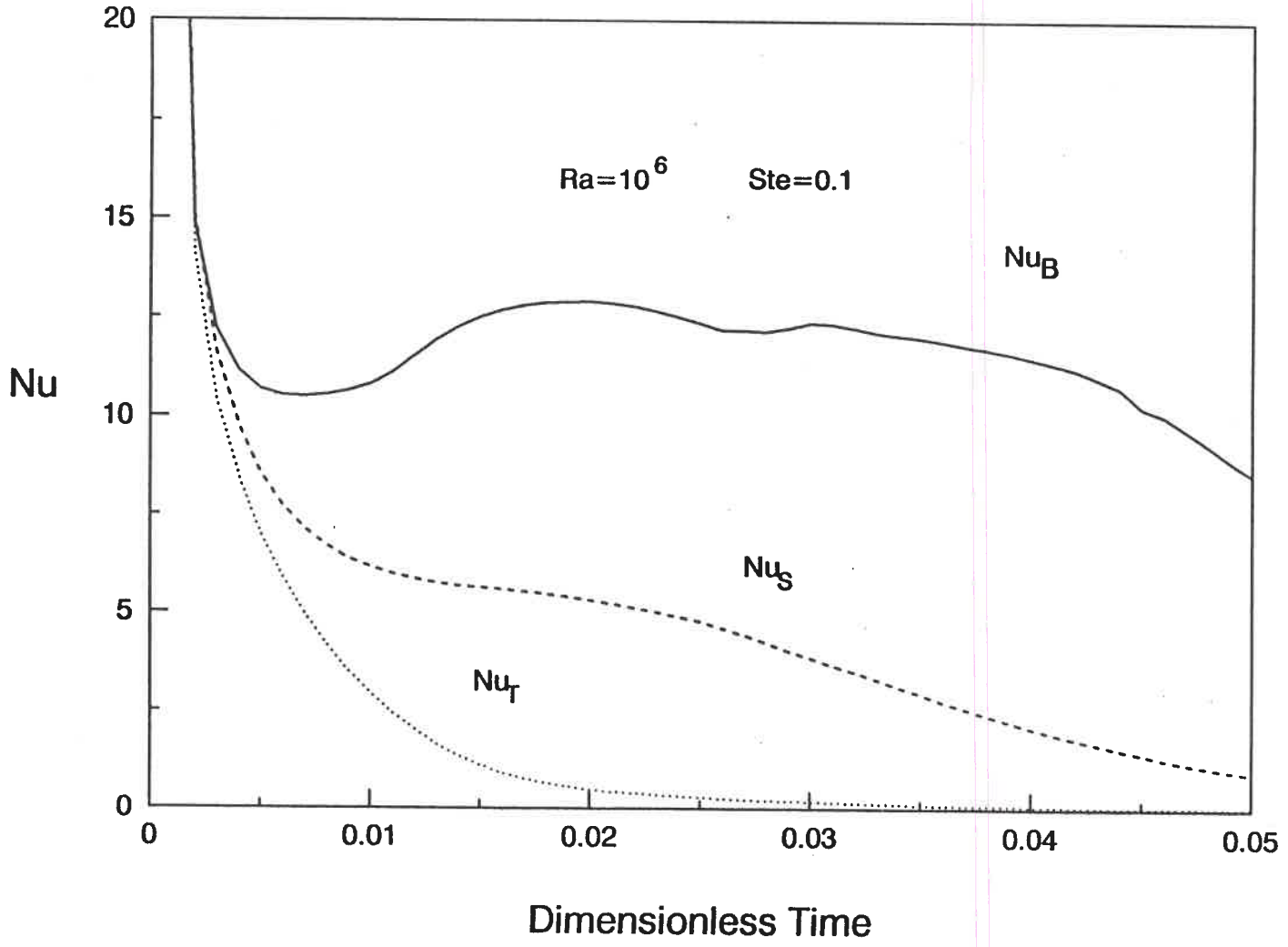

Figure 6.10: Variations of the average Nusselt number with time

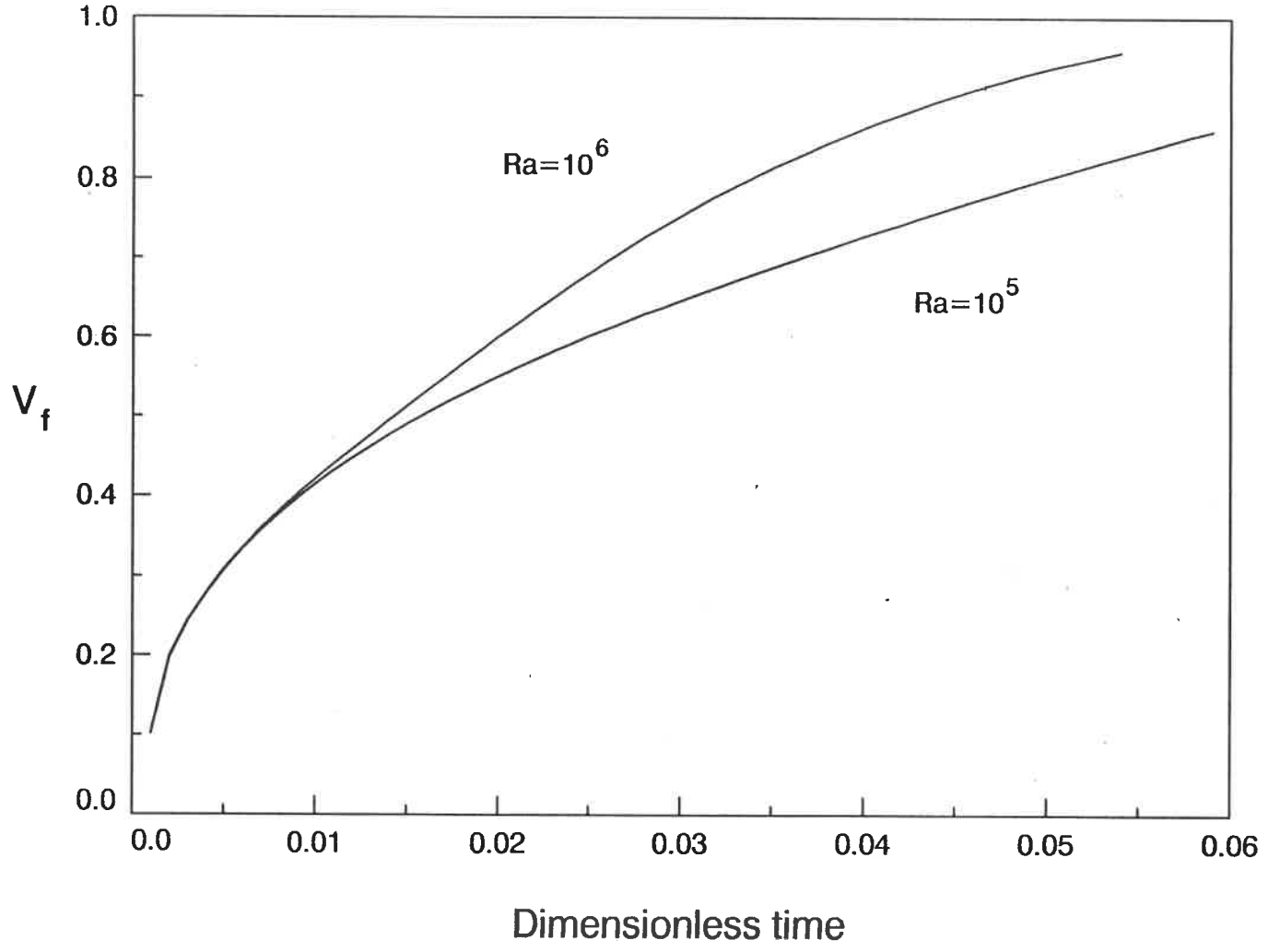

Figure 6.11: Variations of the Molten fraction with time

Chapter 7

A NUMERICAL STUDY OF THE MELTING OF ICE IN A VERTICAL CYLINDER

In recent years the problem of ice melting has been treated by many investigators because of its occurrence in nature as well as its direct applications in industries.

Due to the anomalous thermal expansion of water at about 4^0C, flow reversal may occur in the melt region, resulting in a minimum heat transfer rate. The peculiar nature of the maximum density phenomenon was first investigated by Tkachev[72]. By using photographic techniques he found a minimum Nusselt number for an ice cylinder melting at 5.5^0C. A horizontal ice cylinder immersed in water was studied both theoretically and experimentally by Saitoh[23]. He found that when the temperature was about 6^0C, the Nusselt number attained its minimum value. For the same case, three-dimensional thermal instability was studied by Saitoh and Hirose[73]. They found thermal instability in the temperature range between 5.5^0C and 6.5^0C.

By using a theoretical method, Merk[74] predicted a minimum Nusselt number for a melting sphere at 5.31^0C. Experimental works by Dumore et al[75] generally supported Merk's analysis. The same study was carried out by Vanier et al. [76], who found a minimum Nusselt number at 5.35^0C.

Herrmann et al[51] studied experimentally the influence of density inversion

on the melting of ice around a heated horizontal cylinder. They pointed out a critical condition for the melting process at $T_w = 8^0C$: for $T_w > 8^0C$ natural convection occurs mainly in the upper region of the melt while for $T_w < 8^0C$, melting occurs in the lower part. Ho and Chen[50] studied the same case numerically. They found that the minimum heat transfer rate does not always occur for $T_w = 8^0C$, which is contrary to the results obtained by Herrmann.

Heat transfer during melting of ice confined within a heated horizontal cylinder was studied experimentally and theoretically by Rieger et al. [47]. Two inner diameters of the cylinder were considered. For both radii, heat transfer reached their minimum in the proximity of $T_w = 8^0C$.

To our knowledge, no literature has been published so far on the melting of a vertical ice cylinder. The present work was focused on the influence of the inversion of density on the melting profiles, isotherms and flow patterns, and heat transfer and melting rates for wall temperature varying between 0^0 and 10^0C.

7.1 Governing Equations

The physical problem is schematically pictured in Fig. 7.1.

An ice cylinder of height H and radius r_0 is initially at its fusion temperature. At time $t = 0$, the temperature at the surface of the cylinder is raised, and maintained at a fixed value $T_w > T_f$. As a consequence, the ice cylinder will melt inward. The mathematical formulation of this problem is based on the same assumptions as in the previous chapter, except for that the variation of fluid density with temperature is nonlinear.

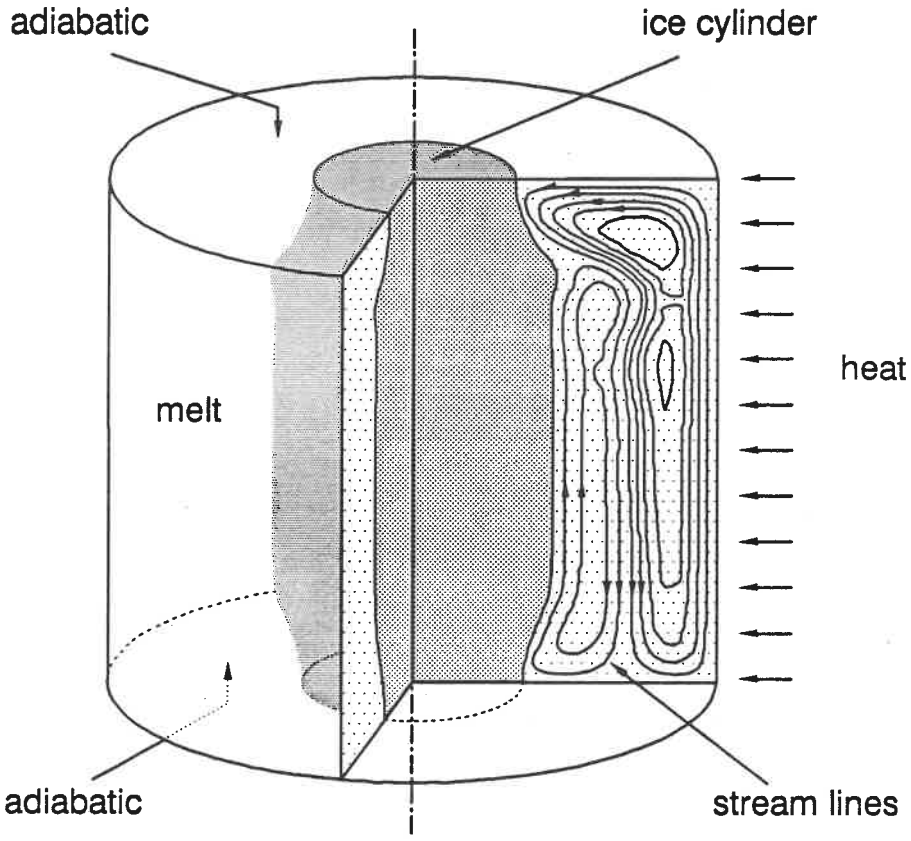

Figure 7.1: Schematic diagram of the physical problem

With those assumptions, the system of governing equations are

Continuity equation:

$$\frac{\partial(ru)}{\partial r} + \frac{\partial(rv)}{\partial z} = 0 \tag{7.1}$$

Momentum equation:

$$\frac{\partial u}{\partial t}+u\frac{\partial u}{\partial r}+v\frac{\partial u}{\partial z}=-\frac{1}{\rho}\frac{\partial p}{\partial r}+\nu(\frac{\partial^2 u}{\partial r^2}+\frac{1}{r}\frac{\partial u}{\partial r}+\frac{\partial^2 u}{\partial z^2}-\frac{u}{r^2}) \tag{7.2}$$

$$\frac{\partial v}{\partial t}+u\frac{\partial v}{\partial r}+v\frac{\partial v}{\partial z}=-\frac{1}{\rho}\frac{\partial p}{\partial z}+\nu(\frac{\partial^2 v}{\partial r^2}+\frac{1}{r}\frac{\partial v}{\partial r}+\frac{\partial^2 v}{\partial z^2})+g\sum_{n=1}^{n}a_n\beta_n(T-T_f)^n \tag{7.3}$$

Energy equation:

$$\frac{\partial T}{\partial t}+u\frac{\partial T}{\partial r}+v\frac{\partial T}{\partial z}=\alpha(\frac{\partial^2 T}{\partial r^2}+\frac{1}{r}\frac{\partial T}{\partial r}+\frac{\partial^2 T}{\partial z^2}) \tag{7.4}$$

Because of the nonlinear variation of the density of water with temperature, the buoyancy force is expressed by a polynomial series, which means that the source term becomes nonlinear.

Energy equation at the ice-water interface:

$$-k\frac{\partial T}{\partial n}=\rho h\frac{\partial n}{\partial t} \tag{7.5}$$

After introducing the dimensionless variables and stream function, the system (7.1)-(7.4) can be written as

$$Ste\frac{\partial \omega}{\partial \tau}+\frac{\partial(U\omega)}{\partial R}+\frac{\partial(V\omega)}{\partial Z}=Pr(\nabla^2\omega-\frac{\omega}{R^2})+Pr\sum_{n=1}^{n}a_nRa_n\frac{\partial\theta^n}{\partial R} \tag{7.6}$$

$$\nabla^2\psi=\frac{2}{R}\frac{\partial\psi}{\partial R}-R\omega \tag{7.7}$$

$$Ste\frac{\partial\theta}{\partial\tau}+U\frac{\partial\theta}{\partial R}+V\frac{\partial\theta}{\partial Z}=\nabla^2\theta \tag{7.8}$$

and the interface energy equation becomes

$$-\frac{\partial\theta}{\partial n}=\frac{\partial n}{\partial\tau} \tag{7.9}$$

The appropriate boundary conditions are

$$\theta=1 \quad \psi=0 \quad at \quad r=1$$

$$\theta=0 \quad \psi=0 \quad along \quad S_i$$

$$\frac{\partial\theta}{\partial z}=0 \quad \psi=0 \quad at \quad z=0,\ A$$

The source term in the vorticity transport equation is nonlinear due to the nature of water density. a_n and β_n are coefficients of the nonlinear expansion, which can be determined as will be shown in the following section.

7.2 Inversion Parameter

To describe the nonlinear variation of water density with temperature, an approximate relation in the range of 0^0 to 10^0C can be used in the following form:

$$\rho=\rho_m[1-\beta(T-T_m)^2] \tag{7.10}$$

Introducing some reference variable with subscript r, the relation becomes

$$\rho=\rho_r[1-2\beta_1(T-T_r)-\beta_2(T-T_r)^2] \tag{7.11}$$

where

$$\rho_r = \rho_m[1 - \beta(T_r - T_m)^2]$$

$$\beta_1 = \beta_2(T_r - T_m)$$

$$\beta_2 = \beta/[1 - \beta(T_r - T_m)]$$

For the present case of water, we need to define two parameters

$$Ra_1 = \frac{g\beta_1 r_0^3(T_w - T_r)}{\alpha\nu} \tag{7.12}$$

$$Ra_2 = \frac{g\beta_2 r_0^3(T_w - T_r)^2}{\alpha\nu} \tag{7.13}$$

The source term in the vorticity transport equation (7.6) then becomes

$$2PrRa_1\frac{\partial\theta}{\partial R} + PrRa_2\frac{\partial\theta^2}{\partial R} \tag{7.14}$$

Introducing an inversion parameter

$$\gamma = \frac{Ra_1}{Ra_2} = -\frac{T_m - T_r}{T_w - T_r} = -\theta_m \tag{7.15}$$

Eq. (7.6) can be written as

$$2Pr\gamma Ra_2\frac{\partial\theta}{\partial R} + PrRa_2\frac{\partial\theta^2}{\partial R} = 2PrRa_2(\gamma + \theta)\frac{\partial\theta}{\partial R} \tag{7.16}$$

Hereafter, instead of Ra_1 and Ra_2, we shall use γ and Ra_2, and the subscript 2 will be omitted for the sake of clarity.

It is worth nothing that if γ is positive, the source term will act qualitatively as in a normal fluid. If γ is negative, it can greatly reduce and even "reverse" the buoyancy force. If we choose the reference temperature $T_r = T_f = 0$, the range of γ is confined to $-\infty < \gamma < 0$. Since θ is defined as $0 \leq \theta \leq 1$, the source term becomes negative for $\gamma < -1$, introducing a buoyancy force in an opposite direction to that of a "normal fluid". For $-1 < \gamma < 0$, the source term can be either positive or negative depending on the dimensionless temperature θ within the melt region. Thus, two counter-rotating vortices can appear within the melt region at the same time, corresponding to the phenomenon of flow reversal.

7.3 Transformed Equations

In order to perform all the computations in a fixed domain (ξ, η), (ξ, η), the physical variables have to be transformed into functions with independent variables ξ and η. Using x and y instead of R and Z as independent variables in the physical plane, the transformed equations become

$$Ste\frac{\partial \omega}{\partial \tau} + \tilde{U}\frac{\partial \omega}{\partial \xi} + \tilde{V}\frac{\partial \omega}{\partial \eta} = Pr\widetilde{\nabla}^2\omega + S_\omega \tag{7.17}$$

$$\widetilde{\nabla}^2\psi = S_\psi \tag{7.18}$$

$$Ste\frac{\partial \theta}{\partial \tau} + \tilde{U}\frac{\partial \theta}{\partial \xi} + \tilde{V}\frac{\partial \theta}{\partial \eta} = \widetilde{\nabla}^2\theta + S_\theta \tag{7.19}$$

and the equations for the moving interface are

$$\frac{\partial x}{\partial \tau} = -\frac{\partial \theta}{\partial \xi}\xi_x \tag{7.20}$$

$$\frac{\partial y}{\partial \tau} = -\frac{\partial \theta}{\partial \xi}\xi_y \tag{7.21}$$

where $\tilde{U}$ and $\tilde{V}$ are contravariant velocities expressed as

$$\tilde{U} = \xi_x U + \xi_y V \tag{7.22}$$

$$\tilde{V} = \eta_x U + \eta_y V \tag{7.23}$$

and

$$\begin{aligned}
U &= \frac{1}{x}(\xi_y \frac{\partial \psi}{\partial \xi} + \eta_y \frac{\partial \psi}{\partial \eta}) \\
V &= -\frac{1}{x}(\xi_x \frac{\partial \psi}{\partial \xi} + \eta_x \frac{\partial \psi}{\partial \eta}) \\
S_\omega &= Ste(\xi_\tau \frac{\partial \omega}{\partial \xi} + \eta_\tau \frac{\partial \omega}{\partial \eta}) + (\frac{U}{x} - \frac{Pr}{x^2})\omega + 2PrRa(\gamma + \theta)(\xi_x \frac{\partial \theta}{\partial \xi} + \eta_x \frac{\partial \theta}{\partial \eta}) \\
S_\psi &= \frac{2}{x}(\xi_x \frac{\partial \psi}{\partial \xi} + \eta_x \frac{\partial \psi}{\partial \eta}) - x\omega \\
S_\theta &= Ste(\xi_\tau \frac{\partial \theta}{\partial \xi} + \eta_\tau \frac{\partial \theta}{\partial \eta}) \\
\widetilde{\nabla}^2 &= g^{11}\frac{\partial^2}{\partial \xi^2} + 2g^{12}\frac{\partial^2}{\partial \xi \eta} + g^{22}\frac{\partial^2}{\partial \eta^2} + P\frac{\partial}{\partial \xi} + Q\frac{\partial}{\partial \eta} + \frac{1}{x}(\xi_x \frac{\partial}{\partial \xi} + \eta_x \frac{\partial}{\partial \eta})
\end{aligned}$$

The transformed boundary conditions are

$$\xi = \xi_{min}: \quad U = 0; \qquad \xi = \xi_{max}: \quad U = 0;$$

$$V = 0; \qquad V = 0;$$

$$\theta = 0; \qquad \theta = 1;$$

$$\psi = 0; \qquad \psi = 0;$$

$$\omega = \xi_x V_\xi - \xi_y U_\xi \qquad \omega = \xi_x V_\xi - \xi_y U_\xi$$

$$\eta = \eta_{min} \quad and \quad \eta = \eta_{max}$$

$$U = 0; \qquad V = 0;$$

$$\psi = 0;$$

$$\omega = \eta_x V_\eta - \eta_y U_\eta;$$

$$g^{22}\theta_\eta + g^{12}\theta_\xi = 0$$

7.4 Results and Discussion

The simulations were carried out with an isothermal boundary condition. For all cases, the Rayleigh number is chosen as 7×10^5, with an aspect ratio $A = 2.0$. The other parameters are given in Table 7.1.

Table 7.1: *Control Parameters*

Parameters	4^0C	6^0C	8^0C	10^0C
γ	-1.0	-0.667	-0.5	-0.4
Pr	11.5	10.55	10.0	9.4
Ste	0.05	0.75	0.10	0.125

Fig. 7.2 displays the velocity profiles, streamlines and isotherms for the case $T_w = 4^0C$. The figure shows a unicellular flow pattern, with a larger melt region in the lower part of the cylinder. This is due to the fact that the water near the cylinder wall has a higher density than that near the interface; thus water near the cylinder wall moves downwards while relatively lighter water near the interface moves upwards. This circulation behavior is opposite to that of normal fluid.

For the case of $T_w = 6^0C$ in the Fig. 7.3, a dual cell flow occurs. As the water with maximum density is located somewhere in the melt region, two counter-rotating circulations are formed. Since the maximum density at 4^0C is closer to the cylinder wall than the interface, the inner circulation is stronger than the outer one. Thus, the melting near the bottom is faster than near the top of the cylinder.

For the case of $T_w = 8^0C$ in Fig. 7.5, the maximum density line is located approximately in the middle of the melt region. Thus, the inner and outer circulations have almost a same intensity. In the early stage of the melting, the melt front is almost vertical as shown in Fig. 7.4. As the melting proceeds, the melting of both the top and bottom regions becomes faster than that in the middle region.

For the case of $T_w = 10^0C$ in Fig. 7.6, the maximum density moves towards the interface and the outer circulation is much stronger than the inner. The melting profiles are similar to those of a normal fluid except for the presence of a counter-rotating circulation in the lower part of the cylinder.

The heat transfer rates are plotted in Fig. 7.7, which shows a maximum Nusselt number at $T_w = 4^0C$ and a minimum at $T_w = 8^0C$. This means that a unicellular circulation in the melt is more efficient in carrying heat from the heated wall to the interface while a flow reversal significantly reduces the heat transport. The variation of the molten volume fraction in Fig. 7.8 shows that the melting velocity has a maximum value when $T_w = 4^0C$ and a minimum value when $T_w = 8^0C$.

7.5 SUMMARY

The melting process of a vertical ice cylinder has been studied numerically. The results show that flow and heat transfer can be strongly affected by the inversion of density. In the temperature range considered, the maximum Nusselt number is obtained at 4^0C, and the minimum at 8^0C.

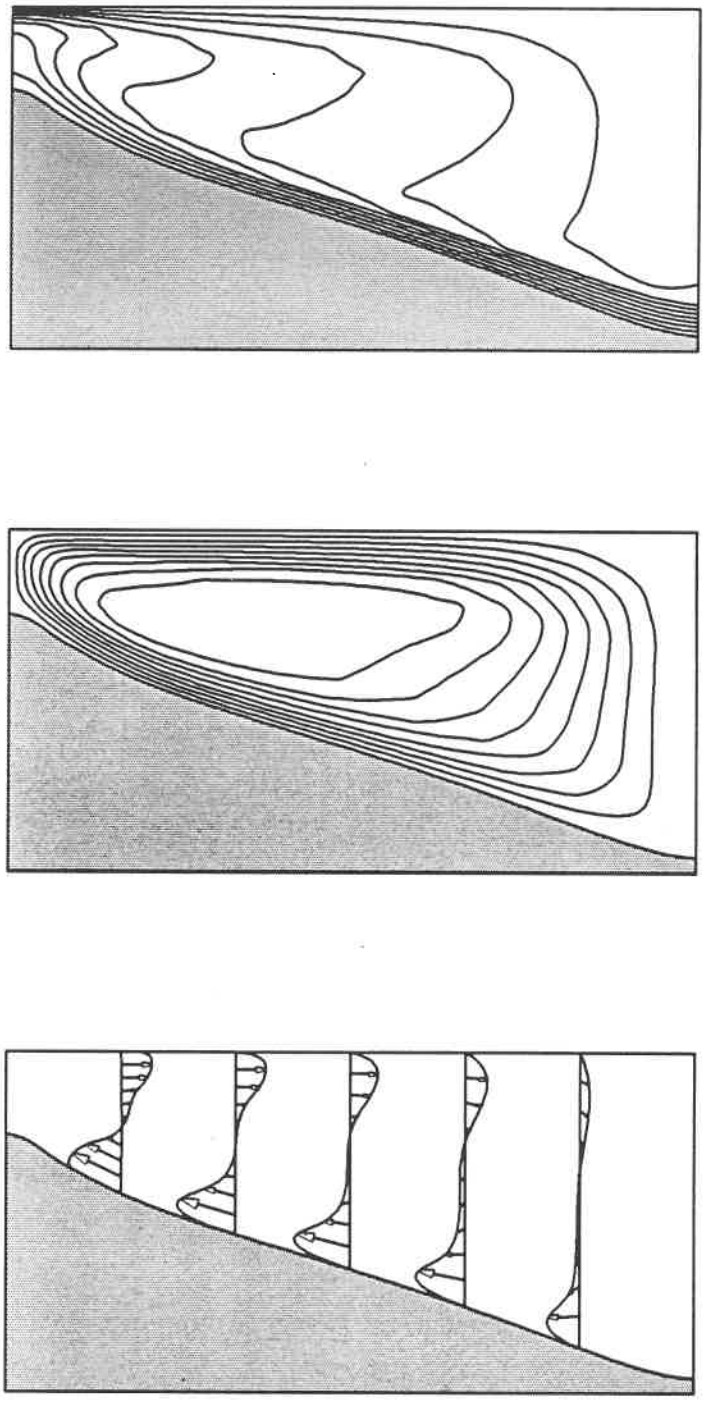

Figure 7.2: Velocity profiles, isotherms and flow pattern of melting at $T_\omega = 4^oC, \tau = 0.06$

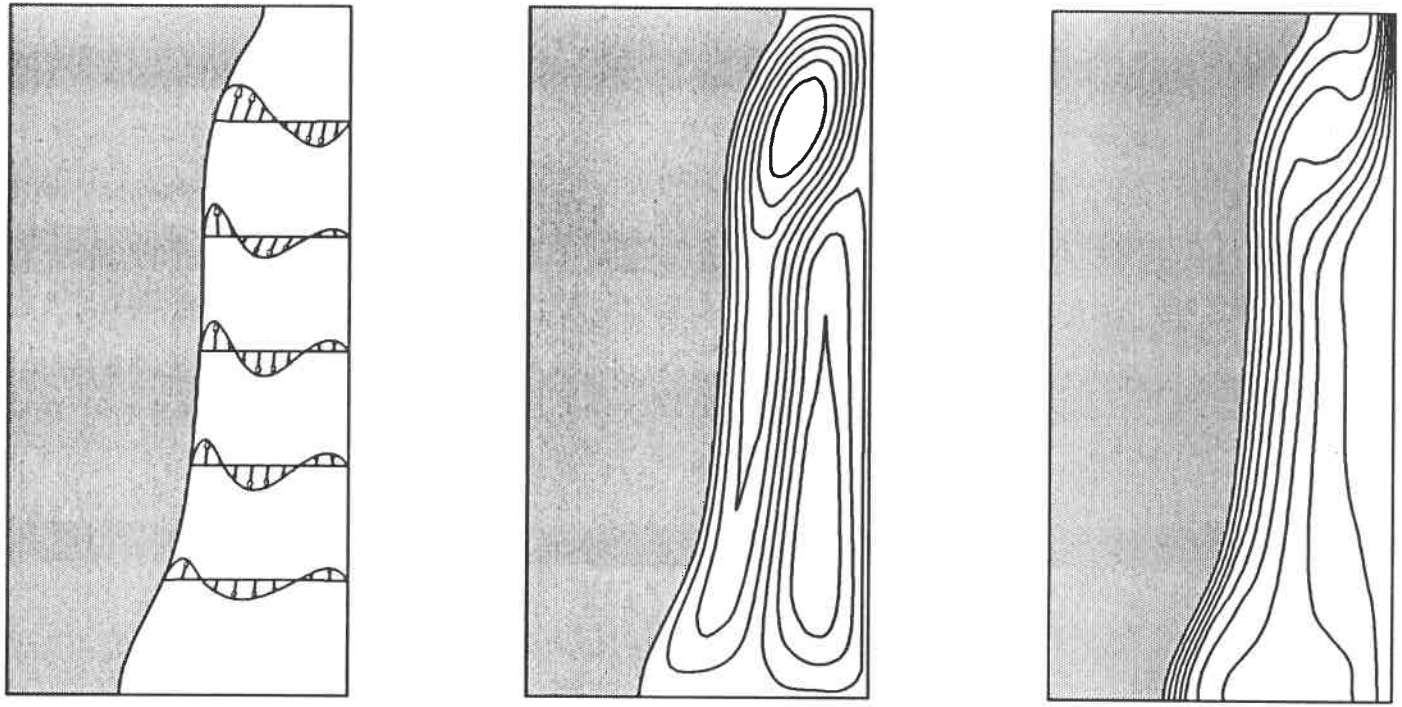

Figure 7.3: Velocity profiles, isotherms and flow pattern of melting at $T_w = 6^0C, \tau = 0.06$

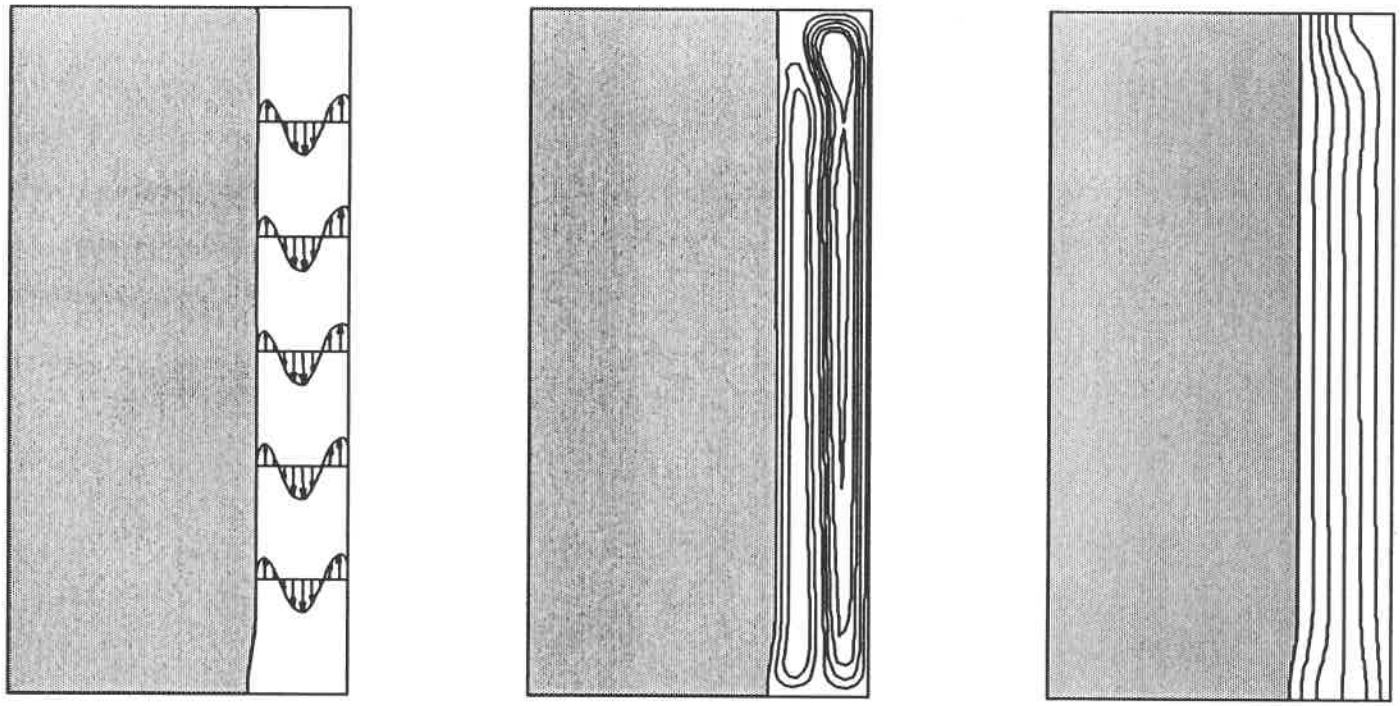

Figure 7.4: Velocity profiles, isotherms and flow pattern of melting at $T_w = 8^0C$, $\tau = 0.03$

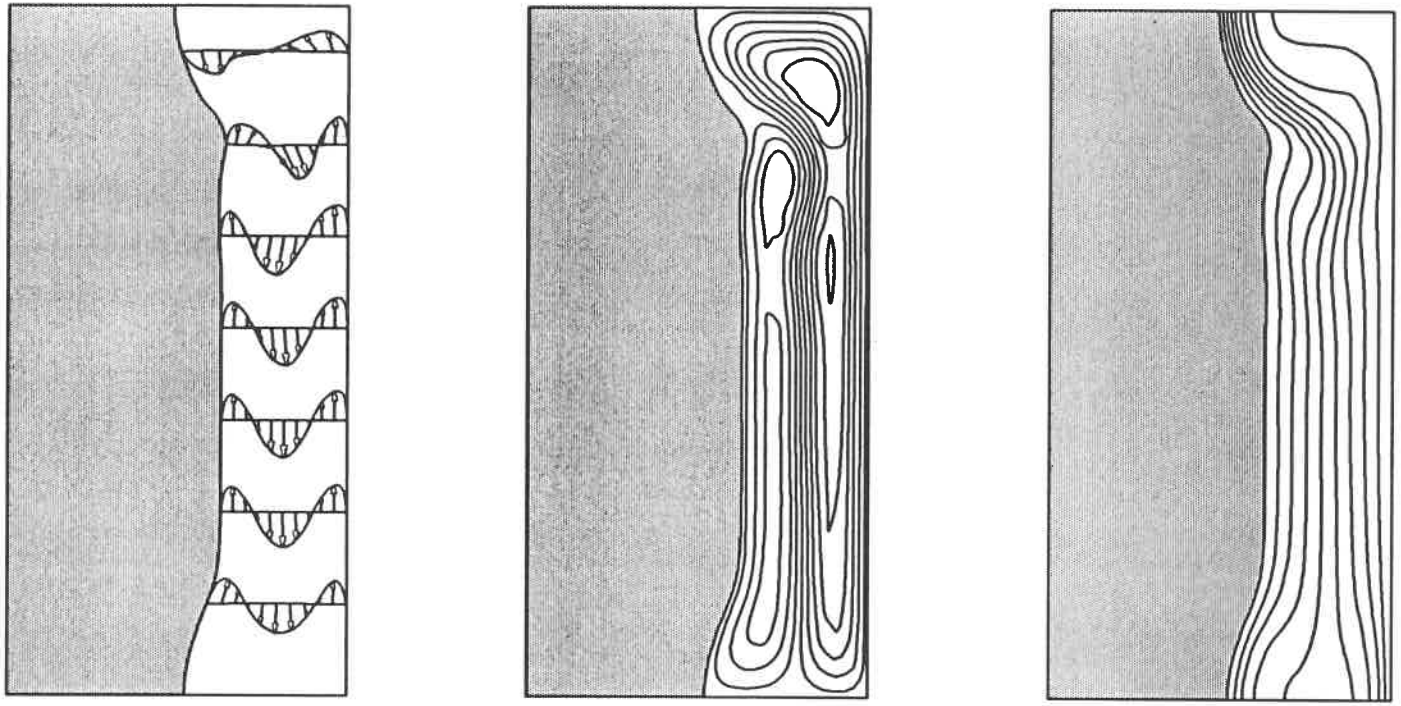

Figure 7.5: Velocity profiles, isotherms and flow pattern of melting at $T_w = 8^0C$, $\tau = 0.70$

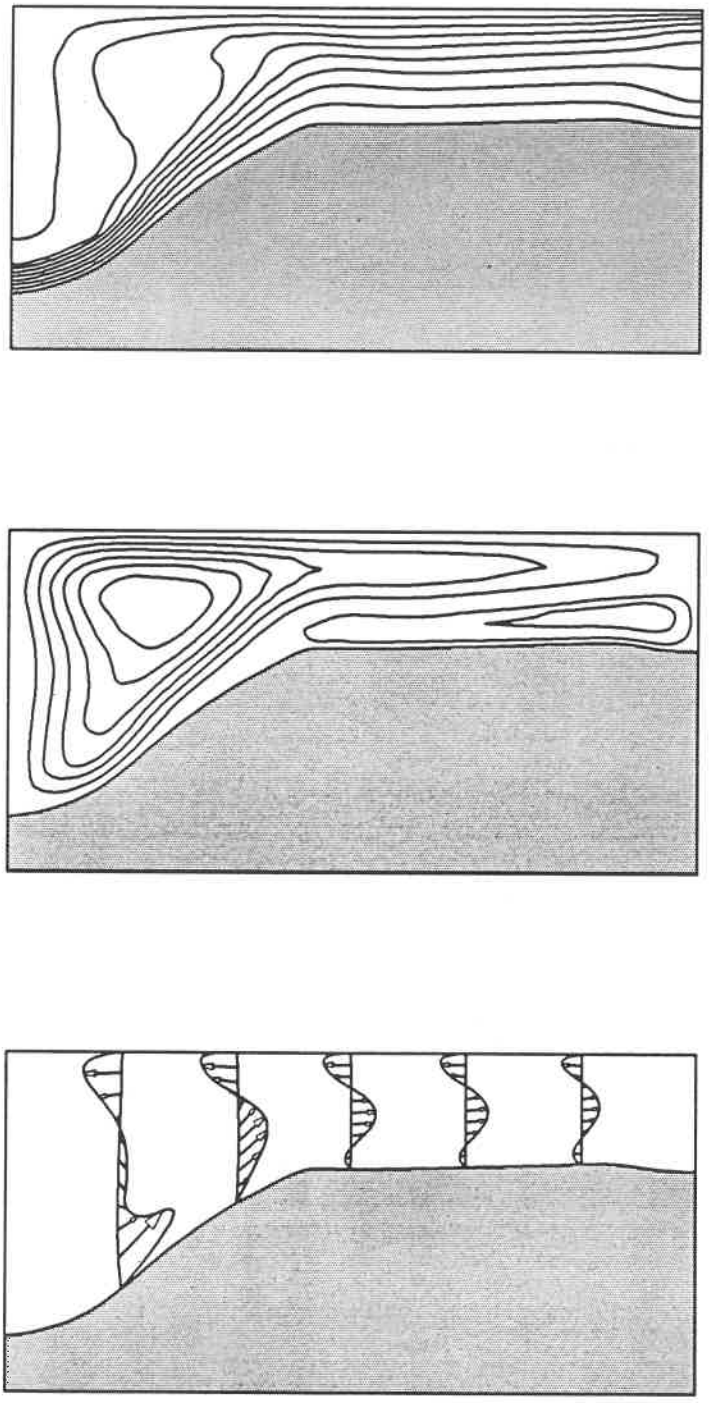

Figure 7.6: Velocity profiles, isotherms and flow pattern of melting at $T_w = 10^oC, \tau = 0.06$

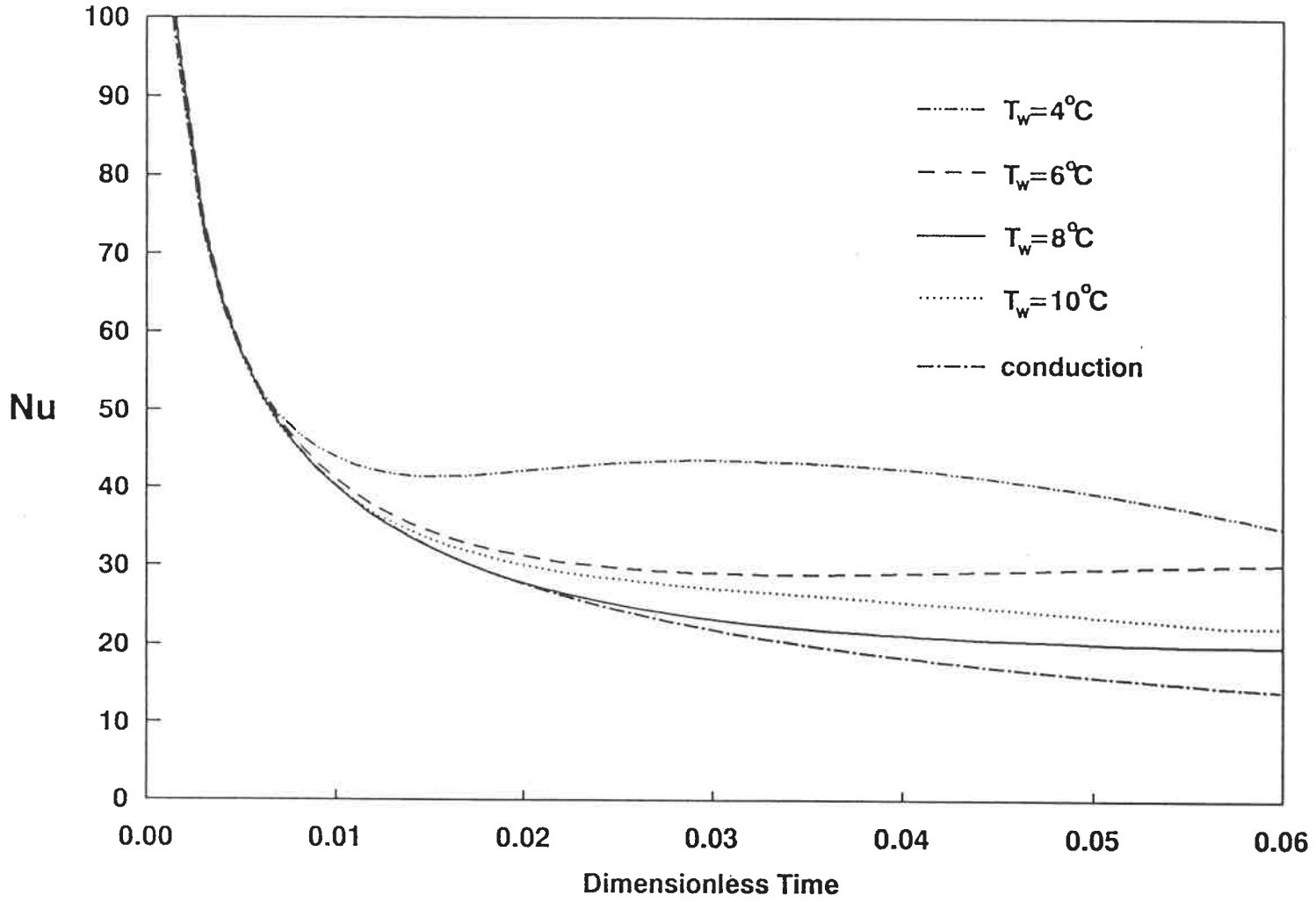

Figure 7.7: Variations of Nusselt number as function of time for $T_w = 4^0, 6^0, 8^0$ and $10^0 C$

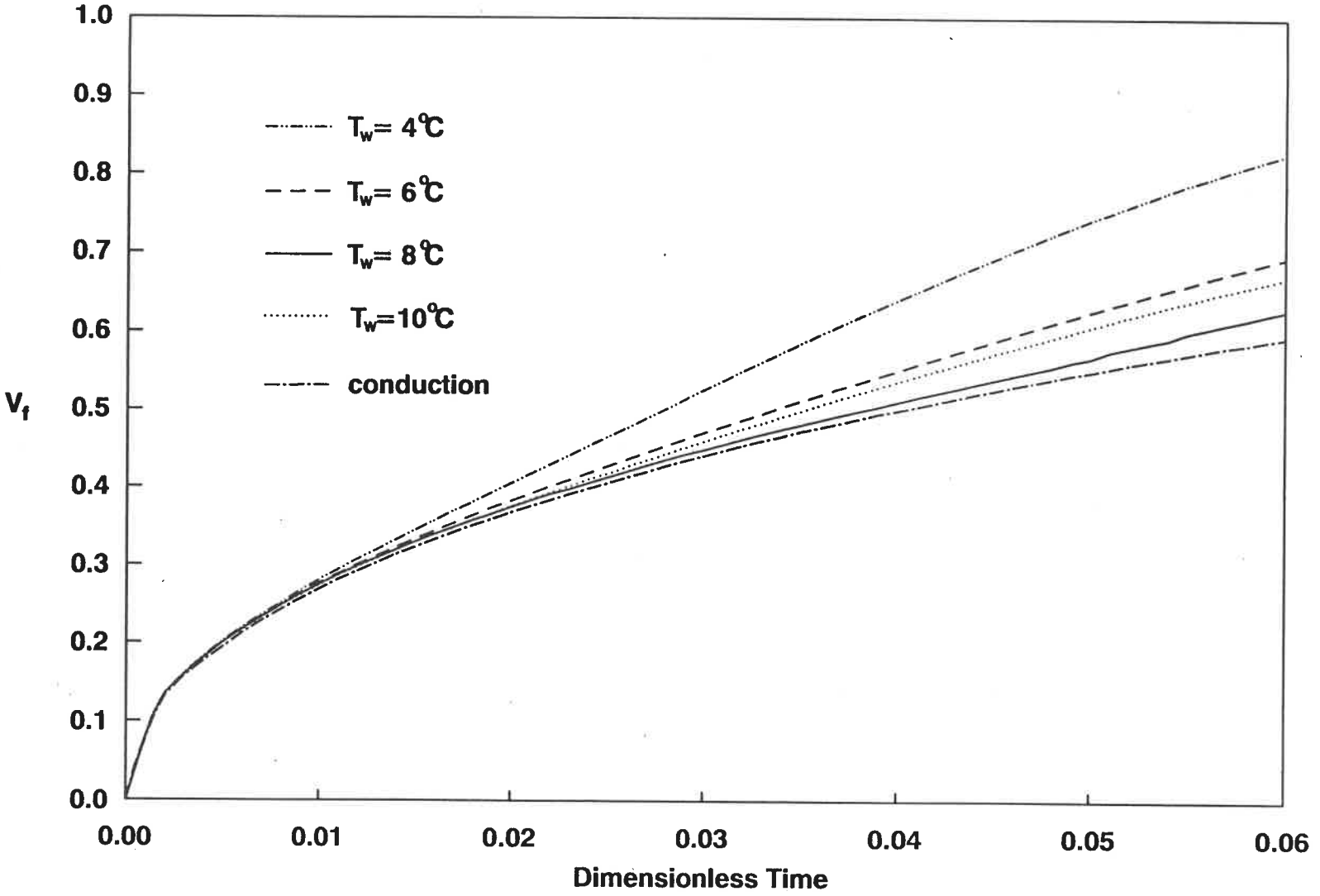

Figure 7.8: Molten fractions as function of time for $T_w = 4^0, 6^0, 8^0$ and $10^0 C$

Chapter 8

CONCLUSIONS AND RECOMMENDATIONS

A numerical method capable of handling a phase-change process has been devised to model melting in a vertical cylinder with different boundary conditions. The governing equations for the phase-change problem have been developed in curvilinear coordinates. The body-fitted coordinate system was employed to deal with complex geometries and a moving boundary. The transformed equations were discretized by the conventional finite difference approach on the transformed plane. The convective terms were treated by the second-order upwind scheme.

The computations have been carried out for several cases: melting outward from a vertical cylinder imbedded in the phase-change material, inward melting within a vertical cylinder, melting in a vertical cylinder with density inversion, melting in a vertical cylinder by heating from the bottom and melting within an isothermal cylindrical enclosure. From this comprehensive analytical study it is concluded that:

- The coordinate transformation has shown its flexibility and effectiveness in handling an irregular domain for a moving boundary problem.
- The "quasi-static" and "smooth interface" approximations can significantly

affect the shape and the velocity of melting profile in the computations, especially at the later times when natural convection becomes dominant.

- Based on several kinds cases of melting in/around a vertical cylinder, natural convection was shown to play a very important role during the melting process. Therefore, the predictions for the melting process based on the conduction mode can significantly differ form those taking into account natural convection.

- Study on the melting of ice in a vertical cylinder has shown that the density inversion can significantly influence the melting process. The single cell circulation affects the effectiveness of heat transfer. The counter-rotating circulation reduce the heat transfer rate. In the temperature range considered in this study, there exists a maximum and a minimum heat transfer rate. They occur at 4^0C and 8^0 respectively.

- Melting with the bottom heating shows the Bénard convection. It has been found that the cells near the symmetry axis are always engulfed by the one next to t. The shape of the melting front and the local Nusselt number profile oscillate with time. The critical Rayleigh number for the onset of convection is 2197.

- In the case of a melting within an isothermal enclosure, the previous three types of melting are interacting. The highest heat transfer rate is found at the bottom wall. The heat transfer rate at the top of the cylinder becomes vanishingly small as the melting progresses.

Because of the time limit, the present research are mainly focused on the melting process without considering heat conduction in the solid. As a matter

of fact, melting with a subcool in the solid occurs quite often in practice. A comprehensive study for melting taking into account heat conduction in the solid will be the subject of a future research.

In the present research, we have taken advantage of the symmetry of a cylinder, where we ensure that the flow in the melt layer is two-dimensional. In the case of a very high Rayleigh number, a three-dimensional flow or Bénard cells may occur as the melt layer become larger. In the study of this case, a complete three-dimensional formulation should be adopted.

Bibliography

[1] L. I. Rubinstein, "The Stefan Problem", *American Mathematics Society Translation of Mathematics Monographs.*, Vol. 27, (1971).

[2] H. S. Carslaw and J. C. Jaeger, "CONDUCTION OF HEAT IN SOLIDS", 2nd Ed., p. 283-353. Oxford University Press, London and New York, (1959).

[3] S. G. Bankoff, "Heat Conduction or Diffusion with Change of Phase", *Advances in Chemical Engineering*, Vol. 5, pp. 75, (1964).

[4] J. P. Hartnett and T. F. Irvine, "ADVANCES IN HEAT TRANSFER", Academic Press Inc., Vol. 19, (1989).

[5] M. S. El-Genk and A. W. Cronenberg, "Solidification in a Semi-Infinite Region with Boundary Conditions of the Second Kind: An Exact Solution", *Letters in Heat and Mass Transfer*, Vol. 6, pp. 321-327, (1979).

[6] S. H. Cho and J. E. Sunderland, "Approximate Temperature Distribution for Phase Change of A Semi-Infinite Body", *ASME Journal of Heat Transfer*, Vol. 103, pp. 401, (1981).

[7] S. H. Cho and J. E. Sunderland, "Heat-Conduction Problems with Melting or Freezing", *ASME Journal of Heat Transfer*, Vol. 91, pp. 421, (1969).

[8] L. S. Yao and W. Cherney, "Transient Phase-Change Around a Horizontal Cylinder", *International Journal of Heat and Mass Transfer*, Vol. 24, pp. 1971, (1981).

[9] G. W. Evans, E. Isaacson, and J. K. L. MacDonald, "Stefan-Like Problems", *Quarterly of Applied Mathematics*, Vol. 8, pp. 312, (1950).

[10] L. N. Tao, "The Stefan Problem with Arbitrary Initial and Boundary Conditions", *Quarterly of Applied Mathematics*, Vol. 36, pp. 223-233, (1979).

[11] L. N. Tao, "On Free Boundary Problems with Radiation Boundary Conditions", *Quarterly of Applied Mathematics*, Vol. 37, pp. 1, (1979).

[12] L. N. Tao, "The Solidifications Problems Including the Density Jump at the Moving Boundary", *Quarterly journal of Mechanics and Applied Mathematics*, Vol. 32, pp. 175-185, (1979).

[13] L. N. Tao, "On Free Boundary Problems with Arbitrary Initial and Flux Conditions", *Journal of Applied Mathematics and Physics*, Vol. 30, pp. 416, (1979).

[14] D. E. Rosner, "Lifetime of a Highly Soluble Dense Spherical Particle", *Journal of Physical Chemistry*, Vol. 73, pp. 382, (1969).

[15] J. L. Duda and J. S. Vrentas, "Perturbation Solutions of Diffusion-Controlled Moving Boundary Problem", *Chemical Engineering Science*, Vol. 24, pp. 461, (1969).

[16] M. Prud'homme and T. H. Nguyen, "Solution par Perturbations Singulères pour un Problème de Stéfan Généralisé", *International Journal of Heat and Mass Transfer*, Vol. 32, No. 8, pp. 1501-1515, (1989).

[17] L. M. Jiji and S. Weinbaum, "Perturbation Solutions for Melting of Freezing in Annular Regions Initially not at the Fusion Temperature", *International Journal of Heat and Mass Transfer*, Vol. 21, pp. 581-592, (1978).

[18] S. Weinbaum and L. M. Jiji, "Singular Perturbation Theory for Melting or Freezing in Finite Domains not at the Fusion Temperature", *Journal of Applied Mechanics*, Vol. 44, pp. 25, (1977).

[19] R. I. Pedroso and G. A. Domoto, "Exact Solution by Perturbation Method for Planar Solidification of a Saturated Liquid with Convection at the Wall", *International Journal of Heat Transfer*, Vol. 16, pp. 1816, (1973).

[20] H. G. Landau, "Heat Conduction in a Melting Solid", *Quarterly Applied Mathematics*, Vol. 8, pp. 81, (1950).

[21] K. T. Yang, "Formation of Ice in Plane Stagnation Flow", *Applied Science Research*, Vol. 17, pp. 377, (1967).

[22] J. L. Duda, M. F. Malone, R. H. Notter, and J. S. Vrentas, "Analysis of Two-Dimensional Diffusion-Controlled Moving Boundary Problems", *International Journal of Heat and Mass Transfer*, Vol. 18, pp. 901, (1975).

[23] T. Saitoh, "Numerical Method for Multidimensional Freezing Problems in Arbitrary Domains", *ASME Journal of Heat and Transfer*, Vol. 100, pp. 294, (1978).

[24] E. M. Sparrow, S. Ramadhyani, and S. V. Partankar, "Effect of Subcooling on Cylindrical Melting", *ASME Journal of Heat Transfer*, Vol. 100, pp. 395-402, (1978).

[25] N. Shamsundar and E. M. Sparrow, "Analysis of Multidimensional Conduction Phase Change Via the Enthalpy Model", *ASME Journal of Heat Transfer*, Vol. 97, pp. 333, (1975).

[26] R. M. Furzeland, "A Comparative Study of Numerical Methods for Moving Boundary Problems", *Journal of Institute of Mathematics and Applications*, Vol. 26, pp 411, (1980).

[27] D. C. Baxter, "The Fusion Times of Slabs and Cylinder", *ASME Journal of Heat Transfer*, Vol. 84, pp317, (1962).

[28] R. Siegel, Boundary Perturbation Methods for Free Boundary Problem in Convectively Cooled Continuous Casting", *ASME Journal of Heat Transfer*, Vol.108, pp. 230, (1986).

[29] P. G. Kroeger and S. Ostrach, "The Solution of a Two-Dimensional Freezing Problem Including Convection Effects in the Liquid Region", *International of Journal of Heat and Mass Transfer*, Vol. 17 pp. 1191-1207, (1974).

[30] J. Crank, "Two Methods for the Numerical Solution of Moving Boundary Problems in Diffusion and Heat Flow", *Quarterly Journal of Mechanics and Applied Mathematics*, Vol. 10, pp. 220, (1975).

[31] Y. K. Chuang and J. Szekely, "On the Use of Green Function for Solving Melting and Solidification Problems", *International of Journal of Heat and Mass Transfer*, Vol. 14, pp. 1285, (1971).

[32] P. K. Banerjee and R. P. Shaw, "Boundary Element Formulation for Melting and Solidification Problems", *Developments in Boundary Element Methods*, Applied Science Public, London, (1982).

[33] C. Tien and Y. C. Yen, "Approximate Solution of a Melting Problem with Natural Convection", *Chemical Engineering Progress Symposium Series*, Vol. 62, pp. 166, (1966).

[34] D. V. Boger and J. W. Westwater, "Effect of Buoyancy on the Melting and Freezing Process", *ASME Journal of Heat Transfer*, Vol. 89, pp. 81, (1967).

[35] N. W. Hale and R. Viskanta, "Solid-Liquid Phase-Change Heat Transfer and Interface Motion in Materials Cooled or Heated from Above or Below", *International Journal of Heat and Mass Transfer*, Vol. 23, pp. 283, (1980).

[36] N. W. Hale and R. Viskanta, "Photographic Observations of the Liquid-Solid Interface Motion During Melting of a Solid Heated from an Isothermal Vertical Wall", *Letters in Heat Transfer*, Vol. 5, pp. 329-337, (1978).

[37] M. Okada, "Analysis of Heat Transfer during Melting from a Vertical Wall", *International Journal of Heat and Mass Transfer*, Vol. 27, pp. 2059, (1984).

[38] A. Gadgil and D. Gobin, "Analysis of Two-Dimensional Melting in Rectangular Enclosures in Presence of Convection", *ASME Journal of Heat Transfer*, Vol. 106, pp. 20, (1984).

[39] C. J. Ho and R. Viskanta, "Heat Transfer during Melting from an Isothermal Vertical Wall", *ASME Journal of Heat Transfer*, Vol. 106, pp. 12-19, (1984).

[40] B. W. Webb and R. Viskanta, "Analysis of Heat Transfer During Melting of a Pure Metal from an Isothermal Wall", *Numerical Heat Transfer*, Vol. 9, pp. 539-558, (1986).

[41] N. Ramachandran, J. P. Gupta, and Y. Jaluria, "Two Dimensional Solidification with Natural Convection in the Melt and Convective and Radiative Boundary Conditions", *Numerical Heat Transfer*, Vol. 4, pp. 469-484, (1981).

[42] N. Ramachandran, J. P. Gupta, and Y. Jaluria, "Thermal and Fluid Flow Effects during Solidification in a Rectangular Enclosure", *International Journal of Heat and Mass Transfer*, Vol. 35, pp. 187-194, (1982).

[43] C. Benard, D. Gobin, and A. Zanoli, "Moving Boundary Problem: Heat Conduction in the Solid Phase of a Phase-Change Material during Melting Driven by Natural Convection in the Liquid", *International Journal of Heat and Mass Transfer*, Vol. 29, pp. 1669-1681, (1986).

[44] A. G. Bathelt, R. Viskanta, and W. Leidenfrost, "An Experimental Investigation of Natural Convection in the Melted Region around a Heated Horizontal Cylinder", *Journal of Fluid Mechanics*, Vol. 90, pp. 227, (1979).

[45] J. Prusa and L. S. Yao, "Melting around a Horizontal Heated Cylinder: Part I - Perturbation and Numerical Solution for Constant Heat Flux Boundary Condition", *ASME Journal of Heat Transfer*, Vol. 106, pp. 376, (1984).

[46] J. Prusa and L. S. Yao, "Melting around a Horizontal Heated Cylinder: Part II - Numerical Solution for Isothermal Boundary Condition". *ASME Journal of Heat Transfer*, Vol. 106, pp. 469, (1984).

[47] H. Rieger, U. Projahn, and H. Beer, "Analysis of the Heat Transport Mechanisms during Melting around a Horizontal Circular Cylinder", *International Journal of Heat and Transfer*, Vol. 25, No. 1, pp. 137-147, (1982).

[48] H. Rieger, U. Projahn, M. Bereiss, and H. Beer, "Heat Transfer During Melting Inside Horizontal Tube", *ASME Journal of Heat Transfer*, Vol. 105, pp. 226-234, (1983).

[49] C. J. Ho and R. Viskanta, "Heat Transfer during inward Melting in a Horizontal Tube", *International Journal of Heat and Mass Transfer* Vol. 27, pp. 705, (1984).

[50] C. J. Ho and S. Chen, "Numerical Simulation of Melting of Ice around a Horizontal Cylinder", *International Journal of Heat and Mass Transfer*, Vol. 29, pp. 1359-1369, (1986).

[51] J. Herrmann, W. Leidenfrost, and R. Viskanta, "Melting of Ice around a Horizontal Isothermal Cylindrical Heat Source, *Chemical Engineering Communication*, Vol. 25, pp. 63-78, (1984).

[52] E. M. Sparrow, S V. Patankar, and S. Ramadhyani, "Analysis of Melting in the Presence of Natural Convection in the Melt Region", *ASME Journal of Heat Transfer*, Vol. 99, pp. 521-526, (1977).

[53] Y. K. Wu, M. Prud'homme, and T. H. Nguyen, Étude numérique de la Fusion autour d'un Cylindre Vertical Soumis à Deux Types de Conditions Limites", *International Journal of Heat and Mass Transfer*, Vol. 32, No. 10, pp. 1927-1938, (1989).

[54] M. Bareiss and H. Beer, "Influence of Natural Convection on the Melting Process in a Vertical Cylindrical Enclosure", *Letter in Heat and Mass Transfer*, Vol. 7, pp. 329-338, (1980).

[55] M. Bareiss and H. Beer, "Experimental Investigation of Melting Heat Transfer with Regard to Different Geometric Arrangements", *Letter in Heat and Mass Transfer*, Vol. 11, pp. 323-333, (1984).

[56] R. G. Kemink and E. M. Sparrow, "Heat Transfer Coefficients of Melting about a Vertical Cylinder with or without Subcooling and for Open or Closed Containment", *International Journal of Heat and Mass Transfer*, Vol. 24, pp. 1699-1710, (1981).

[57] M. Vinokur, "Conservation Equations of Gasdynamics in Curvilinear Coordinate System", *Journal of Computational Physics*, Vol. 14, pp. 105-125, (1974).

[58] R. K. Shah, and A. L. London, "LAMINAR FLOW FORCED CONVECTION IN DUCTS", Academic, New York, (1978).

[59] J. F. Thompson, F. C. Thames, and C. W. Mastin, "Boundary-Fitted Curvilinear

Coordinate Systems for Solution of Partial Difference Equation On Fields Containing any Number of Arbitrary Two-Dimension Bodies", *NASA Contractor Report*, CR-2729, (1977).

[60] J. F. Thompson, Z. U. A. Warsi, and C. W. Mastin, "NUMERICAL GRID GENERATION", *North Holland*, (1985).

[61] A. Goldman and Y. C. Kao, "Numerical Solution to a Two-Dimensional Conduction Problem Using Rectangular and Cylindrical Body-Fitted Coordinate Systems", *ASME Journal of Heat Transfer*, Vol. 103, pp. 753-758, (1981).

[62] J. F. Thompson, Z. U. A. Warsi, and C. W. Mastin, "Boundary-Fitted Coordinate Systems for Numerical Solution of Partial Differential Equations- A Review", Journal of Computational Physics, Vol. 47, pp. 1-108, (1982).

[63] C. W. Mastin and J. F. Thompson, "Elliptic Systems and Numerical Transformations", *Journal of Mathematical Analysis and Applications*, Vol. 62, (1978).

[64] P. D. Thomas and J. F. Middlecoff, "Direct Control of the Grid Point Distribution in Meshes Generated by Elliptic Equations", *AIAA Journal*, Vol. 18, No. 6, pp. 652-656, (1980).

[65] K. Miki and T. Takagi, "Numerical Solution of Poisson's Equation with Arbitrarily Shaped Boundaries Using a Domain Decomposition and Overlapping Technique", *Journal of Computational Physics*, Vol. 67, pp. 263-278, (1986).

[66] W. Shyy and M. E. Braaten, "Three-Dimensional Analysis of the Flow in a Curved Hydraulic Turbine Draft Tube", *International Journal for Numerical Methods in Fluids*, Vol. 6 pp. 861-882, (1986).

[67] B. P. Leonard, "A Stable and Accurate Convective Modelling Procedure Base on Quadratic upstream Interpolation", *Computer methods in Applied Mechanics and Engineering*, Vol. 19, pp. 59-98, (1979).

[68] J. P. Coulter and S. İ. Güçeri, "Laminar and Turbulent Natural Convection within Irregularly Shaped Enclosures", *Numerical Heat Transfer*, Vol. 12, pp. 211-227, (1987).

[69] S. Ramanathan and R. Kumar, "Comparison of Boundary-Fitted Coordinates with Finite-Element Approach for Solution of Conduction Problems", *Numerical Heat Transfer*, Vol. 14, pp. 187-211, (1988).

[70] Wei Shyy, "A Study of Finite Difference Approximations to Steady-State, Convection Dominated Flow Problem", *Journal of Computational Physics*, Vol, 57, pp. 415-483, (1985).

[71] Roache, P. J., "COMPUTATIONAL FLUID DYNAMICS", Hermosa, Albuqerque, New Mexico, (1976).

[72] A.G. Tkachev, "Heat Exchange in Melting and Freezing of Ice", *Problems of Heat Transfer during a Change of State*, AEC-TR 3405, pp. 169-178, (1953).

[73] T. Saitoh, and K. Hirose, "High Rayleigh Number Solutions to Problem of Latent Heat Thermal Energy Storage in a Horizontal Cylinder Capsule", *ASME Journal of Heat Transfer*, Vol. 104, pp. 545-553, (1982).

[74] H. J. Merk, "The Influence of Melting and Anomalous Expansion on the Thermal Convection in Laminar Boundary Layers", *Applied Science Research*, Vol. 4, pp. 435-452, (1954).

[75] J. M. Dumore, H. J. Merk, and J. A. Prins, "Heat Transfer from Water to Ice by Thermal Convection", *Natural*, Vol. 172, pp. 460-461, (1953).

[76] C. R. Vanier, and C. Tien, "Effect of Maximum Density and Melting on Natural Convection Heat Transfer from a Vertical Plate", *Chemical Engineering Progress Symposium Series*, Vol. 64, pp. 240-254, (1968).

[77] S. Ostrach, and D. Pnueli, "The Thermal Instability of Completely Confined Fluids Inside Some Particular Configurations", *ASME Journal of Heat Transfer*, Vol. 85, pp. 346-354, (1963).

[78] M. Sherman and S. Ostrach, "Lower Bounds to the Critical Rayleigh Number in Completely Confined Regions", *ASME Journal of Applied Mechanics*, Vol. 89, pp. 308-312, (1967).

[79] M. R. Samuels and S. W. Churehill, "Stability of a Fluid in a Rectangular Region Heated from Below", *AIChE Journal*, Vol. 13, pp. 77-85, (1967).

[80] E. Schmidt and P. L. Silveston, "Natural Convection in Horizontal Liquid Layers", *Chemical Engineering Progress Symposium Series*, Vol. 55, pp. 163-169, (1959).

[81] I. Catton and D. K. Edwards, "Effect of Side Walls on Natural Convection between Horizontal Plates Heated from Below", *ASME Journal of Heat Transfer*, Vol. 89, pp. 295-299, (1967).

[82] W. L. Heitz and J. W. Westwater, "Critical Rayleigh Numbers for Natural Convection of Water Confined in Square Cells with L/D from 0.5 to 8", *ASME Journal of Heat Transfer*, Vol. 93, pp. 188-196, (1971).

[83] Y. C. Yen, "Onset of Convection in a Layer of Water Formed by Melting Ice from Below", *Physics of Fluids*, Vol. 11, pp. 1263-1270, (1968).

[84] N. Seki, S. Fukusako and M. Sugawara, "A Criterion of Onset of Free Convection in a Horizontal Melted Water Layer with Free Surface", *ASME Journal of Heat Transfer*, Vol. 99, pp. 92-98, (1977).

[85] E. M. Sparrow, L. Lee and N. Shamsundar, "Convective Instability in a Melt Layer Heated from Below", *ASME Journal of Heat Transfer*, Vol. 98, pp. 88-94, (1976).

Appendix A

TRANSFORM RELATIONS IN COVARIANT SCALE FACTORS

The general transformation from a physical plane (x, y) to a rectangular plane (ξ, η) is given by

$$\begin{bmatrix} \xi \\ \eta \end{bmatrix} = \begin{bmatrix} \xi(x,y) \\ \eta(x,y) \end{bmatrix} \tag{A.1}$$

The Jacobian matrix for this transformation is as follows

$$J_1 = \begin{bmatrix} \xi_x & \xi_y \\ \eta_x & \eta_y \end{bmatrix} \tag{A.2}$$

The inverse function or transformation of (1) is given by

$$\begin{bmatrix} x \\ y \end{bmatrix} = \begin{bmatrix} x(\xi,\eta) \\ y(\xi,\eta) \end{bmatrix} \tag{A.3}$$

The Jacobian matrix of (3) is

$$J_2 = \begin{bmatrix} x_\xi & x_\eta \\ y_\xi & y_\eta \end{bmatrix} \tag{A.4}$$

The Jacobian determinant is

$$\begin{aligned} J &= det[J_2] \\ &= x_\xi y_\eta - x_\eta y_\xi \end{aligned} \tag{A.5}$$

The Jacobian matrices (2) and (3) are related by

$$J_1 = [J_2]^{-1} \tag{A.6}$$

i.e.

$$\begin{bmatrix} \xi_x & \xi_y \\ \eta_x & \eta_y \end{bmatrix} = \frac{1}{J} \begin{bmatrix} y_\eta & -x_\eta \\ -y_\xi & x_\xi \end{bmatrix} \tag{A.7}$$

which implies the relations below:

$$\xi_x = y_\eta / J \tag{A.8}$$

$$\xi_y = -x_\eta / J \tag{A.9}$$

$$\eta_x = -y_\xi / J \tag{A.10}$$

$$\eta_y = x_\xi / J \tag{A.11}$$

Using the chain rule, the transformation relations are

$$f_x = (y_\eta f_\xi - y_\xi f_\eta)/J \tag{A.12}$$

$$f_y = (-x_\eta f_\xi + x_\xi f_\eta)/J \tag{A.13}$$

$$\begin{aligned} f_{xx} = {} & (y_\eta^2 f_{\xi\xi} - 2y_\xi y_\eta f_{\xi\eta} + y_\xi^2 f_{\eta\eta})/J^2 \\ & + \left[(y_\eta^2 y_{\xi\xi} - 2y_\xi y_\eta y_{\xi\eta} + y_\xi^2 y_{\eta\eta})(x_\eta f_\xi - x_\xi f_\eta)\right. \\ & \left. +(y_\eta^2 x_{\xi\xi} - 2y_\xi y_\eta x_{\xi\eta} + y_\xi^2 x_{\eta\eta})(y_\xi f_\eta - y_\eta f_\xi)\right]/J^3 \end{aligned} \tag{A.14}$$

$$\begin{aligned} f_{yy} = {} & (x_\eta^2 f_{\xi\xi} - 2x_\xi x_\eta f_{\xi\eta} + x_\xi^2 f_{\eta\eta})/J \\ & + \left[(x_\eta^2 y_{\xi\xi} - 2x_\xi x_\eta y_{\xi\eta} + x_\xi^2 y_{\eta\eta})(x_\eta f_\xi - x_\xi f_\eta)\right. \\ & \left. +(x_\eta^2 x_{\xi\xi} - 2x_\xi x_\eta x_{\eta\eta} + x_\xi^2 x_{\xi\xi})(y_\xi f_\eta - y_\eta f_\xi)\right]/J^3 \end{aligned} \tag{A.15}$$

$$\begin{aligned} \nabla^2 f = {} & g_{22} f_{\xi\xi} - 2g_{12} f_{\xi\eta} + g_{11} f_{\eta\eta} \\ & + [(g_{22} x_{\xi\xi} - 2g_{12} x_{\xi\eta} + g_{11} x_{\eta\eta})(y_\xi f_\eta - y_\eta f_\xi) \\ & +(g_{22} y_{\xi\xi} - 2g_{12} y_{\xi\eta} + g_{11} y_{\eta\eta})(x_\eta f_\xi - x_\xi f_\eta)]/J^3 \end{aligned} \tag{A.16}$$

where

$$g_{11} = x_\xi^2 + y_\xi^2 \tag{A.17}$$

$$g_{22} = x_\eta^2 + y_\eta^2 \tag{A.18}$$

$$g_{12} = x_\xi x_\eta + y_\xi y_\eta \tag{A.19}$$

The relations between g_{ii} and g^{jj} are

$$g^{11} = g_{22}/J^2 \tag{A.20}$$

$$g^{22} = g_{11}/J^2 \tag{A.21}$$

$$g^{12} = -g_{12}/J^2 \tag{A.22}$$

The time derivative can be transformed as below:

$$\begin{aligned} \left.\frac{\partial f}{\partial \tau}\right|_{x,y} &= \frac{\partial(x,y,f)}{\partial(\xi,\eta,\tau)} \Big/ \frac{\partial(x,y,\tau)}{\partial(\xi,\eta,\tau)} \\ &= (f_\tau)_{\xi,\eta} - \frac{x_\tau(f_\xi y_\eta - f_\eta y_\xi)}{J} + \frac{y_\tau(f_\xi x_\eta - f_\eta x_\xi)}{J} \end{aligned} \tag{A.23}$$

The unit vector normal to a line of constant ξ is given in covariant scale factors as

$$\mathbf{n}^{(\xi)} = \frac{1}{\sqrt{g_{22}}}(y_\eta \mathbf{i} - x_\eta \mathbf{j}) \tag{A.24}$$

and for a line of $\eta = constant$ as

$$\mathbf{n}^{(\eta)} = \frac{1}{\sqrt{g_{11}}}(-y_\xi \mathbf{i} + x_\xi \mathbf{j}) \tag{A.25}$$

Gradient of a scalar f is

$$\nabla f = [(y_\eta f_\xi - y_\xi f_\eta)\mathbf{i} + (x_\xi f_\eta - x_\eta f_\xi)\mathbf{j}]/J \tag{A.26}$$

Directional derivatives become

$$\left.\frac{\partial f}{\partial n}\right|_{\xi=const.} = \mathbf{n}\cdot\nabla f = \frac{1}{J\sqrt{g_{22}}}(g_{22}f_\xi - g_{12}f_\eta) \tag{A.27}$$

$$\left.\frac{\partial f}{\partial n}\right|_{\eta=const.} = \mathbf{n}\cdot\nabla f = \frac{1}{J\sqrt{g_{11}}}(g_{11}f_\eta - g_{12}f_\xi) \tag{A.28}$$

Appendix B

UPWIND SCHEMES

Upwind schemes for approximating the convection terms.

(a) First-order upwind:

$$u\frac{\partial\phi}{\partial x}\bigg|_i = u\frac{\phi_i - \phi_{i-1}}{\Delta x} \qquad for \quad u > 0$$

$$= u\frac{\phi_{i+1} - \phi_i}{\Delta x} \qquad for \quad u < 0$$

$$= -\frac{|u|+u}{2\Delta x}\phi_{i-1} + \frac{2|u|}{2\Delta x}\phi_i - \frac{|u|-u}{2\Delta x}\phi_{i+1} \qquad \text{(B.1)}$$

(b) Second-order upwind:

$$u\frac{\partial\phi}{\partial x}\bigg|_i = u\frac{3\phi_i - 4\phi_{i-1} + \phi_{i-2}}{2\Delta x} \qquad for \quad u > 0$$

$$= u\frac{-\phi_{i+2} + 4\phi_{i+1} - 3\phi_i}{2\Delta x} \qquad for \quad u < 0$$

$$= \frac{|u|+u}{4\Delta x}\phi_{i-2} - \frac{|u|+u}{\Delta x}\phi_{i-1} + \frac{2|u|}{3\Delta x}\phi_i - \frac{|u|-u}{\Delta x}\phi_{i+1} + \frac{|u|-u}{4\Delta x}\phi_{i+2} \qquad \text{(B.2)}$$

(c) Third-order upwind:

$$u\frac{\partial\phi}{\partial x}\bigg|_i = u\frac{2\phi_{i+1}+3\phi_i-6\phi_{i-1}+\phi_{i-2}}{6\Delta x} \qquad for \quad u>0$$

$$= u\frac{-\phi_{i+2}+6\phi_{i+1}-3\phi_i-2\phi_{i-1}}{6\Delta x} \qquad for \quad u<0$$

$$= \frac{|u|+u}{12\Delta x}\phi_{i-2} - \frac{|u|+2u}{3\Delta x}\phi_{i-1} + \frac{|u|}{2\Delta x}\phi_i - \frac{|u|-2u}{3\Delta x}\phi_{i+1} + \frac{|u|-u}{12\Delta x}\phi_{i+2} \qquad (B.3)$$

(d) QUICK:

$$u\frac{\partial\phi}{\partial x}\bigg|_i = u\frac{3\phi_{i+1}+3\phi_i-7\phi_{i-1}+\phi_{i-2}}{8\Delta x} \qquad for \quad u>0$$

$$= u\frac{-\phi_{i+2}+7\phi_{i+1}-3\phi_i-3\phi_{i-1}}{8\Delta x} \qquad for \quad u<0$$

$$= \frac{|u|+u}{16\Delta x}\phi_{i-2} - \frac{2|u|+5u}{8\Delta x}\phi_{i-1} + \frac{3|u|}{8\Delta x}\phi_i - \frac{2|u|-5u}{8\Delta x}\phi_{i+1} + \frac{|u|-u}{16\Delta x}\phi_{i+2} \qquad (B.4)$$

To summarize the schemes described above, a general form can be written as follows

$$u\frac{\partial\phi}{\partial x}\bigg|_i = A^u\phi_{i-2} + B^u\phi_{i-1} + C^u\phi_i + D^u\phi_{i+1} + E^u\phi_{i+2} \qquad (B.5)$$

Appendix C

TDMA AND PDMA METHODS

C.1 ALGORITHM FOR A TRIDIAGONAL SYSTEM

The equations to be solved must be of the form

$$A_i x_{i-1} + B_i x_i + C_i x_{i+1} = D_i \tag{C.6}$$

The matrix for these equations are

$$\begin{bmatrix} B_{min} & C_{min} & & & \\ A_{min+1} & B_{min+1} & C_{min+1} & & \\ & \ddots & \ddots & \ddots & \\ & & A_{max} & B_{max} \end{bmatrix} \begin{bmatrix} x_{min} \\ x_{min+1} \\ \vdots \\ x_{max} \end{bmatrix} = \begin{bmatrix} D_{min} \\ D_{min+1} \\ \vdots \\ D_{max} \end{bmatrix}$$

The algorithm for solving this tri-diagonal matrix is listed below

$$\begin{aligned} P_i &= A_i / B_{i-1} \\ B_i &= B_i - C_{i-1} P \\ D_i &= D_i - D_{i-1} P \\ x_{max} &= D_{max} / B_{max} \end{aligned}$$

$$i = min + 1, min + 2, \cdots, max$$

$$x_i = (D_i - x_{i+1} C_i) / B_i$$

$$i = max - 1, max - 2, \cdots, min$$

A subroutine for solving a tridiagonal matrix is listed in Appendix D.

C.2 ALGORITHM OF A PANTA-DIAGONAL SYSTEM

The equations to be solved must be of the form

$$A_i x_{i-2} + B_i x_{i-1} + C_i x_i + D_i x_{i+1} + E_i x_{i+2} = F_i \tag{C.7}$$

The matrix for these equations are

$$\begin{bmatrix} C_{min} & D_{min} & E_{min} & & & \\ B_{min+1} & C_{min+1} & D_{min+1} & E_{min+1} & & \\ A_{min+2} & B_{min+2} & C_{min+2} & D_{min+2} & E_{min+2} & \\ & \ddots & \ddots & \ddots & \ddots & \ddots \\ & & A_{max-1} & B_{max-1} & C_{max-1} & D_{max-1} \\ & & & A_{max} & B_{max} & C_{max} \end{bmatrix} \begin{bmatrix} x_{min} \\ x_{min+1} \\ x_{min+2} \\ \vdots \\ x_{max-1} \\ x_{max} \end{bmatrix} = \begin{bmatrix} F_{min} \\ F_{min+1} \\ F_{min+2} \\ \vdots \\ F_{max-1} \\ F_{max} \end{bmatrix}$$

The algorithm for solving this matrix is listed below

$$\begin{aligned} P &= B_i/C_{i-1} \\ Q &= A_{i+1}/C_{i-1} \\ C_i &= C_i - D_{i-1}P \\ D_i &= D_i - E_{i-1}P \\ F_i &= F_i - F_{i-1}P \\ B_{i+1} &= B_{i+1} - D_{i-1}Q \\ C_{i+1} &= C_{i+1} - E_{i-1}Q \\ F_{i+1} &= F_{i+1} - F_{i-1}Q \\ C_{max} &= C_{max} - D_{max-1}B_{max}/C_{max-1} \\ F_{max} &= F_{max} - F_{max-1}B_{max}/C_{max-1} \\ x_{max} &= F_{max}/C_{max} \\ x_{max-1} &= (F_{max-1} - x_{max}D_{max-1})/C_{max-1} \end{aligned}$$

$$i = min + 1, min + 2, \cdots, max - 1$$

$$x_i = (F_i - D_i * x_{i+1} - E_i * x_{i+2})/C_i$$

$$i = max - 2, max - 3, \cdots, min$$

Appendix D

PROGRAM LIST

D.1 SUBROUTINE OF TDMA

```
      SUBROUTINE TDMA(A,B,C,D,MIN,MAX,N)
C     ==================================================
C     | THIS SUBROUTINE IS TO SOLVE A TRIADIAGNAL MATRIX |
C     |      A(I)*X(I-1)+B(I)*X(I)+C(I)*X(I+1)=D(I)      |
C     |        D ARRAY CONTAINS THE RESULTS OF X         |
C     ==================================================
      IMPLICIT REAL*8 (A-H,O-Z)
      DIMENSION A(N),B(N),C(N),D(N)
      MINP1=MIN+1
      DO 10 I=MINP1,MAX
      P=A(I)/B(I-1)
      B(I)=B(I)-C(I-1)*P
10    D(I)=D(I)-D(I-1)*P
      D(MAX)=D(MAX)/B(MAX)
      DO 20 II=MINP1,MAX
      I=MAX+MIN-II
20    D(I)=(D(I)-D(I+1)*C(I))/B(I)
      RETURN
      END
```

D.2 SUBROUTINE OF PDMA

```
      SUBROUTINE PDMA(A,B,C,D,E,F,MIN,MAX,N)
C     ======================================================
C     | THIS SUBROUTINE IS TO SOLVE A PENTADIAGONAL METRIX |
C     | A(I)*X(I-2)*B(I)*X(I-1)+C(I)*X(I)+D(I)*X(I+1)      |
C     | +E(I)*X(I+2)=F(I)                                  |
C     |         A ARRAY CONTAINS THE RESULTS OF X          |
C     ======================================================
      IMPLICIT REAL*8 (A-H,O-Z)
      DIMENSION A(N),B(N),C(N),D(N),E(N),F(N)
      MAXM1=MAX-1
      MINP1=MIN+1
      DO 10 I=MINP1,MAXM1
      P=B(I)/C(I-1)
      Q=A(I+1)/C(I-1)
      C(I)=C(I)-D(I-1)*P
      D(I)=D(I)-E(I-1)*P
      F(I)=F(I)-F(I-1)*P
      B(I+1)=B(I+1)-D(I-1)*Q
      C(I+1)=C(I+1)-E(I-1)*Q
      F(I+1)=F(I+1)-F(I-1)*Q
10    CONTINUE
      P=B(MAX)/C(MAXM1)
      C(MAX)=C(MAX)-D(MAXM1)*P
      F(MAX)=F(MAX)-F(MAXM1)*P
      A(MAX)=F(MAX)/C(MAX)
      A(MAXM1)=(F(MAXM1)-A(MAX)*D(MAXM1))/C(MAXM1)
      MAXMIN=MAX-MIN
      DO 20 I=2,MAXMIN
      K=MAX-I
      A(K)=(F(K)-D(K)*A(K+1)-E(K)*A(K+2))/C(K)
20    CONTINUE
      RETURN
      END
```

D.3 SUBROUTINE FOR GRID GENERATION

```
      SUBROUTINE GRIGEN(N,M,X,Y,P,Q)
C     ================================================
C     |  THIS SUBROUTINE IS TO SOLVER AN ELLIPTIC    |
C     |  GENERATING SYSTEM FOR NONORTHOGONAL GRIDS   |
C     |  P AND Q ARE THE GRID CONTROL FUNCTIONS      |
C     ================================================
      IMPLICIT REAL*8 (A-H,O-Z)
      DIMENSION X(N,M),Y(N,M),P(N,M),Q(N,M)
      KMAX=300
      RELAX=1.2
      RELG=1.0-RELAX
      DO 500 J=1,M,M-1
      DO 500 I=1,N
      IF (I.EQ.1.OR.I.EQ.N) GOTO 570
      XXI=0.5*(X(I+1,J)-X(I-1,J))
      YXI=0.5*(Y(I+1,J)-Y(I-1,J))
      XXI2=X(I+1,J)-2.*X(I,J)+X(I-1,J)
      YXI2=Y(I+1,J)-2.*Y(I,J)+Y(I-1,J)
      GOTO 580
570   IF (I.EQ.1) THEN
      XXI=0.5*(-3.*X(1,J)+4.*X(2,J)-X(3,J))
      YXI=0.5*(-3.*Y(1,J)+4.*Y(2,J)-Y(3,J))
      XXI2=0.5*(-7.*X(1,J)+8.*X(2,J)-X(3,J))-3.*XXI
      YXI2=0.5*(-7.*Y(1,J)+8.*Y(2,J)-Y(3,J))-3.*YXI
      ELSE
      XXI= 0.5*(3.*X(N,J)-4.*X(N-1,J)+X(N-2,J))
      YXI= 0.5*(3.*Y(N,J)-4.*Y(N-1,J)+Y(N-2,J))
      XXI2=0.5*(-7.*X(N,J)+8.*X(N-1,J)-X(N-2,J))-3.*XXI
      YXI2=0.5*(-7.*Y(N,J)+8.*Y(N-1,J)-Y(N-2,J))-3.*YXI
      ENDIF
580   G11=XXI*XXI+YXI*YXI
      P(I,J)=-(XXI*XXI2+YXI*YXI2)/G11
C      P(I,J)=-XXI2/XXI
500   CONTINUE
      DO 600 I=1,N,N-1
      DO 600 J=1,M
      IF (J.EQ.1.OR.J.EQ.M) GOTO 650
      XETA=0.5*(X(I,J+1)-X(I,J-1))
      YETA=0.5*(Y(I,J+1)-Y(I,J-1))
      XETA2=X(I,J+1)-2.*X(I,J)+X(I,J-1)
      YETA2=Y(I,J+1)-2.*Y(I,J)+Y(I,J-1)
      GOTO 670
650   IF (J.EQ.1) THEN
      XETA= 0.5*(-3.*X(I,1)+4.*X(I,2)-X(I,3))
      YETA= 0.5*(-3.*Y(I,1)+4.*Y(I,2)-Y(I,3))
```

```
      XETA2=0.5*(-7.*X(I,1)+8.*X(I,2)-X(I,3))-3.*XETA
      YETA2=0.5*(-7.*X(I,1)+8.*X(I,2)-X(I,3))-3.*XETA
      ELSE
      XETA= 0.5*(3.*X(I,M)-4.*X(I,M-1)+X(I,M-2))
      YETA= 0.5*(3.*Y(I,M)-4.*Y(I,M-1)+Y(I,M-2))
      XETA2=0.5*(-7.*X(I,M)+8.*X(I,M-1)-X(I,M-2))-3.*XETA
      YETA2=0.5*(-7.*X(I,M)+8.*X(I,M-1)-X(I,M-2))-3.*XETA
      ENDIF
670   G22=XETA*XETA+YETA*YETA
      Q(I,J)=-(XETA*XETA2+YETA*YETA2)/G22
C      Q(I,J)=-YETA2/YETA
600   CONTINUE
      DO 900 I=1,N
      DO 900 J=1,M
      RJ1=FLOAT(M-J)/FLOAT(M-1)
      RJ2=FLOAT(J-1)/FLOAT(M-1)
      RI1=FLOAT(N-I)/FLOAT(N-1)
      RI2=FLOAT(I-1)/FLOAT(N-1)
      P(I,J)=RJ1*P(I,1)+RJ2*P(I,M)
      Q(I,J)=RI1*Q(1,J)+RI2*Q(N,J)
900   CONTINUE
      DO 1000 K=1,KMAX
      ERRX=0.0
      ERRY=0.0
      DO 100 I=2,N-1
      DO 100 J=2,M-1
      XXI=0.5*(X(I+1,J)-X(I-1,J))
      YXI=0.5*(Y(I+1,J)-Y(I-1,J))
      XETA=0.5*(X(I,J+1)-X(I,J-1))
      YETA=0.5*(Y(I,J+1)-Y(I,J-1))
      XXI2=X(I+1,J)+X(I-1,J)
      YXI2=Y(I+1,J)+Y(I-1,J)
      XETA2=X(I,J+1)+X(I,J-1)
      YETA2=Y(I,J+1)+Y(I,J-1)
      XXIETA=0.25*(X(I+1,J+1)-X(I+1,J-1)-X(I-1,J+1)+X(I-1,J-1))
      YXIETA=0.25*(Y(I+1,J+1)-Y(I+1,J-1)-Y(I-1,J+1)+Y(I-1,J-1))
      G11=XXI*XXI+YXI*YXI
      G22=XETA*XETA+YETA*YETA
      G12=XXI*XETA+YXI*YETA
      XTEMP=0.5*(G22*(XXI2+P(I,J)*XXI)+G11*(XETA2+Q(I,J)*XETA)
     / -2.*G12*XXIETA)/(G11+G22)
      YTEMP=0.5*(G22*(YXI2+P(I,J)*YXI)+G11*(YETA2+Q(I,J)*YETA)
     / -2.*G12*YXIETA)/(G11+G22)
      XTEMP=RELAX*XTEMP+RELG*X(I,J)
      YTEMP=RELAX*YTEMP+RELG*Y(I,J)
      ERRD=AMAX1(ERRX,ABS(XTEMP-X(I,J)),ERRY,ABS(YTEMP-Y(I,J)))
      X(I,J)=XTEMP
```

```
      ERRD=DMAX1(ERRX,DABS(XTEMP-X(I,J)),ERRY,DABS(YTEMP-Y(I,J)))
      X(I,J)=XTEMP
      Y(I,J)=YTEMP
100   CONTINUE
      IF (ERRD.LT.1E-5) GOTO 1050
1000  CONTINUE
      WRITE(6,22)
22    FORMAT(//,5X,'*** NOT CONVERGNE GRIDS ***')
      WRITE(6,9) K,ERRD
9     FORMAT(/,5X,'ITERATION=',I3,5X,'ERR=',E11.4)
1050  RETURN
      END
```

D.4 SUBROUTINE FOR CALCULATING THE SCALE FACTORS

```
      SUBROUTINE METRIC(X,Y,N,M,XIX,ETAX,XIY,ETAY,G,G11,G22,G12,P,Q)
C     ================================================
C     |   THIS PROGRAM IS TO COMPUTE ALL THE METRICS   |
C     |   FOR THE TRANSFORMATION                       |
C     ================================================
      IMPLICIT REAL*8 (A-H,O-Z)
      DIMENSION X(N,M),Y(N,M),P(N,M),Q(N,M)
      DIMENSION XIX(N,M),ETAX(N,M),G11(N,M),G(N,M)
      DIMENSION XIY(N,M),ETAY(N,M),G22(N,M),G12(N,M)
      DATA EPS/1E-6/
C     ================================================
      DO 10 I=1,N
      DO 10 J=1,M
      IF (I.EQ.1.OR.I.EQ.N) GOTO 20
      XXI=0.5*(X(I+1,J)-X(I-1,J))
      YXI=0.5*(Y(I+1,J)-Y(I-1,J))
      GOTO 30
20    IF (I.EQ.1) THEN
      XXI=0.5*(-3.0*X(1,J)+4.0*X(2,J)-X(3,J))
      YXI=0.5*(-3.0*Y(1,J)+4.0*Y(2,J)-Y(3,J))
      ELSE
      XXI=0.5*(3.0*X(N,J)-4.0*X(N-1,J)+X(N-2,J))
      YXI=0.5*(3.0*Y(N,J)-4.0*Y(N-1,J)+Y(N-2,J))
      ENDIF
30    IF (J.EQ.1.OR.J.EQ.M) GOTO 40
      XETA=0.5*(X(I,J+1)-X(I,J-1))
      YETA=0.5*(Y(I,J+1)-Y(I,J-1))
      GOTO 50
40    IF (J.EQ.1) THEN
      XETA=0.5*(-3.0*X(I,1)+4.0*X(I,2)-X(I,3))
      YETA=0.5*(-3.0*Y(I,1)+4.0*Y(I,2)-Y(I,3))
      ELSE
      XETA=0.5*(3.0*X(I,M)-4.0*X(I,M-1)+X(I,M-2))
      YETA=0.5*(3.0*Y(I,M)-4.0*Y(I,M-1)+Y(I,M-2))
      ENDIF
50    IF (XXI.LT.EPS) THEN
      XXI=0.0
      ENDIF
      IF (YXI.LT.EPS) THEN
      YXI=0.0
      ENDIF
      IF (XETA.LT.EPS) THEN
      XETA=0.0
      ENDIF
      IF (YETA.LT.EPS) THEN
```

```
      YETA=0.0
      ENDIF
      G(I,J)=XXI*YETA-XETA*YXI
      XIX(I,J)= YETA/G(I,J)
      XIY(I,J)=-XETA/G(I,J)
      ETAX(I,J)=-YXI/G(I,J)
      ETAY(I,J)= XXI/G(I,J)
      G11(I,J)= XIX(I,J)* XIX(I,J)+ XIY(I,J)* XIY(I,J)
      G22(I,J)=ETAX(I,J)*ETAX(I,J)+ETAY(I,J)*ETAY(I,J)
      G12(I,J)= XIX(I,J)*ETAX(I,J)+ XIY(I,J)*ETAY(I,J)
      P(I,J)=P(I,J)*G11(I,J)
      Q(I,J)=Q(I,J)*G22(I,J)
10    CONTINUE
      RETURN
      END
```